Czech Technical University in Prague
Faculty of Electrical Engineering
Department of Electrotechnology

PROPERTY STUDIES OF PLASMA SPRAYED TITANATES

Doctoral Thesis

Jiří Kotlan

Prague, August 2016

Ph.D. Programme: Electrical Engineering and Information Technology
Branch of study: Electrotechnology and Materials

Supervisor: Ing. Pavel Ctibor, Ph.D
Supervisor-Specialist: Ing. Josef Sedláček, CSc.

Preface

This dissertation thesis is meant as a summary of disertant's work in the field of property studies of plasma sprayed titanates which are in sintered form commonly used ceramics for electronic applications. The main focus is on electrical properties of these functional oxides and the role of deposition conditions and consequent thermal treatment on the electrical properties. The thesis is written as a collection of published papers in impacted journals related to the topic including brief introduction to plasma spraying and current state of the art in the field of plasma sprayed ceramics for electrical engineering. This thesis presents the results obtained from the beginning of the authors masters degree program at Czech Technical University in Prague until today.

Acknowledgements

Declaration

I hereby declare that this thesis is the result of my own work and all the sources I used are in the list of references, in accordance with the Methodological Instructions on Ethical Principles in the Preparation of University Theses.

In Prague 3rd of August 2016   ....

                                                            Jiri Kotlan

Abstrakt

V mnoha technologických aplikacích jsou plazmové nástřiky díky svým vlastnostem nenahraditelnou součástí průmyslové výroby. Jedná se převážně o aplikace jakými jsou tepelné bariéry či otěruvzdorné vrstvy. Využití plazmových nástřiků v elektrotechnickém průmyslu zaostává za jejich možnostmi i díky tomu, že studiu elektrických vlastností takto připravených vrstev je celosvětově přikládána nižší pozornost. Tato práce přináší nové poznatky o elektrických a strukturních vlastnostech titaničitanů, které se ve slinutém stavu používají v elektrotechnickém průmyslu jako dielektrika. Titaničitan vápenatý a titaničitan barnato-strontnatý jakožto perspektivní materiály pro použití v podobě nástřiku byly vybrány jako modelové materiály v této disertaci. Oproti slinutému materiálu vykazují plazmové nástřiky rozdílnou mikrostrukturu a často i chemické a fázové složení. Nástřiky pro tuto práci byly vytvořeny pomocí standardního plynem stabilizovaného plazmového hořáku i pomocí unikátního vodou stabilizovaného systému. Bylo použito mnoho experimentálních metod, které přinesly nové poznatky o těchto materiálech. Elektrické vlastnosti byly studovány na základě frekvenčních závislostí relativní permitivity a ztrátového činitele či pomocí měření elektrické pevnosti, elektrické rezistivity nebo stanovení šířky zakázaného pásu. Morfologie nástřiků byla studována, jak světelnou, tak i elektronovou mikroskopií. Fázové složení bylo charakterizováno pomocí rentgenové difrakční analýzy včetně použití vysokoteplotních měření. Ramanova spektroskopie a rentgenová fotoelektronová spektroskopie byly použity k analýze chemického složení. Mechanické vlastnosti byly studovány pomocí měření mikrotvrdosti a modulu pružnosti. Všechna tato měření a diskuze nad získanými výsledky přinesla nové poznatky o chování plazmových nástřiků vybraných titaničitanů a tím přispěla k možnému většímu uplatnění těchto materiálů v elektrotechnickém průmyslu.

Abstract

Use of plasma sprayed coatings is an important part of industrial production in many applications. This technique is mainly used for applications such as thermal barrier and wear resistant layers. Application of plasma sprayed coatings in the electronics industry lags behind its possibilities because there was lower attention to electrical properties of these coatings worldwide. This work provides new knowledge about the electrical and structural properties of titanates which are in the sintered state used as a dielectrics. Calcium titanate and barium-strontium titanate as promising materials in the form of the coating were selected as proper materials in this dissertation. Plasma deposited coatings exhibit different microstructure and often phase and chemical composition when compared to the sintered material. Coatings were prepared by the conventional gas stabilized plasma torch as well as water stabilized plasma technology. Many experimental methods were used to bring a new knowledge about these materials. The electrical properties were studied by frequency dependence of relative permittivity and loss factor or by measuring electrical breakdown strength, electrical resistivity and determination of band gap. The morphology of coatings was studied by both light and electron microscopy. Phase composition was characterized by X-ray diffraction analysis including high temperature in-situ experiments. Raman spectroscopy and X-ray photoelectron spectroscopy were used to analyze the chemical composition. The mechanical properties were analyzed by microhardness and elastic modulus measurements. All these measurements and discussion of the results bring a new knowledge about plasma deposited titanates and thereby contribute to greater potential application of these materials in the electronics industry.

Contents

List of Figures

Chapter 1

Aims of this Thesis

The purpose of this doctoral thesis is to expand our knowledge of electrical properties of plasma sprayed titanates deposited in form of coatings or self-supported parts. The main focus of the work is to bring a new approach to preparing high quality dielectric coatings by plasma spraying techniques. Employment of plasma spraying in the field of electrical engineering is rare but promising for future development of interesting industrial production. Possibility of deposition of functional ceramics onto various substrates has much larger industrial potential to current use. Based on bibliographic research, titanates as an important part of dielectric materials were used as material of choice in this work. Different coatings and consequent modifications of their materials properties were studied as well as development of a new deposition method based on reactive suspension plasma spraying. Not only characterization of prepared coatings but spraying conditions and parameters of plasma deposition are points of interests in this work.

Chapter 2

Introduction

Plasma spraying, also known as atmospheric plasma spraying (APS), is one of thermal spray methods used to deposit coatings onto various substrates. Metallic, ceramic or composite materials can be deposited onto substrate where serve as a layer which improves substrates properties. For example, thermal barrier coatings (TBC) prepared by thermal spraying are used as a protective coating for environment with high temperature loads. These coatings are widely used for protecting of turbine blades, parts of combustion engines or furnaces for thermal treatment. Coatings with high abrasion resistance find application anywhere the quality or lifetime of the component rapidly depend on abrasion resistance. Protection of walls of molds can be given as one of many examples. Chemical and corrosion resistance are crucial properties not only for chemical engineering. All those coatings have one same attribute. Usability of systems without them is reduced or even precluded. Not only coatings but even free-standing parts can be produced by thermal spraying using procedures leading to striping thick coating out of the substrate. Basic systems of plasma spraying are described below.

Material in the form of powder, rod, suspension or solution is melted in plasma jet and propelled towards to the substrate where typical lamellar microstructure is formed (see Fig. 2.1). Single molten particles are mechanically mounted to the substrate. By particles are meant droplets and not elementary particles of the matter - plasma spraying is not a technique forming layers "atom-after-atom". A molten particle undergoes rapid deformation and after solidification on the substrate is called splat. Roughness of the substrate affects adhesion of the sprayed layer [8]. Due to that fact is the substrate usually grit blasted before spraying. As is illustrated in Fig. 2.1, the coating may contain unmelted particles, which are mostly unwanted. Amount of these particles can be minimized by optimization of the spraying parameters and size of the powder [9]. During plasma spraying of metallic materials in open atmosphere, their oxidation usually takes place. Molten material interacts with oxygen coming into the jet from the surrounding atmosphere due to entrainment of the ambient air. Pure argon or mixture of argon and hydrogen may be used as a shroud gas for elimination of oxides [10]. Both intrasplat or intersplat porosity is typical for thermally sprayed coatings. Some applications as thermal barriers require high porosity because decreases coating's thermal conductivity [11] but for many other applications porosity

Fig. 2.1: Typical microstructure of plasma sprayed coatings [1].
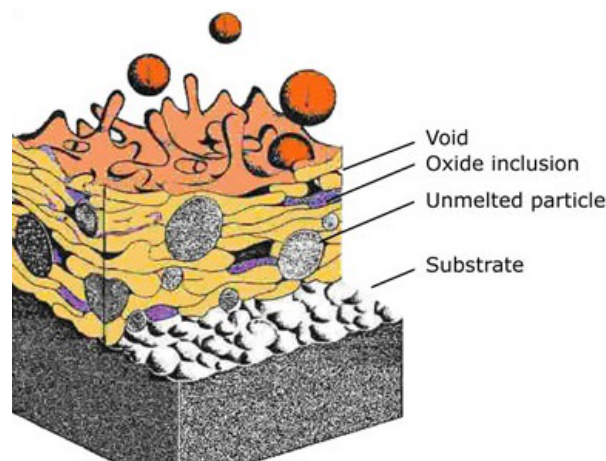
is unwanted because it affects significantly mechanical, dielectric and other properties [12]. Chemical and phase composition of the feedstock material is often changed during the interaction with plasma [13], and it changes materials properties as well. Finding of the optimal spraying conditions is a crucial task for preparation of coatings with required properties.
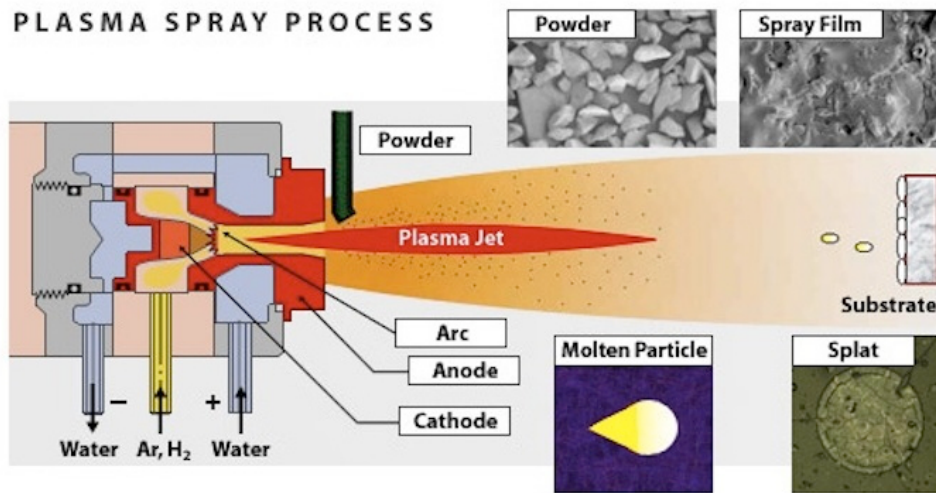
Fig. 2.2: Plasma spray process [2].

2.1 Plasma Spraying

In plasma spraying, an electric arc generates plasma throughout ionization of working gases. This electrical arc is struck between an anode and cathode. The gases flowing through this arc are heated up to their ionization level and plasma jet is formed. The most common working gas is mixture of argon and hydrogen. Hydrogen is used to increase plasma enthalpy. Another combination of working gases (nitrogen, helium) are not so widely used. The rapid expansion of ionized gases results in high plasma velocity. Typical peak exit nozzle velocities range from 500 m/s to 2500 m/s and peak plasma temperatures at the nozzle exit is 12 000 K to 15 000 K. Both parameters depends on torch design, process parameters and plasma gases. Employment of water cooling is necessary for increasing lifetime of the electrodes.

Feedstock material in the form of powder, suspension or solution is injected radially or less common axially into the plasma jet where it becomes melted and accelerated toward to the substrate where coating is formed by rapid solidification of molten or semi-molted droplets. Plasma spray process is illustrated, Fig. 2.2.

When plasma spraying is operated at ambient atmosphere, the process is called Atmospheric Plasma Spray (APS). Deposition process can also be carried out in reduced pressure as Low Pressure Plasma Spraying (LPPS) or spraying in vacuum chamber is termed as Vacuum Plasma Spray (VPS). Spraying at normal atmosphere was the only one technique used for samples manufactured in this thesis.

2.2 Water Stabilized Plasma Technology

Flow of a gas is not the only mean of plasma stabilization as it has been principally proved in 1922 by Siemens engineers Gerdien and Lotz [14]. The first use of liquid stabilization of plasma torch was reported in 1962. The main difference from standard APS torch is the chamber construction, Fig. 2.3. Evaporation from the inner wall of water vortex, surrounding the arc column, and heating and ionization of produced steam, are principal mechanisms that produce arc plasma. The evaporation is induced by the absorption of a fraction of heat power dissipated within the conducting arc core. Water vortex is created in cylindrical chamber with tangential injection. Rotating copper anode is placed outside of arc chamber. Due to that construction lifetime of electrode rapidly increases.

Water chamber is the heart of the water based plasma spray systems (WSP). Temperature of formed plasma jet is up to 30 000 K. Standard operation temperature is about 25 000 K. Plasma torch based on water stabilized technology is favorable for large coatings areas because the large amount of material can be processed per hour. For ceramics it is up to 50 kg/h and metals 100 kg/h. The cause is in the
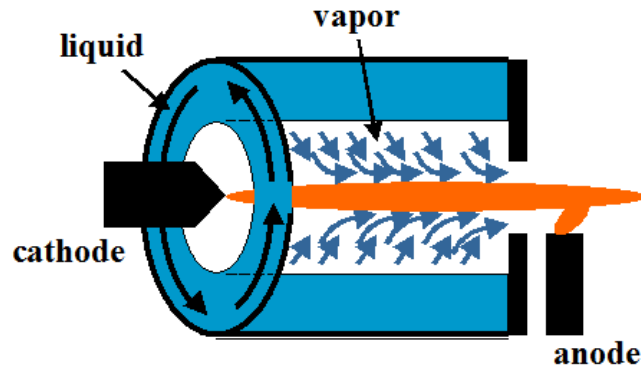
Fig. 2.3: Principle of water stabilized plasma torch (WSP) in detail, courtesy of IPP Prague.
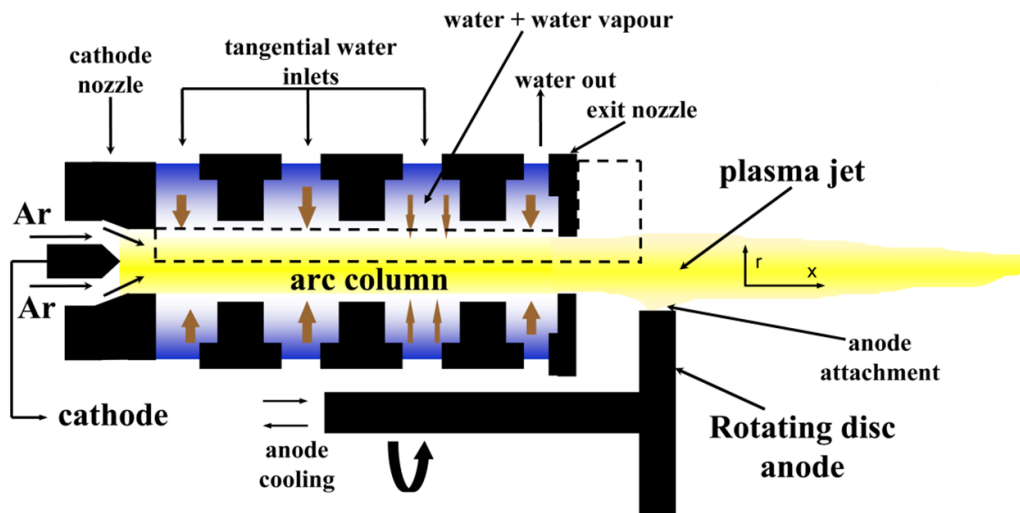
Fig. 2.4: Principle scheme of hybrid argon-water stabilized plasma torch (WSP-H) [3].

high power of the system (80 - 160 kW) and about ten times higher plasma enthalpy when compare to standard APS torches. Powder feeding injector is radial and outside of the chamber. Versatility of used external feeding system allows to find optimal feeding parameters by change in feeding distance (i.e. distance between plasma nozzle and feeding point) and feeding angle. Absence of working gases decreases operation costs, as only water with average consumption of about 3 l/h is used for plasma generation. Disadvantage of this pure water based system lies in the consumable graphite cathode, which delimits maximal operating time. Ignition of the torch is done by short circuit of graphite cathode and external copper anode by metallic wire which is melted by high power supply. That results in electric discharge between electrodes and ignition of arc in the water chamber.

Since the beginning of development of water stabilized plasma technology (WSP) was the water stabilized plasma torch developed into the novel hybrid argon-water stabilized form (WSP-H), Fig. 2.4. For plasma spraying, where plasma jets are used to heat and accelerate particles injected into plasma jet, the high-enthalpy jets generated in water torches ensure a high level of efficiency of the particle heating and thus high throughputs, while low plasma flow rates and density result in lower efficiency of the particle acceleration. Thus, it was desirable to create a plasma torch with thermal characteristics typical for the water torches but with increased plasma flow rates and densities. These ideas led to the development of the hybrid water–gas torch where principles of arc stabilization by gas flow and water vortex are combined [15]. The design of chamber is more complicated when compared to WSP. Gas part was added to the system also in order to omit ignition by shortcut wire. This design allows high voltage impulse
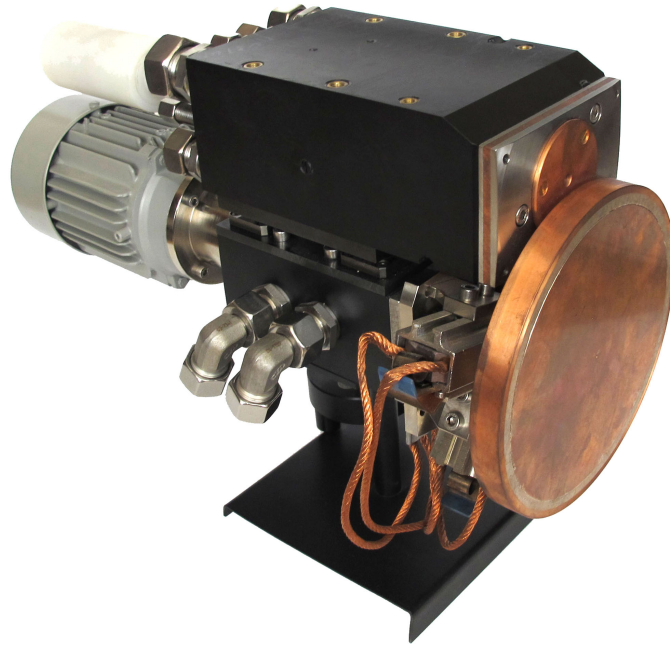
Fig. 2.5: Hybrid argon-water stabilized plasma torch (WSP-H), courtesy of IPP Prague.

torch ignition. Moreover, gas flow in the cathode part protects a cathode tip and thus a consumable carbon cathode used in water torches could be replaced by a fixed tungsten cathode. In combination with employing simple ignition this solution brings easy operation equivalent to APS. Typical cathode life time is up to 200 operating hours (as in 2016) and typical argon consumption is between 10 - 15 slpm when operating at power of 160 kW. Complete spray system including water cooling unit was introduced to the market by ProjectSoft HK a.s., Czech Republic. Figure of the WPS-H 500 plasma torch is given, Fig. 2.5

Chapter 3

Introduction to Electrical Properties of Thermal Spray Coatings

This chapter introduces the reader into published works in the field of thermally sprayed ceramics with enhanced properties useful for possible electronics applications. However, the most of thermally sprayed coatings serve as a passive protecting layer of underlying substrate against harsh environment. Thermal barrier coatings protect substrate against high thermal load. Usability of mechanical parts with contact damage increases by application of wear resistive coatings. Another example of passive layer is coating protecting substrate against surrounding chemical environment. When speaking about functional coatings more than the barrier effect is required. Material must provide sensory function and ability to replace basic components for electronic applications such as capacitor, conductor or semiconductor.

3.1 Dielectrics

Relative permittivity (ϵ_r) which evaluates ratio of electric energy stored in the material to electric energy stored in vacuum of the same dimensions (also well known as dielectric constant) is an important parameter to determine quality of dielectrics. Loss factor ($tg\delta$) determines electrical properties as well. It describes the contribution of loss current in a capacitor. The latter results from polarization as well as electron or ion conduction. Both these parameters are frequency dependent, because the polarization mechanism of a dielectric varies with frequency.

Alumina (Al_2O_3) is widely studied material from several points of technical utilization including electrical properties. Not surprisingly electrical properties of alumina coatings strongly depend on microstructure and spray conditions. Pawlowski reported relative permittivity of plasma sprayed alumina in the range 5.9–8.3 depending on the feedstock powder and spray process parameters [16]. Presence of metastable γ-phase in thermally sprayed alumina is well known [17]. The γ-phase is highly hygroscopic which may lead to an increase in the dielectric constant of alumina coatings [18]. Ctibor et al., reported relative permittivity value of about 14 for frequency 200 Hz [19]. Toma et al. made the comparative study of the depence of humidity on electrical properties and characteristics of thermally sprayed alumina and magnesium spinel coatings sprayed by APS and High Velocity Oxy Fuel (HVOF). At low humidity levels, the electrical resistivity of alumina and spinel coatings was comparable (10^{11} Ω·m). At a very high humidity level (95 % RH, Relative air Humidity), a dramatic decrease in resistivity of about five orders of magnitude for alumina coatings, and about four orders of magnitude for spinel coatings was observed. This decrease was mainly due to the increase in water adsorption on the coatings, generating ionic conductivity [6]. Both surface as well as volume resistivity are commonly influenced by moisture due to the porosity of coatings opened towards to the surface.

Sintered barium titanate ($BaTiO_3$) and its doped variants received a lot of attention in the past decades. This material has interesting electrical properties in the form of coating but still there is a lack of publications coming from thermal spray community. Dent et al. successfully deposited $BaTiO_3$ and $(Ba,Sr)TiO_3$. Relative permittivity value for frequency 10 kHz was low for such kind of material when comparede with sintered material. The value varied in between 23 and 152 in the case of HVOF spraying. For plasma deposited coatings, the range was between 65 and 240. Loss factor was lower than 0.16 for all samples. The main conclusion is that the dielectric properties of the sprayed material are directly related to their degree of crystallinity; coatings containing more crystalline material have higher dielectric constants [20]. Increase in crystallinity induced by thermal annealing resulted in increasing of relative
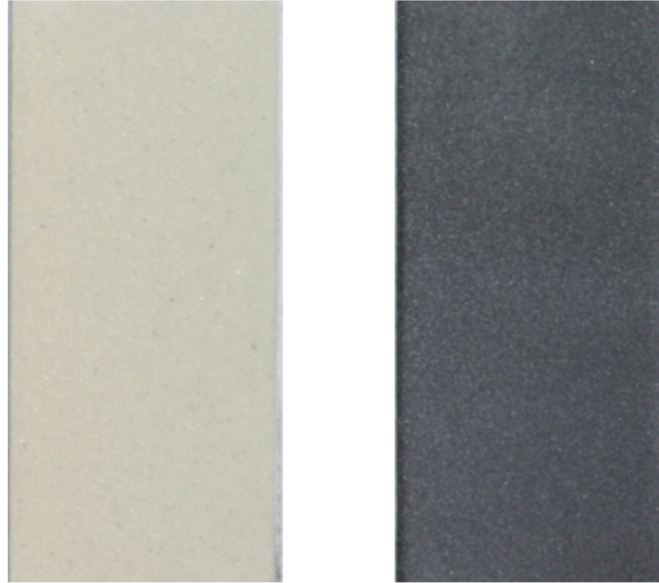
Fig. 3.1: Comparison of long spray distance (190 mm) and short spray distance (100 mm) BaTiO$_3$ coatings surfaces the dark color of the short SD coating (right) indicates oxygen deficiency; sample width is 25 mm [4].

permittivity [21]. Ctibor et al. reported BaTiO$_3$ thick coatings sprayed by F4 plasma torch. Dielectric properties were measured in the temperature range 280–400 K with result that the maximum permittivity value lies near to the theorethical transition temperature from tetragonal to cubic crystallographic phase [22]. The study was later extended to taking into account photocatalytical activity of these coatings [4]. The paper also shows influence of spray distance on oxygen deficiency which is often indicated by the change in color to the different shades of grey, Fig.3.1.

BaTiO$_3$ coatings were successfully sprayed by employing the supersonic plasma spray system HEP-Jet [23]. Obtained coating was dense, with low porosity and high hardness. The average bond strength between the coating and substrate (measured by standardized pull-off test) was 42 MPa. Dielectric constant is significantly higher when compared to the previous published works on different torches. The value for frequency 5 kHz was about 1500 for the whole temperature range 300–420 K. The importance of substrate temperature during plasma spray deposition of coatings was demonstrated in a study, which showed that with the increase in substrate temperature the inter-splat bonding increases and this consequently results in the increase in the relative permittivity values by the factor of 3 [5]. Micro-graphs of fracture surfaces for this study is given in Fig. 3.2. Thermal post treatment of plasma sprayed (BaTiO$_3$) significantly decreased loss factor. Final value dropped from 0.8 to less than 0.1 and become almost frequently independent up to the frequency 500 kHz. Relative permittivity dropped from 800 to approximately 200 and was not sensitive to frequency change as well [24]. Increase of relative permittivity of deposited coating by thermal annealing due to the recrystallization was reported as the last work by this time [25].

Papers focused on uncommon materials which were prepared in the form of the coating. Dielectric properties of less common materials as synthetic mullite, steatite and spodumene as well as natural olivine-forsterite were studied in the work of deposites sprayed by WSP technology [26]. Complex study on plasma sprayed diopside which represents an inexpensive natural material partially studied dielectric properties was published [27].

3.2   Insulators

The purpose of electric insulator is to separate areas with different electrical potential. This ability is caused by the absence (very limited number) of free electric charges in the material. Typical application of insulators is in high voltage power lines where insulator separates power lines and pylons. These insulators are made of ceramics or polymer materials. Thermally sprayed coatings are applicable where
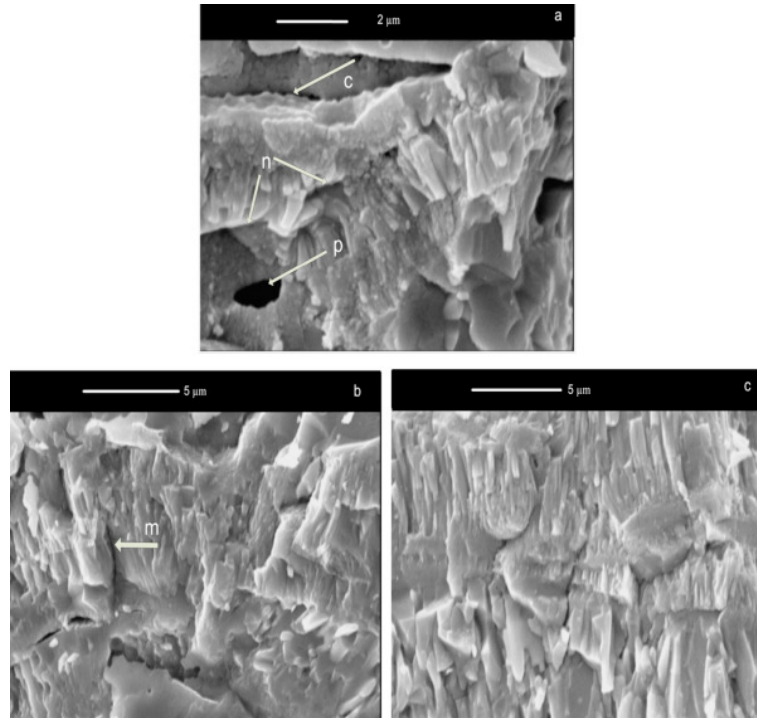
Fig. 3.2: Fracture surface of $BaTiO_3$ film deposited on substrate held at different temperatures: (a) room temperature, (b) 300 °C and (c) 600 °C (c: poor contact between splats, n: non-bounded interfaces, p: pore, m: micro-crack) [5].

the surface of metallic material could serve as a electrical isolation as well as a mechanical protection of this part. Isolation ability is limited by the micro-structure of the deposits. In general, denser micro-structure results in higher electrical breakdown strength which is traditionally defined as breakdown voltage divided by coatings thickness. One way to improve breakdown strengths is to optimize spray conditions in order to obtain denser micro-structure or use sealants. Research on the dielectric strength of plasma sprayed ceramics has been limited mostly to alumina and alumina based materials. Pawlowski states that the crucial parameter that can affect the breakdown strengths results is the volume percentage of porosity present in the coatings. He reported dielectric strength values ranging between 9 and 18 kV/mm for coatings deposited by spraying different alumina powders [16]. The effect of role of coatings thickness on the dielectric strength was analyzed by Toma et al., [6] The maximum dielectric strength was found to be 24 kV/mm for APS sprayed alumina. Of about 10 kV/mm higher value was observed for HVOF coatings, Fig. 3.3. Dielectric breakdown strength decreased with increasing of coatings thickness. The reason may be cumulation of micro-structure defects.

An ultra-dense alumina coating with a porosity lower than 1 vol. % prepared by low pressure plasma spray technique can exhibit a maximum dielectric strength of 45 kV/mm [28]. Kim et al. [7], showed that breakdown voltage for coatings surface of which was ground compared to as-sprayed alumina-titania coatings was similar, Fig. 3.4 - Left.

Increase in breakdown voltage of about 50 % caused by the appropriate sealant penetration into the coating was reported in this study as well, Fig. 3.4 - Right. Plasma sprayed alumina coating for operation in extreme environment related to the nuclear waste processing was investigated. Electrical breakdown strength was one of the studied parameters for these coatings characterization. The evolution of the electrical insulation of these sealed ceramic coatings is sensitive to the degradation of the microstructure [29].
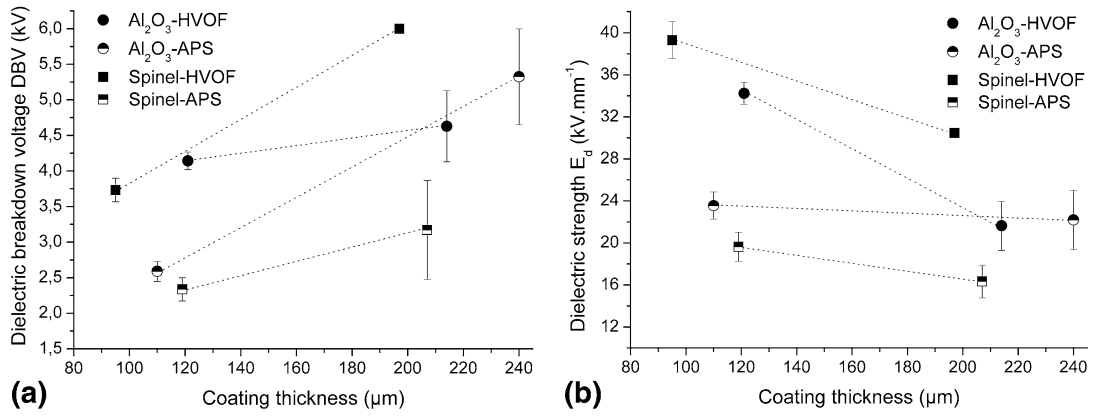
Fig. 3.3: Dielectric properties as a function of coating composition and coating thickness: (a) dielectric breakdown voltage; and (b) dielectric strength (dotted lines are for orientation purposes only) [6].
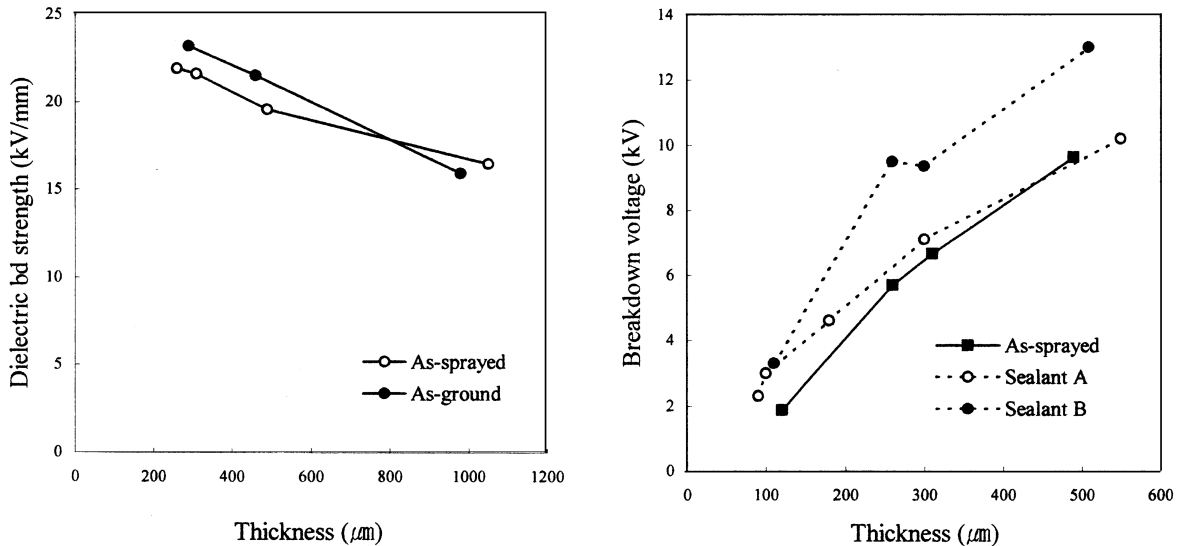
Fig. 3.4: Left - dielectric strength of as-sprayed and as-ground coating samples as a function of ceramic coating thickness; Right - the effect of sealing on the dielectric breakdown voltage of coating samples as a function of ceramic coating thickness. [7].

Chapter 4

Collection of Papers

This chapter contains six original papers published in journals with impact factor related to the thesis topic. Papers are in logical order by their subject. The first three papers are focused on property studies of plasma sprayed calcium titanate as an alternative to commonly studied barium titanate which exhibits not well satisfying electrical properties in the form of deposits. The first paper origins from authors masters thesis and is focused on plasma deposition of calcium titanate by APS as well as WSP. Two other papers studied effect of thermal post treatment on the dielectric properties of these coatings as a method for improving their electrical properties. The fourth paper deals with electric breakdown strengths of plasma sprayed barium-strontium titanate and four other industrially well established materials. An interesting correlation between electrical breakdown strength and amorphous phase content was observed for plasma sprayed barium-strontium titanate in this publication. This observation resulted in fifth paper which is focused on the role of amorphous phase content on the electrical properties of atmospheric plasma sprayed barium-strontium titanate. Different amount of amorphous phase content resulted in significantly different behavior in electrical field. The last paper introduced a new method for plasma spraying of calcium titanate. The technique is based on reactive suspension plasma spraying of precursors $CaCO_3$ and TiO_2 resulting in formation of calcium titanate coating. The study did not deal with tailoring of coatings properties but presented new technique with potential benefits resulting from the direct spraying of precursor.

4.1 Dielectric properties of CaTiO$_3$ coatings prepared by plasma spraying

The paper deals with dielectric properties of calcium titanate prepared by plasma spraying using WSP and APS. Please note, GSP abbreviation represents APS process in the terminology of this thesis. Sample GSP 100 exhibited the best dielectric properties, in the meaning of low loss factor and well frequency stable relative permittivity value, within all samples in this study. At this moment is necessary to highlight gas composition during the APS spraying. Used setup with 65 slpm of Ar and only 2.5. slpm of H$_2$ resulted in less reductive plasma atmosphere and consequently lower oxygen reduction of sprayed material. This is most likely reason for such good electrical properties of APS sprayed calcium titanate.

Dielectric properties of CaTiO$_3$ coatings prepared by plasma spraying

J. Sedlacek[1], P. Ctibor*[2], J. Kotlan[1] and Z. Pala[2]

This paper presents a study of dielectric properties, namely the relative permittivity and loss factor dependence on the frequency of a weak electric field. Perovskite CaTiO$_3$ was studied in the form of coatings and self-supporting plates made by plasma spraying. A conventional gas stabilised plasma gun (GSP) as well as a water stabilised plasma gun (WSP) were employed. It was observed that plasma sprayed titanates exhibit a strong relaxation of permittivity and loss factor decrease with a frequency rise. These properties are influenced by spray technique and spraying parameters, but the relaxation character in general is preserved in all cases. The volume resistivity of the samples was studied as well. Several aspects of the structural features of plasma deposits, especially the phase composition, porosity character, and their influence on dielectric properties are discussed.

Keywords: Plasma, Ceramics, CaTiO$_3$, Permittivity, Resistivity

Introduction

In recent decades plasma spraying has become a well accepted coating method for metallic and ceramic materials and has been used in a variety of fields including electrical engineering.[1,2] Plasma sprayed coatings are produced by introducing powder particles of a material into a plasma jet, which melts and propels them towards the substrate. Coating is formed as a result of the interaction between a droplet and the substrate or the previously deposited layers. The lamellar character of a body formed in this way induces a particular character of porosity.[3] Besides the chemical and phase composition, the porosity is main factor affecting almost all of the mechanical, thermal and electric properties of coatings.

Various works on dielectric properties of plasma sprayed titanate ceramics have been published,[4,5,6] but there is a lack of research comparing plasma sprayed samples produced with different spray techniques. Such a study has got to be done with advantage employing CaTiO$_3$ because it is a material well known and widely used as a dielectric in a sintered state. Dielectric behaviour of CaTiO$_3$ is described in several comprehensive textbooks.[7,8] A small drop of permittivity with frequency is reported there based on one source of the experimental data but an increase above 10^5 Hz by another source.

Titanates, in general, form a wide ranging and important group of dielectric ceramics. CaTiO$_3$ is often used in complex ceramic systems where its content governs the temperature dependence of relative permittivity or resonant frequency.[9–15] Sintered CaTiO$_3$ is a high permittivity linear dielectric[16] and at the time a material whose suitability for plasma spray processing was already demonstrated by the authors.[17,18]

For the present set of experiments CaTiO$_3$ had been preferred compared to more complicated microstructures[17] of several 'ATiO$_3$–type' dielectrics. Perovskite (CaTiO$_3$) and its mixture with synthetic geikielite (MgTiO$_3$) were studied by the authors in the past.[17,18] First of all, they were examined from the point of view of their sprayability, chemical as well as phase composition, microstructure,[17] mechanical properties[17,18] and partly dielectric properties.[18] The results indicate that anomalous behaviour in dielectric response is introduced to the high permittivitty materials by plasma spray processing.[17–19] The hypothesis that water adsorbed within voids is responsible for dielectric behaviour of as sprayed ceramics was repudiated for a material such as CaTiO$_3$ whose permittivity is much higher than those of water.[17,20,21]

There exists a demand for linear dielectrics enabling to minimize a cross-coupling with conductors.[9] For example a non-stoichiometric composition of CaO–Li$_2$O–RE$_2$O$_3$–TiO$_2$ (RE is rare earth) was mentioned as a temperature stable dielectric material.[10] CaTiO$_3$ doped with Nd[11] was used mainly for this reason, whereas CaTiO$_3$ doped with Pr[12] offers also interesting optical properties. CaTiO$_3$ also can host on the Ca-site Er^{3+}, Tm^{3+} or Yb^{3+} ions to exhibit luminescence properties under 976 nm diode excitation.[13] Ferroelectric-like domains were observed in pure and also doped CaTiO$_3$.[11] Band-gap energy 3·67 eV at volume resistivity 5×10^8 Ω cm[14] was reported; elsewhere only 3·25 eV was the value of the band-gap and resistivity was not simultaneously mentioned.[15] For pristine CaTiO$_3$ the optical absorption edge was observed in the vicinity of a wavelength of 330 nm.[12]

[1]Department of Electrotechnology, Faculty of Electrical Engineering Czech Technical University, 166 27 Prague 6, Czech Republic
[2]Materials Engineering Department, Institute of Plasma, Physics Academy of Sciences of the Czech Republic, 182 21 Prague 8, Czech Republic

*Corresponding author, email ctibor@ipp.cas.cz

CaTiO₃ based materials are applied in the industry as capacitors, sensors, resonators, dielectric duplexers and band pass filters. This paper summarises plasma spraying of calcium titanate, its basic microstructural characterisation, detailed study of the relative permittivity and dielectric losses between 15 Hz and 5 MHz, and finally dependence of the volume resistivity on voltage between 1 and 100 V.

Experimental

Powder and its plasma spraying

CaTiO₃ was obtained in the form of tablets of industrial purity, produced by the conventional reactive sintering of calcium carbonate ($CaCO_3$) and titanium oxide (TiO_2) micropowders. CaTiO₃ powder was sintered without any additives, often used for decreasing the sintering temperature. Sintered tablets were subsequently crushed and sieved into a powder of the correct size for spraying, 63–125 μm.

One series of samples was produced using a high feedrate water stabilised plasma spray system WSP (WSP 500, IPP ASCR, Prague, Czech Republic).[17] This system operates at about 160 kW arc power and can process large amount of material per hour. In the current experiment powder feedrate between 22 and 24 kg h⁻¹ was used. Spray distance, i.e. the distance between the plasma nozzle and the substrate, was set before spraying to 350 mm and for other spray test to 450 mm. The reason lies in a different thermal history of particles corresponding to different spraying distances. Spray distance (SD) is one of the main variable parameters at the spraying process.

A conventional atmospheric plasma spray system equipped with a gas stabilised plasma gun F4,[22] was used for spraying of the other set of samples, labelled GSP. Spray parameters are summarised in the Table 1.

The substrates, $120 \times 25 \times 2·5$ mm, made of flat carbon steel as well as stainless steel, were grit blasted by alumina (0·4–0·7 mm in size) before spraying. Degreasing was done by acetone.

The feedstock powder had the same size for all spray tests. The deposited thickness was about 1·8 mm for WSP SD 350 mm, about 1·2 mm for WSP SD 450 mm, and about 0·5 mm for GSP. Thick (i.e. WSP) deposits were stripped from the substrates by thermal cycling between approximately +150 and −70°C.

Characterisation: specimen preparation

The surface of specimens was ground after spraying to eliminate roughness, which is an inherent property of plasma sprayed coatings. There exist two types of specimen. The first one is stripped-out from the substrate and ground from both sides to produce planparallel plates with a smooth surface. Such specimens are in principle monoblock capacitors with dimensions $10 \times 10 \times 1$ mm.

The second type is a coating on the metallic substrate. For this type only the topside was ground to build monoblock capacitors with dimensions $10 \times 10 \times (0·5$ mm plus 2·5 mm substrate). A thin layer of aluminium as the top electrode (at self-standing plates from both sides) was sputtered in a reduced pressure on the ground surface. A three-electrode measurement fixture was used to evaluate dielectric parameters of all samples. A working electrode was the top central circle separated by a gap (produced via surface masking) from the earth electrode covering whole the rest of the topside surface. The bottom side was covered completely with an Al layer serving as the second working electrode.

Characterisation: description of electric measurements

The electric field was applied along the spray direction (i.e. perpendicular to the substrate surface). Capacity was measured in the frequency range from 15 Hz to 5 MHz using a programmable Hioki 3522-50 LCR HiTester (for the range15 Hz –100 kHz) and Agilent 4285 (for the range 75 kHz–5 MHz). The frequency step was progressively increased and applied AC voltage kept constant (1 V). The stabilised electric source was equipped with a micrometric capacitor as recommended in the relevant standard.[23] Relative permittivity ε_r was calculated from measured capacities and specimen dimensions.[24]

These same LCR-meters were used for the loss factor measurement. Loss factor tg δ was measured at the same frequencies as capacity.

Electric DC resistance was measured with a special adapter to fulfill ASTM recommendations.[25] The electric field was applied by a regulated high voltage supply and the values read by a multipurpose electrometer (617, Keithley Instruments, USA). Applied voltage varied between 1 V and 100 V DC ($\pm 2\%$ of the nominal value). Volume resistivity was calculated from the measured resistance and specimen dimensions.[25] The mean values are average of 6–10 specimens (individual coated substrates) for each sample (i.e. WSP SD 350, WSP SD 450 and GSP). All electric measurements took place in air conditioned room with relative humidity of approximately 50% during the whole measurement. Before the measurements samples were kept on a heater plate for 15 min at 120°C to remove the moisture.

Characterisation of microstructure

Porosity was determined on light microscopy images of cross-sections via image analysis software Lucia G (Laboratory Imaging, Prague, Czech Republic). Images were taken from 10 randomly selected areas for each sample at $\times 250$ magnification. In addition to simple quantification of porosity, other factors of the coatings were also examined. Circularity of pores (planar 2D projections) is equal to zero for a line and to 1 for a circle. Plasma sprayed coating contains

Table 1 Plasma spray parameters

Parameter	WSP	GSP
Power/kW	154 (320 V, 480 A)	24 (48 V, 500 A)
Primary gas/slpm	…	Ar, 65
Secondary gas/slpm	…	H₂, 2·5
Powder feeding medium	air	Ar
Spray distance/mm	350; 450	100
Substrate material	Stainless steel	Carbon steel

Table 2 Porosity parameters

Sample	Porosity/%	Circularity	No. of pores per mm²
GSP	22·8	0·412	2556
WSP SD 350	11·7	0·422	1987
WSP SD 450	13·6	0·378	2033
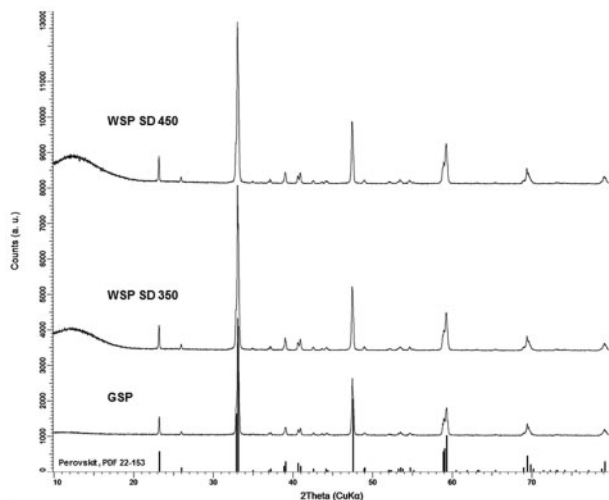
1 X-ray diffraction patterns of all three plasma sprayed deposits

typically pores flattened parallel with the surface as a result of the lamella (splat) formation.

X-ray diffraction analysis was carried out on all three samples after removal of approximately 100 μm thick surface layer. Filtered Cu K_α radiation and 1D multiple strip detector mounted in D8 Discover Bruker diffractometer was used for measuring diffraction patterns with 0·015°2θ step in the range from 10 to 80°2θ. The correct position of the sample surface respecting the Bragg-Brentano semifocusing was checked with laser beams. Beside the phase composition determination, the obtained diffraction patterns were used for calculation of microstrains and mean crystallite sizes in the irradiated volume employing Williamson–Hall plot. The observed diffraction profile is a convolution of instrumental function and the physical function of the sample; in order to get the profile corresponding purely to the physical function, the instrumental profile was approximated by measuring CaF$_2$ standard.

Results and discussion

Phase composition

Only perovskite phase (PDF card no. 22–153) was detected by XRD in the feedstock powder (pattern not given) as well as in all sprayed CaTiO$_3$ samples (Fig. 1). Diffraction patterns and positions of the diffraction maxima correspond to the sole crystallite phase,
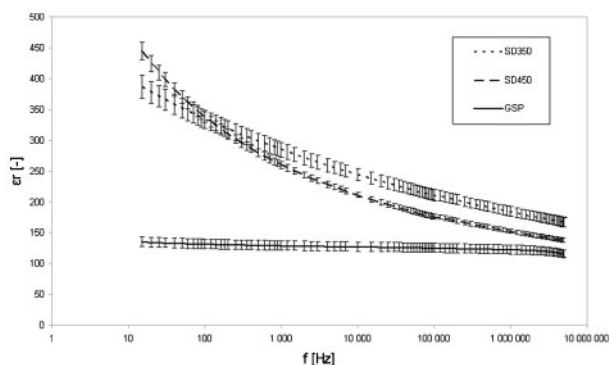
2 Relative permittivity of plasma sprayed deposits, standard deviation is indicated by vertical bars
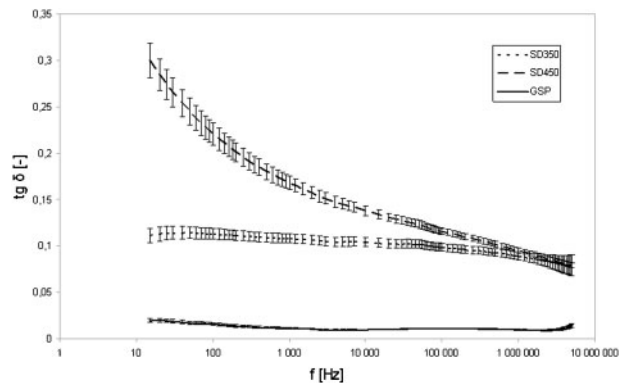
3 Loss factor of plasma sprayed deposits, standard deviation is indicated by vertical bars

orthorhombic CaTiO$_3$ or perovskite. Both WSP samples can be distinguished by a halo in the very low range of 2θ which gives evidence of amorphous phase/phases presence in the irradiated volume, as mentioned in Ref. 26. The diffraction patterns measured before the removal of 100 μm thick surface layer did not exhibit such feature. All three Williamson–Hall plots indicated no broadening due to size effects, i.e. they intersected the integral width axe in its origin. The microstrains calculated from the plots' slopes were 8·60, 8·18 and 8·57 × 10^{-4} for GSP, WSP SD 350 and WSP SD 450 respectively. Since the sizes of CaTiO$_3$ crystallites, or more precisely areas of coherent scattering, had no effect on the diffraction peaks broadening, it can be estimated that they are in the above-micrometre range.

In our previous papers on the topic of calcium titanate[17,18] we used an older XRD equipment and the amorphous fraction remained undetected. Presence of the amorphous phase has a dramatic influence on the dielectric behaviour of the material, as discussed below.

Permittivity and losses

Figure 2 shows that both WSP samples have very high relative permittivity at frequencies lower than 1 kHz. The permittivity is strongly frequency dependent and it does not drop below 130. The WSP sample with the spraying distance of 450 mm (SD450) starts with a relative permittivity of about 450 at 15 Hz and therefore its permittivity drop is stronger. However both WSP samples do not have the same value up to 5 MHz. Over 1 kHz relative permittivity is not strongly dependent on spraying distance and over 50 kHz it obtains approximately the same value as a sintered calcium titanate ($\sim$170),[7,8] but drops further. Also the polarisation does not disappear (relax) completely below 5 MHz. The GSP sample has lower relative permittivity, and also with much more stable values versus the tuned frequency. Over 1 MHz it however starts to drop. In the whole frequency range tested, the values of the GSP are lower than permittivity of a sintered calcium titanate. The dielectric permittivity of most dielectric materials is frequency dependent. In the presence of an alternating electric field, the dipole moments inside the material oscillate with the direction of the electric field.[27]

In the Fig. 3, the loss factor dependence on frequency for all calcium titanate coatings is given. The most significant is the high loss factor of the deposit from a long spraying distance SD 450 mm. Sample SD350 has lower and much less frequency dependent losses. At
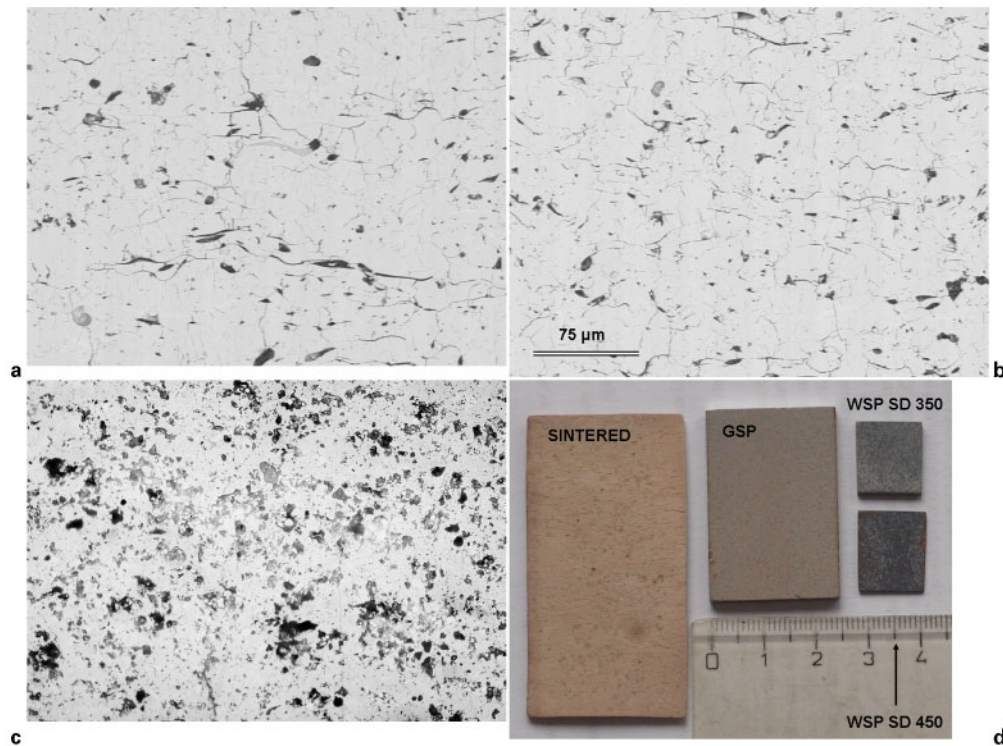
4 **Micrographs of cross-sections of coatings:** *a* **SD 350,** *b* **SD 450; both SEM-SE;** *c* **GSP coating; light microscopy (all micrographs in the same scale); and** *d* **macrophotography showing colours of various CaTiO₃ samples**

~2 MHz the value of both samples is the same, ~0·1. The GSP sample has rather frequency independent loss factor, which is moreover more than 10 times lower than for WSP SD 450 – only about 0·01. In combination with the permittivity character (drop) of the GSP sample we can predict that a relaxation frequency appears sure not far above 5 MHz. Sintered CaTiO₃ should have loss factor about 0·001 at room temperature.[7]

The amorphous phase manifests itself by a halo at very low angular positions of the diffraction patterns, 10 to 17°2θ, which correspond to large nearest neighbour distance as a criterion of certain short range order in amorphous material. We can consider presence of large dipoles in the structure of both WSP coatings. Such dipoles exhibit high permittivity as well as high losses at low frequency. The larger the dipoles, the lower the frequency when they stop to be able to follow a change of the field.[27] Also they must relax at higher frequency.

The color of WSP sprayed CaTiO₃ is significantly darker then the colour of the feedstock powder, sintered CaTiO₃ or also compare to the GSP coating, see Fig. 4*d*. This darkening is an indication of oxygen vacancies, similarly as in the case of plasma sprayed TiO₂.[28] Owing to large crystallites of our CaTiO₃, the loss of some oxygen atoms does not insert much difference in lattice strain among individual coatings and, hence only small lattice distortion is taking place.

At low frequency all type of polarisations are present, but space charge is the most prominent one. The values of dielectric constant and loss factor increase with increase in space charge polarisation. It may be due to a large concentration of defects. The low frequency dispersion in the loss curves of the WSP coatings may be an indication of presence of charge carriers arising from defects like oxygen vacancies caused by hydrogen present in the water stabilised plasma.[28] Any peak in the

loss curves is observed. This is probably due to dominance of weakly bound electronic or ionic charges capable of hopping over extended distances in the amorphous phase.

Volume resistivity

Volume DC resistivity was calculated from the measured resistance and specimen dimensions. Results are summarised in Fig. 5. WSP deposit SD450 exhibits volume resistivity lower by 2–3 orders compared to GSP sample and WSP SD350 sample. The SD450 sample, which, due to low resistivity, was the only one measurable already from 1 V, shows a drop of resistivity, when the voltage increases from 1 to 30 V. At higher voltage its drop is less strong. The WSP SD 350 sample also exhibits a resistance drop with increasing voltage. The GSP sample exhibits an opposite trend – the resistivity increases slightly with increasing voltage. Its values are markedly
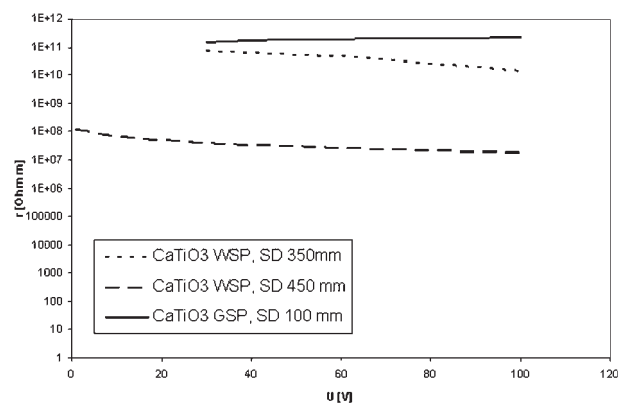
5 **Resistivity of plasma sprayed deposits in dependence on variable voltage**

higher than for WSP SD 450 and only slightly higher than for WSP SD 350.

Porosity and microstructure

Porosity is summarized in Table 2. The GSP coating has approximately two times larger porosity, but the number of pores per mm^2 is just 25% larger than for other specimen. In other words its pores must be the largest. Circularity of pores of this coating is between both WSP coatings. The coating WSP SD 350 has the lowest porosity with highest circularity, and also the lowest number of pores per mm^2. Also its dielectric properties are more intrinsic properties of CaTiO₃ compared to WSP SD450, which is more porous with higher quantity of pores that are in the same time flatter (less circular). According to the literature, CaTiO₃ ceramics are difficult to densify also by sintering techniques[29] and the porosity tends to be high. The permittivity of the GSP coating is lower than permittivity of a sintered calcium titanate because of large coating porosity.

The micrographs of cross-sections of all coatings are provided in the Fig. 4a–c. The WSP coatings contain networks of fine cracks and flat pores; few rounded pores are present as well. The GSP coating contains more pores, but only limited amount of cracks. The typical lamellar microstructure with individual splats is more pronounced in the case of WSP coatings.

Conclusion

It was observed in this paper that plasma sprayed calcium titanate exhibits a strong relaxation of permittivity when it is measured in a state of coating sprayed by a water stabilised plasma gun (WSP). When sprayed by the gas stabilised plasma gun (GSP), the behaviour is different, without any pronounced relaxation. The frequency dependence of permittivity and loss factor is influenced by the spraying parameters at WSP, but the relaxation character in general is always preserved. The volume resistivity of the WSP samples is voltage dependent, whereas in the case of GSP it is not. All these features are connected with amorphous fraction present in WSP coatings, as found by XRD. The dark WSP coatings contain oxygen deficient structures providing dipoles easily movable at low frequencies namely due to partly amorphous structure. Porosity, splat sizes and its boundary character can also play a minor role and are responsible mainly for the behaviour of GSP coating. Plasma spraying broadens the technological variability in the production of dielectric ceramics[1–4] giving the possibility to cover substrates of various shapes made from various materials.[30–32] At the same time the role of microstructure of coatings is important to control. A wide ranging field for further study is open to precise correspondences between the physical nature of plasma sprayed ceramic parts and their dielectric behaviour.

Acknowledgement

References

1. S. Sampath: 'Thermal spray applications in electronics and sensors: past, present, and future', *J. Thermal Spray Technol.*, 2010, **19**, (5), 921–949.
2. F.-L. Toma, S. Scheitz, R. Puschmann and L.-M. Berger: 'Development of ceramic heating elements produced by thermal spray technology', Proc. Intl. Thermal Spray Conf., Düsseldorf, Germany, 2011, DVS, 912–917.
3. P. Ctibor, R. Lechnerová and V. Beneš: 'Quantitative analysis of pores of two types in a plasma-sprayed coating', *Mater. Character.*, 2006, **56**, 297–304.
4. C. Friedrich, R. Gadow and A. Killinger: 'Thermally sprayed multilayer coatings as electrodes and dielectrics in high efficiency ozonizer tubes', Proc. United Thermal Spray Conf. '99, Düsseldorf, Germany, 1999, 676–682.
5. T. Jansing, R. Fleck, J. Decker and C. Verpoort: 'Separation and insulating layers of atmospheric plasma-sprayed ceramics for high temperature fuel cells - development and implementation', Proc. United Thermal Spray Conf. '99, Düsseldorf, Germany, 1999, 69–75
6. A. H. Dent, A. Patel, J. Gutleber, E. Tormey, S. Sampath and H. Herman: 'High velocity oxy-fuel and plasma deposition of BaTiO₃ and (Ba,Sr)TiO₃', *Mater. Sci. Eng. B*, 2001, **87B**, 23–30.
7. 'Gmelins handbook of inorganic chemistry', Vol. 41–42; 1951, Leipzig.
8. H. Landolt and R. Boernstein: 'Values and functions in physics, chemistry, astronomy, geophysics and technology', Vol. IV, Part 3; 1957, Berlin, Springer Verlag.
9. S. Parida, S. K. Rout, N. Gupta and V. R. Gupta: 'Solubility limits and microwave dielectric properties of Ca(Zr$_x$Ti$_{1-x}$)O₃ solid solution', *J. Alloys Compd*, 2013, **546**, 216–223.
10. X. Chen, S. Bai and W. Zhang: 'Low temperature sintering and microwave dielectric properties of Bi₄B₂O₉-added 0·25CaTiO₃–0·75(Li$_{1/2}$Nd$_{1/2}$)TiO₃ ceramics', *J. Alloys Compd.*, 2012, **541**, 132–136.
11. R. Lowndes, F. Azough, R. Cernik and R. Freer: 'Structures and microwave dielectric properties of Ca$_{(1-x)}$Nd$_{2x/3}$TiO₃ ceramics', *J. Eur. Ceram. Soc.*, 2012, **32**, 3791–3799.
12. Y. Inaguma, T. Tsuchiya, Y. Mori, Y. Imade, N. Sato, T. Katsumata and D. Mori: 'Temperature dependence of luminescence properties of praseodymium-doped perovskite CaTiO₃:Pr^{3+}', *Thermochimica Acta*, 2012, **532**, 168–171.
13. X. Chen, Y. Li, F. Kong, L. Li, Q. Sun and F. Wang: 'Red, green, blue and bright white upconversion luminescence of CaTiO₃: Er^{3+}/Tm^{3+}/Yb^{3+} nanocrystals', *J. Alloys Compd*, 2012, **541**, 505–509.
14. D. T. M. Huong, N. H. Nam, L. V. Vu and N. N. Long: 'Preparation and optical characterization of Eu^{3+}-doped CaTiO₃ perovskite powders', *J. Alloys Compd.*, 2012, **537**, 54–59.
15. K. C. Bhamu, A. Dashora, G. Arora and B. L. Ahuja: 'Nature of bonding in CaTiO₃ and SrTiO₃: a compton scattering study', *Rad. Phys. Chem.*, 2012, **81**, 728–734.
16. 'Structure and properties of ceramics', (ed. A. Koller), 496; 1994, Elsevier.
17. P. Ctibor and J. Sedlacek: 'Dielectric properties of plasma sprayed titanates', *J. Europ. Ceram. Soc.*, 2001, **21**, 1685–1688.
18. P. Ctibor, J. Sedlacek, K. Neufuss and P. Chraska: 'Dielectric relaxation in calcium titanate-containing ceramics prepared by plasma', *Ceram. Int.*, 2003, **29**, 955–960.
19. P. Ctibor and J. Sedlacek: in 'Advances in ceramics - characterization, raw materials, processing, properties, degradation and healing', (ed. C. Sikalidis), 19–38; 2011, Wien, InTech.
20. P. Ctibor, Z. Pala, H. Boldyryeva, J. Sedlacek and V. Kmetik: 'Microstructure and properties of plasma sprayed lead zirconate titanate (PZT) ceramics', *Coatings*, 2012, **2**, 64–75.
21. M. Sindhu, N. Ahlawat, S. Sanghi, A. Agarwal, R. Dahiya and N. Ahlawat: 'Rietveld refinement and impedance spectroscopy of calcium titanate', *Current Appl. Phys.*, 2012, **12**, 1429–1435.
22. R. Ahmadi-Pidani, R. Shoja-Razavi, R. Mozafarinia and H. Jamali: 'Laser surface modification of plasma sprayed CYSZ thermal barrier coatings', *Ceram. Intl.*, 2012, **38**, 6613–6620.
23. Czech Standard CSN IEC 250, Czech Institute for Standardization, Prague, 1997.
24. O. Morey, P. Goeuriot, D. Juve and D. Treheux: 'Dielectric investigations on 'MgAlON' compounds: role of nitrogen content', *J. Eur. Ceram. Soc.*, 2003, **23**, 345–355.
25. 'US Standard ASTM D 257–66: standard test methods for DC resistance or conductance of insulating materials', ASTM International, West Conshohocken, PA, 19428–2959.
26. E. F. Rejda, D. F. Socie and T. Itoh: 'Deformation behavior of plasma-sprayed thick thermal barrier coatings', *Surf. Coat. Technol.*, 1999, **113**, 218–226.

27. N. E. Hill: 'Dielectric properties and molecular behaviour'; 1969, London, Van Nostrand-Reinhold.
28. P. Ctibor, V. Stengl, I. Pis, T. Zahoranova and V. Nehasil: 'Plasma sprayed TiO_2: the influence of power of an electric supply on relations among stoichiometry, surface state and photocatalytic decomposition of acetone', *Ceram. Int.*, 2012, **38**, 3453–3458.
29. L. Taibi Benziada, A. Mezroua and R. Von Der Muhll: 'CaTiO₃ related materials for resonators', *Ceramics Silikaty*, 2004, **48**, 180–184.
30. V. Cannillo, F. Pierli, S. Sampath and C. Siligardi: 'Thermal and physical characterisation of apatite/wollastonite bioactive glass–ceramics', *J. Eur. Ceram. Soc.*, 2009, **29**, 611–619.
31. K. Bobzin, T. Schlaefer, M. Begard, M. Bruehl, G. Bolelli, L. Lusvarghi, D. Lisjak, A. Hujanen, P. Lintunen, U. Kanerva, T. Varis and M. Pasquale: 'Development of Ba-hexaferrite coatings for electromagnetic wave absorption applications', *Surf. Coat. Technol.*, 2010, **205**, 1015–1020.
32. T. Hejwowski: 'Comparative study of thermal barrier coatings for internal combustion engine', *Vacuum*, 2010, **85**, 610–616.

4.2 Improving dielectric properties of plasma sprayed calcium titanate (CaTiO$_3$) coatings by thermal annealing

This study is focused on effect of thermal post treatment of calcium titanate coatings on their dielectric properties. As-sprayed samples were annealed in air at atmospheric pressure for 2 hours at variety of temperatures ranging from 530 to 1 170 °C. In general, samples annealed at a higher temperatures exhibit better dielectric properties. Loss factor rapidly decreased and relative permittivity became more frequency stable with frequency tuning. Chemical composition was studies by the X-ray Photoelectron Spectroscopy. All details including microstructure and phase composition changes during annealing are given in detail in the paper.

Improving dielectric properties of plasma sprayed calcium titanate ($CaTiO_3$) coatings by thermal annealing

Jiri Kotlan[a,b,*], Pavel Ctibor[a,b], Zdenek Pala[b], Petr Homola[c], Vaclav Nehasil[c]

[a]Department of Electrotechnology, Faculty of Electrical Engineering, Czech Technical University in Prague, Technicka 2, Prague 6, Czech Republic
[b]Materials Engineering Department, Institute of Plasma Physics ASCR, v.v.i., Za Slovankou 3, Prague 8, Czech Republic
[c]Department of Surface and Plasma Science, Faculty of Mathematics and Physics, Charles University, V Holesovickach 2, Prague 8, Czech Republic

Abstract

Self-supported $CaTiO_3$ coatings prepared by plasma-spraying technology and effect of annealing on dielectric properties and microstructure of these coatings are studied in this work. A water stabilized plasma gun WSP (IPP ASCR, Prague) as well as a widely used conventional gas stabilized plasma gun GSP were employed. Prepared samples were annealed in air atmosphere up to 1170 °C. The work is focused on dielectric properties of these specimens. Relative permittivity and loss factor were measured in a frequency range of 30 Hz–30 MHz. Microstructure was studied using light microscopy, microhardness measurements, X-ray diffraction – including high-temperature XRD measurements, and X-ray photoelectron spectroscopy. The work studies the influence of annealing temperature on dielectric properties, crystalline structure and porosity of plasma deposited calcium titanate. Results obtained show significant improvement in $CaTiO_3$ coating properties after thermal annealing.
© 2014 Elsevier Ltd and Techna Group S.r.l. All rights reserved.

Keywords: A. X-ray methods; C. Dielectric properties; D. Perovskites; Plasma spraying

1. Introduction

Perovskite materials have received a lot of attention in recent decades for their technical importance and excellent properties in many areas [1,2]. Calcium titanate ($CaTiO_3$) is one of the alkaline earth titanates like barium titanate ($BaTiO_3$), magnesium titanium oxide ($MgTiO_3$) and strontium titanate ($SrTiO_3$). These titanates have recently attracted attention of many researchers because some titanates are used as ferroelectric, semi-conductive, photorefractive materials and catalysts [3]. Dielectrics based on calcium titanate are widely used in different fields of electronics applications [4–6]. For its high relative permittivity and low dielectric losses $CaTiO_3$ is recommended as a prospective ceramic material for microwave applications [7]. Dielectric ceramics are used for

production of a variety of components such as oscillators, filters and resonators for microwave systems.

Plasma spraying has become a widely accepted method for preparing coatings, self-supported parts in different industrial applications including electrical engineering. $BaTiO_3$ coatings were also successfully sprayed employing the HEPJet spraying system. The final coating was dense, with low porosity and high hardness. Results show that defects in $BaTiO_3$ coatings prepared by supersonic plasma spraying reduced the piezo-electric effect [8]. Dielectric properties of plasma sprayed $BaTiO_3$ were investigated as well [9]. High relative permittivity – but high loss factor – was observed. Calcium titanate ($CaTiO_3$) as a representative of the low-loss dielectric materials group was chosen as the material for this study. Selected properties of plasma sprayed calcium titanate were studied by authors in the past [10]. The results obtained were the basis for further research to improve the properties of plasma sprayed calcium titanate. Thermal properties of the plasma-sprayed $CaTiO_3$ and mixture of $MgTiO_3$–$CaTiO_3$ were studied with the

---

*Corresponding author. Tel.: +420 266 053717.
E-mail address: kotlan@ipp.cas.cz (J. Kotlan).

result that the thermal diffusivity of both materials decreases with increasing temperature [11]. Improving the dielectric properties, respective to the quality of the coatings, is the point of interest in this study.

2. Experimental details

2.1. Sample preparation

Industrial purity calcium titanate ($CaTiO_3$) tablets were used. Rietveld analysis of XRD patterns showed a 98.72% content of orthorhombic perovskite phase and 1.28% of rutile TiO_2. The tablets were produced by reactive sintering of calcium carbonate ($CaCO_3$) and titanium dioxide (TiO_2) micro-powders. The final powder, $CaTiO_3$ suitable for spraying (63–125 µm), was produced by mechanical crushing and sieving the sintered tablets.

Three sets of samples were produced in this experiment. Two of them were produced using a high feed-rate water-stabilized plasma spray system WSP (WSP 500, IPP ASCR, Prague, Czech Republic) [12]. The distance between the plasma nozzle and the substrate (Spray distance, SD), was set to 350 mm and 450 mm for another spray test. Samples were labeled WSP 350 and WSP 450. Spray distance is one of the main parameters in the spraying process. For short spraying distances the substrate could be overheated and coating thermally affected and in case of too long spraying distances the propelled particles become too cold to deposit correctly. The gas stabilized plasma gun (GSP) operates with a lower temperature and plasma enthalpy compared to the water stabilized plasma gun (WSP). Due to this fact spraying distance is shorter than for WSP. In the current experiment, powder feed-rate was between 22 and 24 kg/h. A conventionally used atmospheric plasma-spray system equipped with a gas-stabilized plasma gun F4 [13] was used for spraying the other set of samples labeled GSP 100. Spray parameters for both methods are summarized in Table 1.

All coatings were stripped from the substrates by thermal cycling between approximately $+150\ °C$ and $-70\ °C$.

All samples were annealed in air at atmospheric pressure for 2 h at a variety of temperatures ranging from 530 to 1170 °C in order to study changes in the structural and electrical properties according to the annealing temperature. Samples were annealed in a furnace together in the same heat cycle. A programmable furnace was employed for the experiment. A typical temperature step was performed at 80 °C with heating and cooling ramps set to 7 °C/min for all temperature ranges.

2.2. Characterization

Aluminum electrodes were sputtered in reduced pressure to surfaces of plan-parallel samples after grinding (sample dimensions of approximately $10 \times 10 \times 1.5$ mm). Capacity was measured in a frequency range from 30 Hz to 30 MHz. For low frequency measurements (10 Hz–100 kHz) a Hioki 3522-50 LCR HiTester was used. The device was set to four times the average of all values. Agilent 4285 with a sample fixture Agilent 16451B employs frequency range measurements from 75 kHz to 30 MHz. The frequency step was progressively increased and applied AC voltage of 1 V kept constant in both devices. A three electrode measuring system was employed. The electric field was applied along the spray direction (i.e., perpendicular to the substrate surface). Relative permittivity ε_r was calculated from measured capacities and specimen dimensions. The same LCR-meters were, at the same moment, used for the loss factor measurement. Loss factor $tg\delta$ was measured for the same frequencies as capacity.

All annealed samples were analyzed by X-ray diffraction. Measurements were done on a D8 Discover Bruker diffractometer using filtered $CuK\alpha$ radiation and 1D LynxEye detector. A high-temperature XRD in-situ experiment was employed in a selected non-annealed sample as well.

Porosity was studied in light microscopy cross-section images taken from 10 randomly selected areas at a magnification of 250 times for each sample. Evaluation was done by the image analysis software Lucia G (Laboratory Imaging, Prague, Czech Republic).

Precise microhardness tester Nexus 4504 (Innovatest, the Netherlands) equipped with a Vickers indenter was used for the evaluation of microhardness. Measuring on polished cross sections applying a 3 kg load and dwell time of 10 s was performed. Mean value of microhardness was calculated from 11 indentations and standard deviation of measured values was calculated as well.

The X-ray photoelectron spectroscopy (XPS) was measured on coatings and compared with the feedstock powder. Experiments were carried out in an ultra-high vacuum chamber with a base pressure lower than 5×10^{-7} Pa. XPS experiments were performed using an Omicron EA 125 multichannel hemispherical analyzer with the Al Kα line (1486.6 eV) as a primary photon source. Where an XPS-based percentage of an element in a compound is expressed in this paper, the meaning is how much from the atomic concentration of the element in the sample belongs to the compound.

3. Results and discussion

Dependence of relative permittivity of annealed WSP 350 samples in a frequency range from 30 Hz to 30 MHz is given in the Fig. 1. In general, it drops with growing frequency, as it is usual for titanates [14]. Permittivity increases and becomes more stable with the increase of the annealing temperature.

Table 1
Plasma spray parameters.

Parameter	WSP	GSP
Power [kW]	154	24
Primary gas [slpm]	–	Ar; 65
Secondary gas [slpm]	–	H_2; 2.5
Powder feeding medium	Air	Ar
Spray distance [mm]	350; 450	100
Substrate (steel)	Stainless	Carbon

Fig. 1. Frequency dependence of relative permittivity for annealed WSP 350.
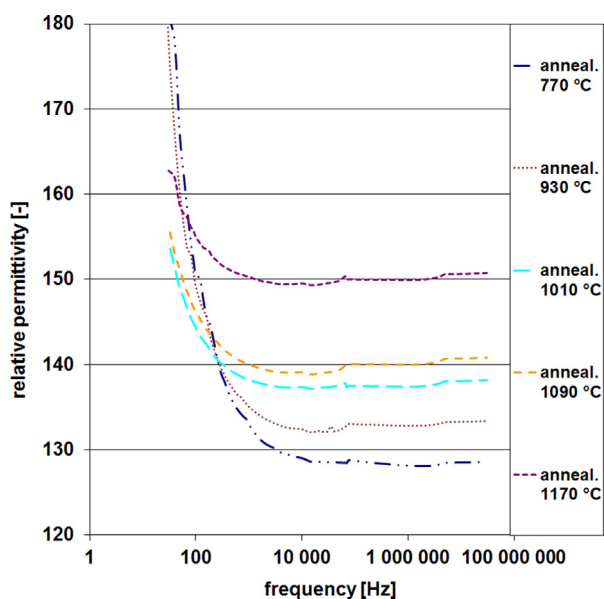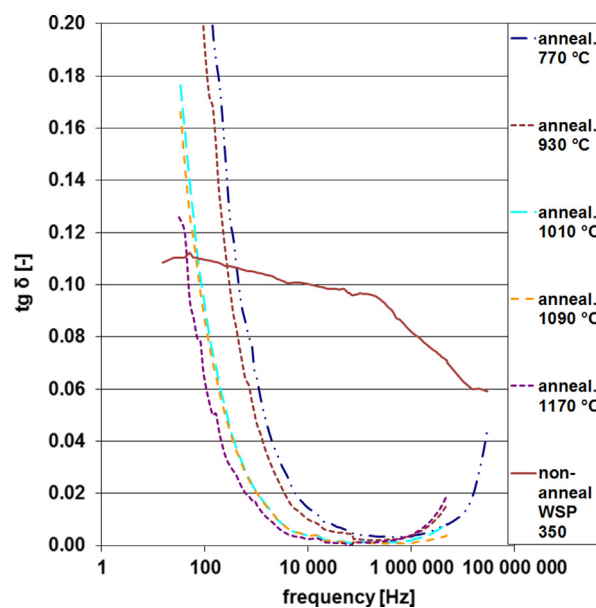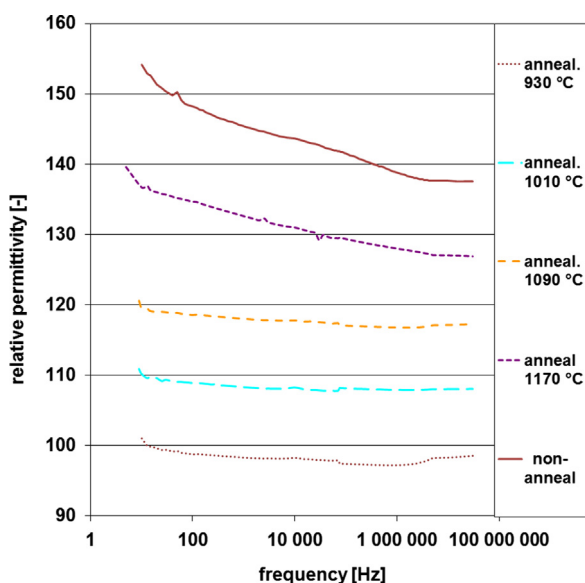

Fig. 2. Frequency dependence of relative permittivity for GSP 100.

Fig. 3. Frequency dependence of dielectric loss factor (tan δ) for WSP 350.
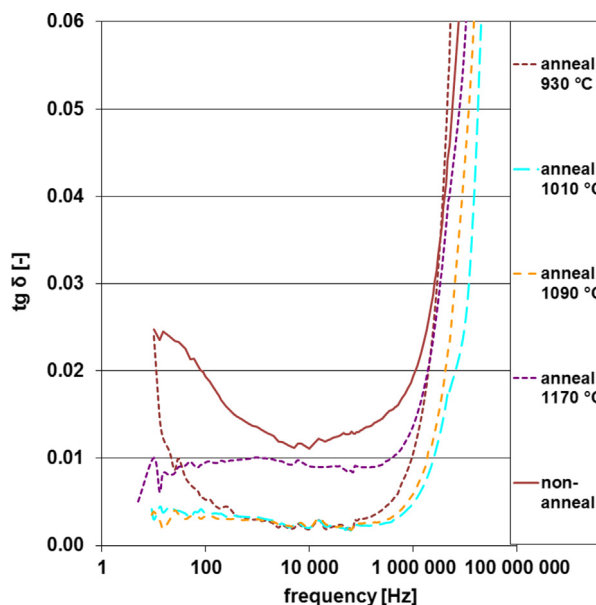

Fig. 4. Frequency dependence of dielectric loss factor (tan δ) for GSP 100.

The same character of dependence was observed for WSP 450 samples. The maximum value of the plateau on the relative permittivity curve was shifted slightly down to 140 for the WSP 450 sample annealed at 1170 °C. Non-annealed samples prepared by water stabilized plasma gun WSP 350 and WSP 450 exhibited significantly higher permittivities. For 10 kHz the value for a non-annealed sample WSP 350 was 240 and for 100 Hz permittivity about 330 [10]. The same influence of thermal annealing on relative permittivity was observed (Fig. 2) for GSP 100 samples. The character of the permittivity was more stable with tuned frequency over the whole frequency range than for samples prepared by the WSP device, but, in general, permittivity also increased with the annealing temperature. The frequency dependence was not very strong. An almost linear change of relative permittivity

with the annealing temperature was observed at GSP 100 samples.

Frequency dependence of dielectric loss factor *tg δ* for WSP 350 is shown in Fig. 3. Samples annealed at a lower temperature had higher losses. The sample WSP 350, annealed at 1170 °C, had the best dielectric properties; for 500 kHz the loss factor is below 0.003.

The non-annealed sample had a much higher loss factor; the observed value was about 0.09. Thermal annealing reduced the loss factor dramatically. In other words, it greatly improved the quality of the dielectric, because the loss factor represents power losses in a capacitor. A similar character was observed for the WSP 450 set of samples. Samples produced by the gas

stabilized plasma spray system had better dielectric properties in a non-annealed state than non-annealed WSP samples [10]. The loss factor was below 0.017 at 500 kHz. Annealed samples had a lower loss factor, but the sample annealed at the highest temperature of 1170 °C had a higher loss factor (0.01 at 500 kHz) than the other annealed samples. This phenomenon was not consistent with other curves. The sample annealed at 1090 °C had a loss factor below 0.004 at a frequency of 500 kHz.

All characteristics of GSP 100 samples are shown in the Fig. 4. Relative permittivity of plasma sprayed $CaTiO_3$ decreased after thermal annealing, but the loss factor decreased as well.

Selected annealed samples were analyzed by X-ray diffraction to determine whether any changes occurred in phase composition, crystallinity or peak broadening. The obtained diffraction patterns for selected annealed samples (Fig. 5) are characteristic for purely crystalline materials, i.e. the so called "amorphous halo" is not observed as it was in case of both non-annealed WSP samples [10]. Only one phase, orthorhombic perovskite (PDF card no. 22-153), was present in the irradiated volume. Furthermore, diffraction profile analysis carried out within the frame of the Rietveld method in TOPAS 4.2 software revealed no differences either in preferred orientation, grain size or microstrain.

Besides the XRD measurement of annealed samples, one non-annealed WSP 350 sample was subjected to a high-temperature XRD in-situ experiment. The starting material was converted into powder and placed on a platinum heating filament in the high-temperature chamber TC-BASIC by MRI. In-situ thermal experiments were performed in two phases. Firstly, the temperature range from 300 °C to 550 °C was increased by 10 °C increments with a heating rate of 10 °C/min and the dwell time for temperature stabilization was set to 20 min. In the second test, the temperatures of annealing were replicated, therefore, the $CaTiO_3$ powder was measured at 590, 600, 610, 680, 780, 850, 930, 1010 and 1090 °C with the same heating rate and dwell time as in the first test.

Since the diffraction patterns obtained in the first test revealed merely the expected 2θ shift to lower angles with increasing temperatures, only the second phase diffraction patterns were processed by Rietveld refinement. Starting with

the temperature of 1010 °C, the structural model of orthorhombic $CaTiO_3$ (Pbnm space group) is not valid, and tetragonal $CaTiO_3$ (I4/mcm space group) was more suitable.

This fact can also be seen in Figs. 6 and 7 as the temperature evolution of diffraction profiles of 200, 121, and 002 planes of orthorhombic lattice transitions into 020 of tetragonal lattice and, likewise, 321, 240, 042, 123 into 024. Moreover, several of the orthorhombic phase diffraction profiles vanished completely such as 111, 311 and 113, for example.

Thermal annealing affected microstructure of the coatings significantly. Results of porosity measurements are shown in Table 2. Character of porosity for WSP 350 was changed considerably as can be seen in Fig. 8. Long wide cracks between splats shrank and divided into several smaller ones. Some of the smaller pores are closed after annealing. The microstructure became finer with smaller amount of pores but the number and volume of bigger circular pores, which are presented in as-sprayed state, increased slightly. This results in a higher total circularity of pores of about 15%. Circularity (CIR) of pores (planar 2D projections) is equal to zero for a line and 1 for a circle. This parameter is slightly higher for GSP 100 samples. These two main effects are the cause of
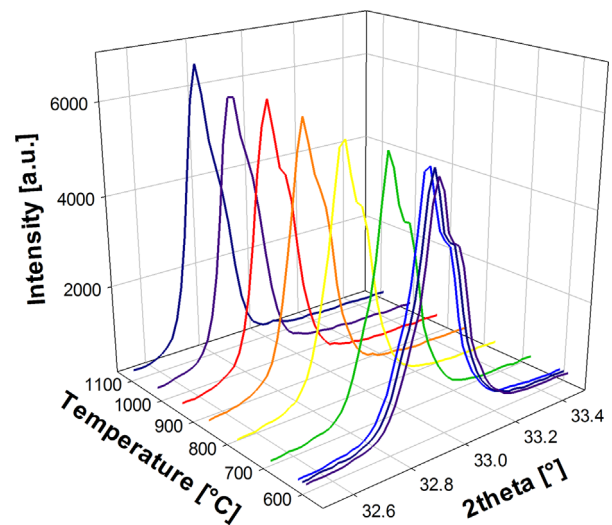

Fig. 6. X-ray diffraction profile of 200, 121, and 002 planes of orthorhombic $CaTiO_3$ (WSP 350) transitioning into 020 planes of tetragonal $CaTiO_3$.
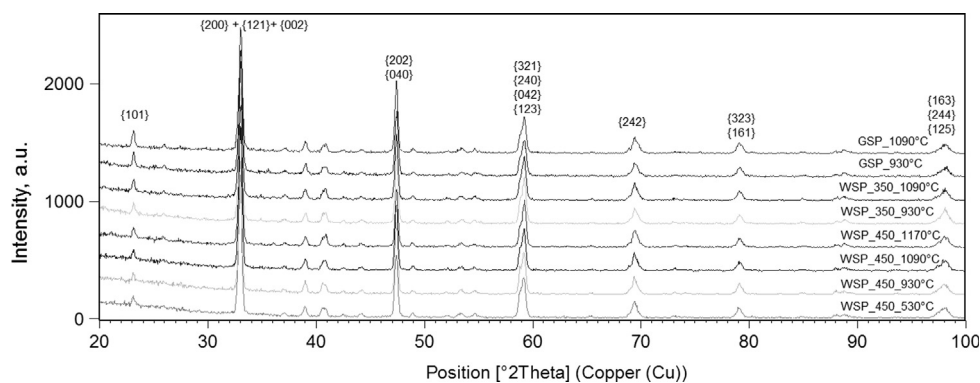

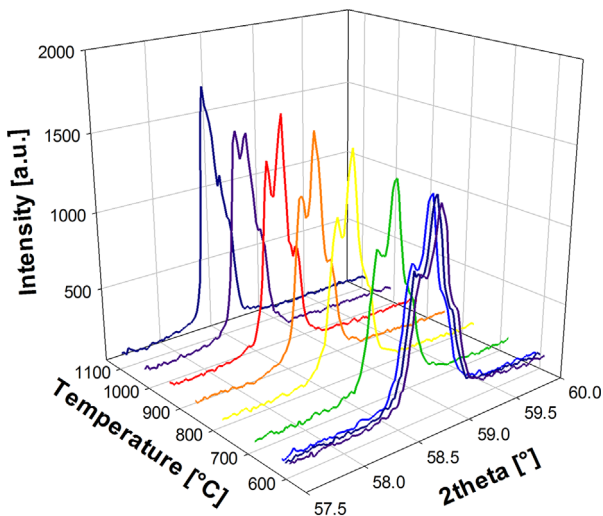Fig. 5. X-ray diffraction patterns of all non-annealed samples.

Fig. 7. X-ray diffraction profile of 321, 240, 042, and 123 planes of orthorhombic $CaTiO_3$ (WSP 350) transitioning into 024 planes of tetragonal $CaTiO_3$.

Table 2
Results of the porosity and microhardness measurements of selected samples.

Sample	$T_{anneal.}$ [°C]	Porosity [%]	N. Por. [mm^{-2}]	CIR [–]	HV3 [–]
WSP 350	–	11.7	1987	0.422	323 ± 24
	930	14.2	912	0.492	452 ± 66
	1090	14.0	1155	0.436	481 ± 39
WSP 450	–	13.6	2033	0.378	276 ± 24
	530	12.0	1275	0.430	374 ± 32
	930	13.9	965	0.471	372 ± 64
	1090	18.0	1378	0.401	408 ± 58
	1170	16.9	1196	0.422	506 ± 51
GSP 100	–	22.8	2556	0.412	240 ± 29
	930	19.4	1832	0.499	216 ± 37
	1090	25.3	2202	0.525	220 ± 45

slightly increasing total porosity but the total number of pores was reduced. Increasing of circularity and decreasing of the total number of pores after annealing were observed for all three types of coatings. In general, porosity increases with increased annealing temperature. The observed trend for total porosity of GSP samples is not too significant taking into account the uncertainty of the porosity measurements. WSP 450 samples exhibit thermal coagulation of pores in the interval between 1090–1170 °C. GSP 100 samples have the highest porosity with the highest number of pores. Samples prepared by the WSP system have a similar porosity and number of pores (N. Por.) as well. Only pores bigger than 3 µm in diameter were taken into account in porosity measurements.

Microhardness (Table 2) of WSP samples increased with increasing annealing temperature. Both WSP samples annealed at 1090 °C had the hardness value of about 50% higher compared to the as-sprayed state. That could be caused by decreasing the total number of pores and reduction of cracks during sintering. There were no significant trends for GSP

samples. Possible explanation of this fact may be the higher initial porosity of GSP compared to WSP and not the strong effect of thermal annealing to porosity of the coatings.

Initial high porosity of GSP samples was influenced by the fact that the coating was sprayed using rather coarse powder for this technique.

Chemical composition of all the three types of samples was analyzed by X-ray Photoelectron Spectroscopy. The samples were analyzed as-sprayed as well as after annealing. Spectra of Ca 2p doublet for $CaTiO_3$ powder are given in Fig. 9. Obtained spectra can be fitted to two components. The first one corresponds to calcium titanate at Ca $2p_{5/2}$ binding energy 346.4 eV and the second one represents calcium carbonate at Ca $2p_{5/2}$ binding energy 347.5 eV. In other words, the presence of calcium carbonate in $CaTiO_3$ powder was detected. Determined composition of the sample WSP 450 annealed at 610, 770 and 1010 °C are presented in Fig. 10. When we compare the as-sprayed material with the annealed one, we can detect a clear decrease of $CaCO_3$ after annealing and an increase of $CaTiO_3$. The results obtained from XPS measurements have not shown a clear tendency in development of chemical composition with the annealing temperature. The amount of calcium carbonate $CaCO_3$ obtained from the Ca 2p doublet is about 40% after $CaTiO_3$ deposition and it seems to decrease a little after heating. But the observed change is in a range of fitting errors (see Fig. 10). That is why we suppose that the concentration of $CaCO_3$ does not depend on the annealing temperature or that this dependence is negligible. Average amount of $CaCO_3$ obtained from the Ca 2p doublet is approximately 31% in the set of WSP 450 samples (amounts of $CaCO_3$ in WSP 350 and GSP samples are 34% and 31%, respectively).

The interpretation becomes more complicated if we compare the results obtained from Ca 2p and Ti 2p spectra. The concentration of $CaTiO_3$, which is the second component recognized in Ca 2p spectra and which is estimated from them, is constant or slowly increasing with temperature. On the other hand, we can see the temperature decrease of concentration of this species estimated using the fitted Ti 2p spectra. But the Ti spectra are much more complicated and their fits exhibit a higher error. That is why we find the values determined from Ca 2p spectra more valid. In every case, the concentration of $CaTiO_3$ estimated from the spectra, Ca 2p as well as Ti 2p, reaches the value close to 70%. It means that with respect to all possible errors we can conclude that it is a dominant component in our material as received as well as after annealing.

By annealing the loss factor diminished more than ten times in the frequency range 10 kHz to 1 MHz. This is a substantial improvement. Relative permittivity decreased at the same time by 20–50%. Relative permittivity becomes frequency independent above 10 kHz. High relative permittivity of the as-sprayed samples was too frequency-dependent. This is associated with slow polarization phenomena which disappeared after annealing. Amorphous component, which was observed in the as-sprayed state, affects the mobility of ions in the structure. At very low frequencies this will play an important role.
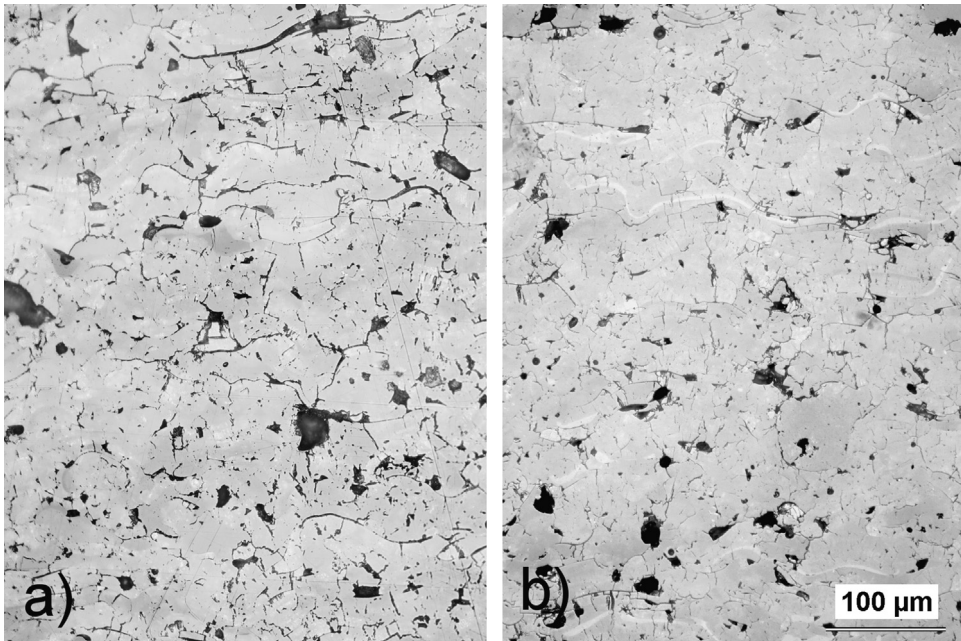
Fig. 8. Optical micrograph of polished cross-sections of the coating samples (a) as-sprayed WSP 350 and (b) WSP 350 annealed at 930 °C.
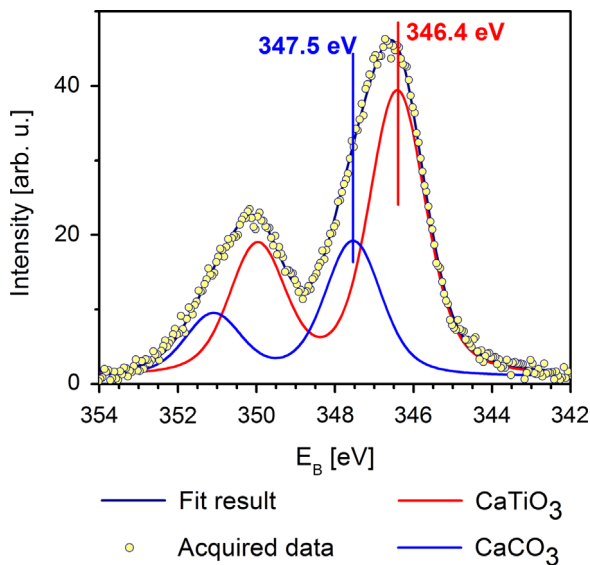

Fig. 9. XPS spectra of $CaTiO_3$ powder, Ca 2p doublet.

Fig. 10. Dependence of area contributions of $CaTiO_3$ and $CaCO_3$ species in Ca 2p and Ti 2p doublets on annealing temperature.

Besides microstructural aspects which are listed in our results the electrical character of the grain boundaries also was most probably affected by annealing. The $CaCO_3$ component of the Ca peak at XPS decreased and the $CaTiO_3$ component increased comparing the annealed state with the as-sprayed one. On the other hand, the TiO_2 component of the Ti peak at XPS increased at the expense of the $CaTiO_3$ component if the annealed state is compared with the as-sprayed one. Ca in the structure of any as-sprayed coating is highly reactive to the CaO form with atmospheric oxygen. At about 600 °C a relative shrinkage of about 2% [15] occurred in $CaCO_3$. This helps to relax the internal stress existing in thermal sprayed coatings. For GSP, this was annealed together with the

substrate. This effect is rather suppressed and the change of dielectric parameters with annealing is therefore rather mild. For WSP coatings annealed without substrates it is more pronounced.

4. Conclusions

This paper studies material properties and characterization of plasma sprayed calcium titanate. The influence of thermal annealing on dielectric properties was also examined. Samples annealed at a higher temperature exhibit better dielectric properties. The loss factor rapidly decreased and relative permittivity increased and became more stable with frequency tuning. Samples prepared using a gas stabilized plasma gun had less frequency dependent dielectric properties compared to samples prepared by the water stabilized plasma gun.

All annealed samples exhibited presence of pure crystalline orthorhombic perovskite phase only. Changes in the porosity and microhardness were caused by the typical character of porosity for plasma sprayed coatings. The results obtained show the possibility of achieving good dielectric materials by plasma spraying techniques. This material will be advantageous for sensors on curved surfaces and capacitors. For industrial use authors could suggest using the GSP technology applied with finer powder. The spraying followed by annealing to more than $600\,^\circ\text{C}$ would then lead to $CaTiO_3$ with a rather high structural stability and probably the best dielectric properties.

Acknowledgments

References

[1] M.A. Peña, J.L.G. Fierro, Chemical structures and performance of perovskite oxides, Chem. Rev. 101 (2001) 1981–2018.

[2] W. Janosik, C. Randall, M. Lanagan, Thermodynamic and electrical effects of residual carbon in glass barium titanate composites for MLCC applications, J. Am. Ceram. Soc. 90 (2007) 2415–2419.

[3] F. Zhao, Z. Yue, J. Pei, H. Zhuang, Z. Gui, L. Li, Structure and microwave dielectric properties of hexagonal $Ba[Ti_{1-x}(Ni_{1/2}W_{1/2})_x]O_3$ ceramics, J. Am. Ceram. Soc. 90 (2007) 2461–2466.

[4] E.E.C. Oliveira, A.G. D'Assunção, J.B.L. Oliveira, A.M. Cabral, Small size dual-band rectangular dielectric resonator antenna based on calcium titanate ($CaTiO_3$), Microw. Opt. Technol. Lett. 54 (4) (2012) 976–979.

[5] A. Krause, W. Weber, A. Jahn, K. Richter, D. Pohl, B. Rellinghaus, U. Schröder, J. Heitmann, T. Mikolajick, Evaluation of the electrical and physical properties of thin calcium titanate high-k insulators for capacitor applications, J. Vac. Sci. Technol. B 29 (1) (2011) 01AC07–05A.

[6] Ch.L. Huang, S.H. Lin, Y.B. Chen, New dielectric material system of Nd $(Mg_{1/2}Ti_{1/2})O_3$–$CaTiO_3$ with V_2O_5 addition for microwave applications, J. Alloys Compd. 489 (2) (2010) 719–721.

[7] R.C. Kell, A.C. Greenham, G.C.E. Olds, High-permittivity temperature-stable ceramic dielectrics with low microwave loss, J. Am. Ceram. Soc. 56 (7) (1973) 352–354.

[8] Z. Xing, H. Wang, L. Zhu, X. Zhou, Y. Huang, Properties of the $BaTiO_3$ coating prepared by supersonic plasma spraying, J. Alloys Compd. 582 (2014) 246–252.

[9] P. Ctibor, H. Seiner, J. Sedlacek, Z. Pala, P. Vanek, Phase stabilization in plasma sprayed $BaTiO_3$, Ceram. Int. 39 (2013) 5039–5048.

[10] J. Sedlacek, P. Ctibor, J. Kotlan, Z. Pala, Dielectric properties of $CaTiO_3$ coatings prepared by plasma spraying, Surf. Eng. 29 (5) (2013) 384–389.

[11] K. Neufuss, A. Rudajevova, Thermal properties of the plasma-sprayed $MgTiO_3$–$CaTiO_3$ and $CaTiO_3$, Ceram. Int. 28 (2002) 93–97.

[12] P. Ctibor, J. Sedlacek, Dielectric properties of plasma sprayed titanates, J. Eur. Ceram. Soc. 21 (10–11) (2001) 1685–1688.

[13] R. Ahmadi-Pidani, R. Shoja-Razavi, R. Mozafarinia, H. Jamali, Laser surface modification of plasma sprayed CYSZ thermal barrier coatings, Ceram. Int. 39 (3) (2012) 2473–2480.

[14] T.S. Kumar, R.K. Bhuyan, D. Pamu, Effect of post annealing on structural, optical and dielectric properties of $MgTiO_3$ thin films deposited by RF magnetron sputtering, Appl. Surf. Sci. 264 (2013) 184–190.

[15] I.R. Evans, J.A.K. Howard, T. Sreckovic, M.M. Ristic, Variable temperature in situ X-ray diffraction study of mechanically activated synthesis of calcium titanate, CaTiO3, Mater. Res. Bull. 38 (2003) 1203–1213.

4.3 Calcium titanate (CaTiO$_3$) dielectrics prepared by plasma spray and post-deposition thermal treatment

Research described in this paper follows previous two papers. Knowledge of the effect of thermal annealing on dielectric properties of plasma sprayed calcium titanate were enhanced by using Raman spectroscopy, band-gap energy measurements and AC conductivity measurements. The final conclusion origins from these three consecutive papers is that plasma plasma spraying and consequent thermal annealing may serve as a production method for high quality dielectric layers or even free standing parts. These parts can be easily manufactured by high throughput WSP plasma torch.

Calcium titanate (CaTiO₃) dielectrics prepared by plasma spray and post-deposition thermal treatment

Pavel Ctibor[a], Jiri Kotlan[a,b,*], Zdenek Pala[a], Josef Sedlacek[b], Zuzana Hajkova[c], Tomas Matys Grygar[c]

[a] Materials Engineering Department, Institute of Plasma Physics ASCR, v.v.i., Za Slovankou 3, Prague 8, Czech Republic
[b] Department of Electrotechnology, Faculty of Electrical Engineering, Czech Technical University in Prague, Technicka 2, Prague 6, Czech Republic
[c] Institute of Inorganic Chemistry ASCR, v.v.i., Husinec-Rez 1001, Rez, Czech Republic

ABSTRACT

This paper studies calcium titanate (CaTiO₃) dielectrics prepared by plasma spray technology. A water stabilized plasma gun (WSP) as well as a widely used gas stabilized plasma gun (GSP) were employed in this study to deposit three sample sets at different spray conditions. Prepared specimens were annealed in air at atmospheric pressure for 2 h at various temperatures from 530 to 1170 °C. X-ray diffraction (XRD), Raman spectroscopy and porosity measurements were used for sample characterization. Dielectric spectroscopy was applied to obtain relative permittivity, conductivity and loss factor frequency dependence. Band gap energy was estimated from reflectance measurements. The work is focused on the explanation of changes in microstructure and properties of a plasma sprayed deposit after thermal annealing. Obtained results show significant improvement of dielectric properties after thermal annealing.

© 2015 Elsevier Ltd. All rights reserved.

1. Introduction

Materials with perovskite structure have received a lot of attention in recent years not only for their possible application in solid oxide fuel cells [1,2] but for their technical importance and excellent properties in a number of areas [3,4]. Calcium titanate (CaTiO₃) is one alkaline earth titanate like barium titanate (BaTiO₃), magnesium titanium oxide (MgTiO₃) and strontium titanate (SrTiO₃). These titanates have recently attracted attention because some titanates are used as semi-conductive, ferroelectric and photorefractive materials. Dielectrics based on calcium titanate are widely used in different fields of electronics applications [5–7]. For its high relative permittivity and low dielectric losses CaTiO₃ is recommended as a prospective ceramic material for high frequency electronics applications. Dielectric ceramics are used for production of a variety of components such as capacitors, oscillators, filters and resonators for microwave systems.

Plasma spray has become a widely accepted method for preparing coatings with different properties especially thermal barrier coatings which are widely used in the aerospace and power industries. However, coatings or self-supported parts have a variety of other industrial applications including those in electrical engineering. BaTiO₃ coatings were successfully sprayed employing the HEPJet spray system. Final coating microstructures were dense, with low porosity and high hardness. Results show that defects in BaTiO₃ coatings prepared by supersonic plasma spray reduce the piezoelectric effect [8]. Dielectric properties of plasma sprayed BaTiO₃ were investigated as well [9]. High relative permittivity and high loss factor were observed. For this study calcium titanate (CaTiO₃), with a tabulated relative permittivity value of 160–170 was chosen to be representative of the low-loss dielectric materials group. Previous studies on properties of plasma sprayed calcium titanate have been completed [10]. Thermal properties of plasma sprayed CaTiO₃ and mixtures of MgTiO₃–CaTiO₃ were studied with results indicating that the thermal diffusivity of both materials decrease with increasing temperature [11]. Thermal post treatment plays an important role in modification of materials properties. This work is focused on explanation of changes in microstructure and properties of plasma sprayed deposits after thermal annealing using several analytical methods described below.

* Corresponding author at: Institute of Plasma Physics AS CR, v.v.i. Materials Engineering Department, Za Slovankou 1782/3, Prague 18200, Czech Republic.
E-mail address: kotlan@ipp.cas.cz (J. Kotlan).

2. Experimental

2.1. Sample preparation

Industrial purity calcium titanate ($CaTiO_3$) sintered tablets were used. Rietveld analysis of XRD patterns showed a 98.72% content of orthorhombic perovskite phase and 1.28% of rutile TiO_2. Tablets were produced by reactive sintering of calcium carbonate ($CaCO_3$) and titanium dioxide (TiO_2) micro-powders. The final $CaTiO_3$ powder was produced by mechanical crushing and sieving of the sintered tablets to ensure a particle size suitable for spraying (63–125 μm).

Three sample sets were deposited for study in this experiment. Two were produced using a high feed rate water stabilized plasma spray system WSP (WSP 500, IPP ASCR, Prague, Czech Republic) [12]. The distance between the plasma nozzle and substrate, or spray distance (SD), was set to 350 mm and 450 mm for each spray run. Samples were labeled WSP 350 and WSP 450. Spray distance is one of the main parameters in the spray process. At short spray distances the substrate can overheat and affect the coating. In the case of long spray distances, the propelled particles experience cooling and this affects coating deposition. The gas stabilized plasma gun (GSP) operates at a lower temperature and plasma enthalpy compared to the water stabilized plasma gun (WSP). Due to this fact, spray distance is shorter than for WSP. In the current experiment, powder feed-rate was between 22 and 24 kg/h for WSP deposition. A conventionally used atmospheric plasma spray (APS) system equipped with a gas-stabilized plasma gun, F4 [13], was used for spraying the third set of samples. This sample set was sprayed at a standoff of 100 mm and labeled GSP 100. Powder feed-rate was between 2 and 4 kg/h for GSP 100 samples. Substrate was preheated to 150 °C before spraying for all deposits. Spray parameters for both methods are summarized in Table 1.

Coatings were stripped from the substrates by thermal cycling between approximately +150 °C and −70 °C. All samples were annealed in air at atmospheric pressure for 2 h at various temperatures ranging from 530 to 1170 °C to study the induced effects of variable annealing temperatures. The temperature range was chosen with respect to aim of this work, to study annealing effect below $CaTiO_3$ sintering temperature, approximately 1200–1300 °C [12]. Annealing time was selected according to the previous results concerning annealing effect on plasma sprayed deposits [14,15]. A programmable furnace was employed for the experiment and three samples, one from each spray run, were simultaneously annealed during each heat cycle. A typical temperature step was 80 °C with heating and cooling ramps of 7 °C/min for all temperature ranges.

2.2. Characterization

After grinding, in a reduced pressure environment aluminum electrodes were sputtered to surfaces of plan-parallel samples (sample dimensions of approximately $10 \times 10 \times 1.5$ mm). Capacity was measured in a frequency range of 30 Hz–30 MHz. For low frequency measurements (30 Hz–100 kHz) a Hioki 3522-50 LCR HiTester was used. The device was set to take the average of four capacity values. Agilent 4285 with a sample fixture Agilent 16451B employs frequency range measurements from 75 kHz to 30 MHz. The frequency step was progressively increased and an applied AC voltage of 1 V was kept constant in both devices. A three electrode measuring system was utilized because this system improves measurement accuracy due to minimizing of the surface currents effect. The electric field was applied along the spray direction (i.e., perpendicular to the substrate surface). Relative permittivity, ε_r, was calculated from measured capacities and specimen dimensions. Simultaneously LCR-meters were used for loss factor measurements. Loss factor, $tg\ \delta$, was measured for the same frequencies as capacity and electrical conductivity was calculated from measured values.

All annealed samples were analyzed by X-ray diffraction. Measurements were performed on a D8 Discover Bruker diffractometer using filtered CuKα radiation and a 1D LynxEye detector. Diffraction profiles were analyzed within the frame of the Rietveld method in TOPAS 4.2 software.

Diffuse reflectance was measured by UV–vis–NIR scanning spectrophotometer (Shimadzu, Japan) with a multi-purpose large sample compartment and corresponding band gap energy was estimated. The reflectance curves obtained between 200 and 2000 nm were converted to absorbance and recalculated [16] to band gap energy, E_{bg}.

Microstructure of $CaTiO_3$ powder was observed using EVO MA 15 scanning electron microscope (Carl Zeiss SMT, Germany). Porosity was studied on polished cross-sections by light microscopy. Ten images of each sample were taken from randomly selected areas at a magnification of 250 times. Evaluation of porosity parameters was completed using image analysis software Lucia G (Laboratory Imaging, Prague, Czech Republic). Only pores larger than 3 μm in diameter were accounted for in the porosity measurements.

Raman spectra were acquired using a DXR Raman microscope by Thermo Scientific Nicolet (USA) using a green laser (532 nm) and power of 3 mW under an objective of 10 magnification with a scanning time of 16 s (8 two-second scans). For calibration samples, mixtures were prepared from pure $CaTiO_3$ and pure
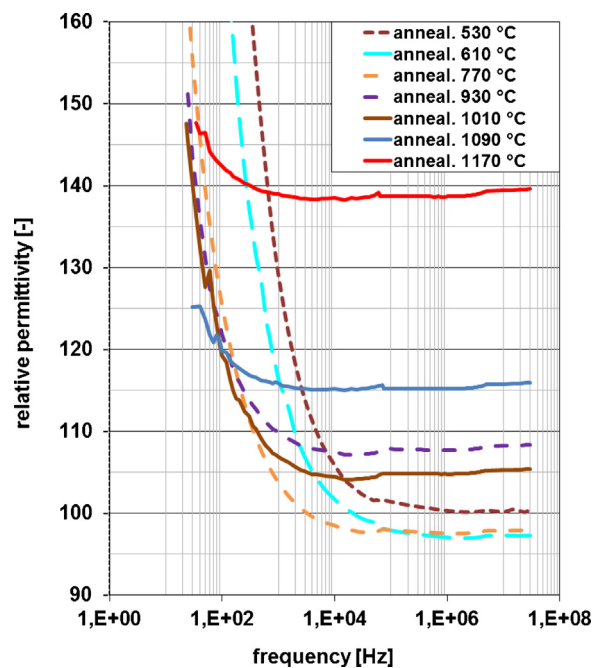
Table 1
Plasma spray parameters.

Parameter	WSP	GSP
Power (kW)	154	24
Primary gas (slpm)	–	Ar; 65
Secondary gas (slpm)	–	H_2; 2.5
Powder feeding medium	Air	Ar
Spray distance (mm)	350; 450	100

Fig. 1. Frequency dependence of relative permittivity for annealed WSP 450 samples.

Fig. 2. Frequency dependence of relative permittivity for annealed WSP 350 samples.

Fig. 4. Frequency dependence of relative permittivity for GSP 100 samples.

TiO_2 annealed at 600 °C for 4 h. Mixtures were homogenized by manual grinding. Calibration mixtures were measured under the same conditions as samples, but with a power of 0.1 mW.

3. Results and discussion
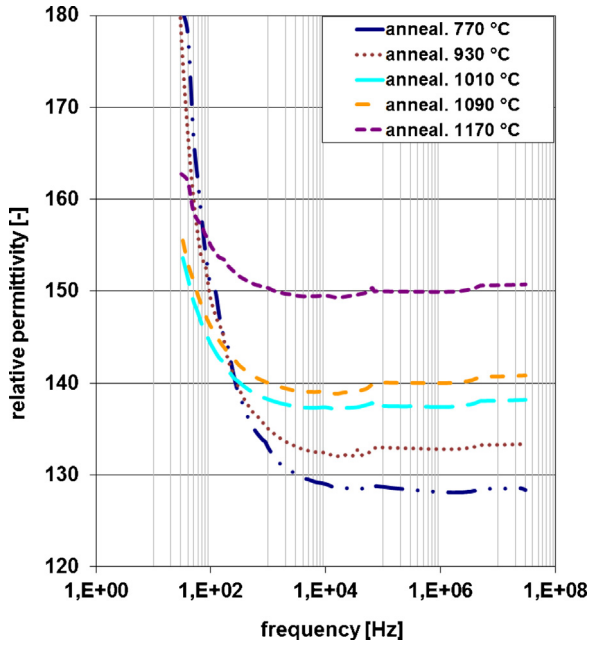
Frequency dependence of relative permittivity for annealed WSP 450 samples for a range of 30 Hz–30 MHz is given in the Fig. 1.

In general, it drops with growing frequency, which is expected for titanates [17]. Permittivity increases and becomes more stable with an increase in annealing temperature. The sample annealed at
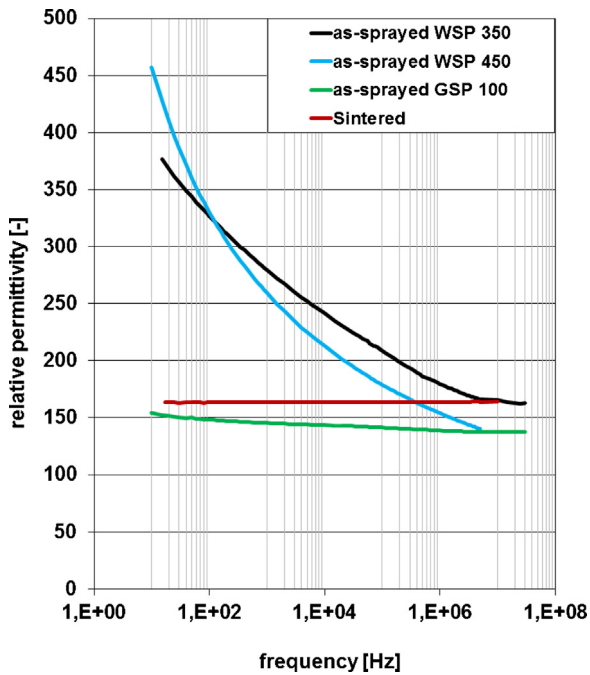
the highest temperature, 1170 °C, exhibit the highest relative permittivity value of 140 and display almost frequency independent behavior. In general, the same character of dependence was observed for WSP 350 samples (Fig. 2).

The maximum value of the plateau on the relative permittivity curve has shifted slightly up to 150 for the WSP 350 sample annealed at 1170 °C. Non-annealed WSP 350 and WSP 450 samples prepared by water stabilized plasma gun exhibited significantly higher permittivity (Fig. 3).

For a non-annealed WSP 450 sample at 10 kHz frequency the permittivity value was 210 and for 100 Hz frequency the permittivity was about 330 [10]. Frequency dependence of

Fig. 3. Frequency dependence of relative permittivity for sintered and as-sprayed samples.

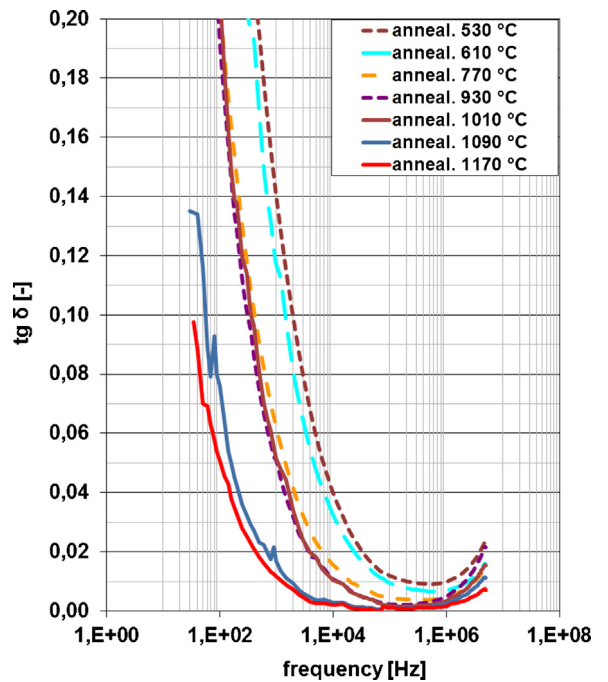**Fig. 5.** Frequency dependence of dielectric loss factor (tan δ) for WSP 450 samples.
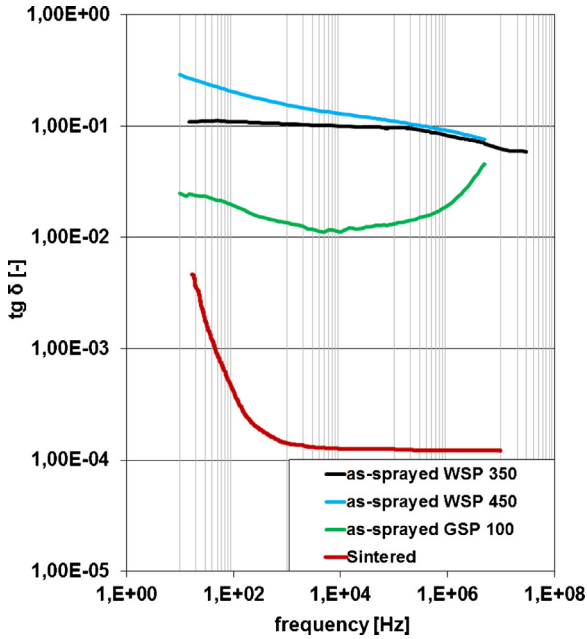
Fig. 6. Frequency dependence of dielectric loss factor ($\tan \delta$) for sintered and as-sprayed samples.

as-sprayed GSP 100 sample has more or less the same character as for sintered sample. The same influence of thermal annealing on relative permittivity was observed for GSP 100 samples (Fig. 4).

The character of the permittivity was more stable with tuned frequency especially at low frequencies than for samples prepared by the WSP device, but, in general, permittivity also increased with the annealing temperature. An almost linear change in relative permittivity with annealing temperature was observed for GSP 100 samples. The frequency dependence for the GSP 100 sample annealed at 1170 °C was not very strong but there were slightly higher linear decreases observed with frequencies over 200 Hz compared to the WSP 450 sample annealed at the same temperature.
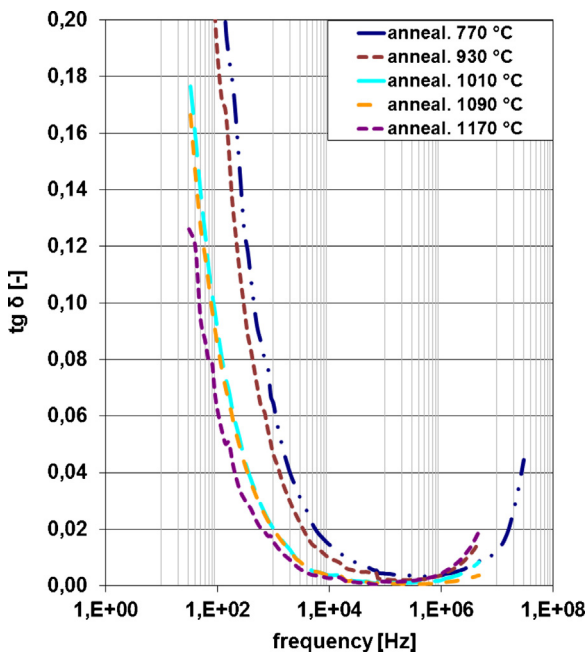

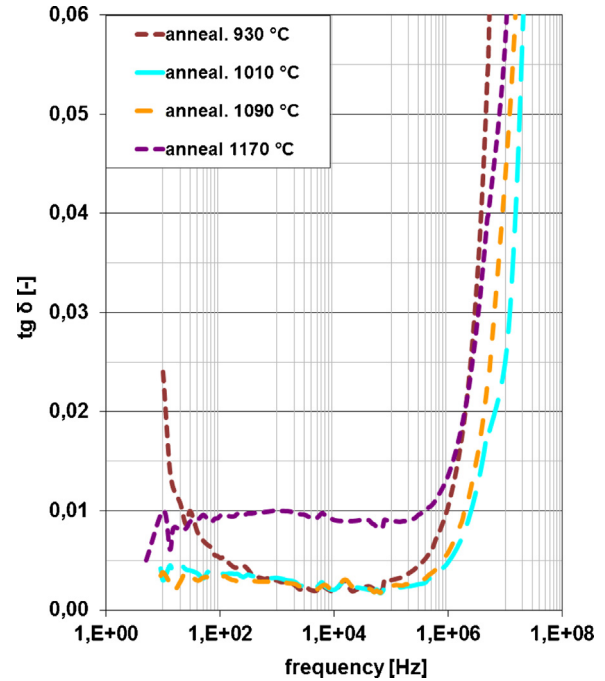**Fig. 7.** Frequency dependence of dielectric loss factor ($\tan \delta$) for WSP 350 samples.

Fig. 8. Frequency dependence of dielectric loss factor ($\tan \delta$) for GSP 100 samples.

Frequency dependence of dielectric loss factor, $tg \ \delta$, for WSP 450 is shown in Fig. 5.

Samples annealed at lower temperatures had higher losses. The WSP 450 sample annealed at 1170 °C, had the best dielectric properties; for frequency range 3 kHz–3 MHz the loss factor is below 0.005. The non-annealed sample had a much higher loss factor, with an observed value varying between 0.14 and 0.08, respectively (Fig. 6). All as-sprayed samples have significantly higher (up to 3 orders of magnitude) compare to industrially sintered sample.

Thermal annealing reduced the loss factor dramatically. In other words, it greatly improved the quality of the dielectric because loss factor represents power loss in a capacitor. A similar trend was observed for the WSP 350 set of samples (Fig. 7).

Samples produced by the GSP system had better dielectric properties in a non-annealed state than non-annealed WSP samples [10].

The loss factor for GSP samples was between 0.012 and 0.034 at a frequency range of 3 kHz–3 MHz, respectively. Annealed GSP 100 samples had a lower loss factor, but the sample annealed at the highest temperature of 1170 °C had a higher loss factor (0.01 at 500 kHz) than the other annealed samples. This phenomenon was not consistent with other curves. The sample annealed at 1090 °C had a loss factor below 0.004 at a frequency of 500 kHz. All characteristics of GSP 100 samples are shown in Fig. 8.

Both relative permittivity and loss factor of plasma sprayed CaTiO$_3$ decreased after thermal annealing.

The frequency dependence of AC conductivity for all non-annealed samples is given by Fig. 9.

The observed GSP 100 curve shows a threshold frequency, f_1, at 3 MHz, separating the curve in to two regions:

(a) Moderate frequency region, $f < 3$ MHz; the conductivity increases linearly with the frequency. This reveals that the conduction mechanism in this region corresponds to the translational hopping motion [18,19].
(b) High frequency region, $f > 3$ MHz; the conductivity increases linearly with the frequency, but at a different slope. The
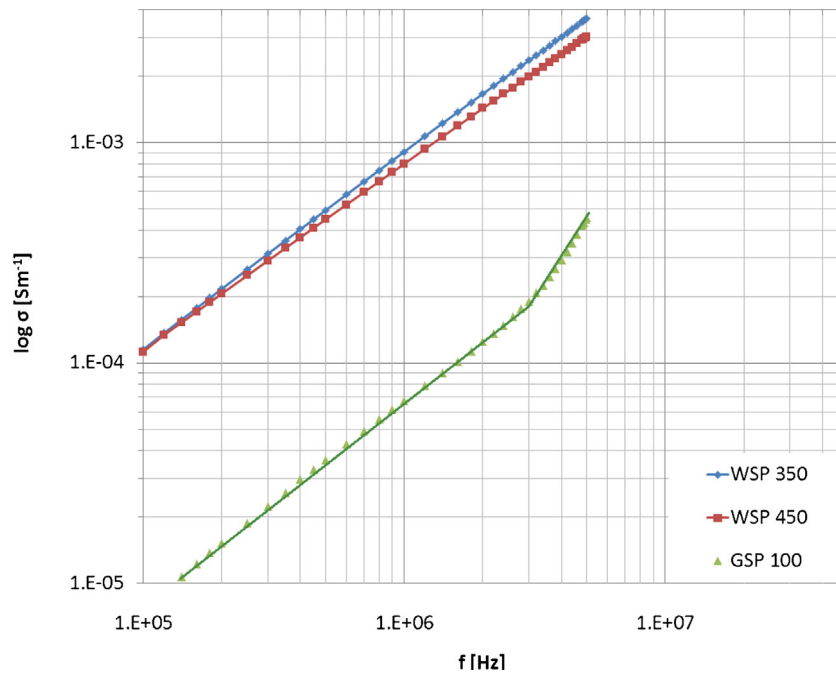
Fig. 9. AC conductivity versus frequency.

conduction mechanism in this range of frequency corresponds partly to a translational hopping motion and partly to a well-localized hopping and/or reorientation motion [16,19].

This is why the growth of the loss factor is higher at frequencies over 3 MHz for GSP samples. The ratio $tg\,\delta$ (at 3 MHz)/$tg\,\delta$ (at 3 kHz) is about 3 for non-annealed GSP 100, while it is only about 0.6 for non-annealed WSP 450. When we try to express it even more fundamentally, the next paragraph is a hypothesis adopted from other class of materials [19]. Under influence of the electric field, both long-range inter-well hopping and short-range intra-well hopping can occur [19]. The long-range inter-well hopping of holes takes place between sites located in adjacent defect-potential wells, while the short-range intra-well hopping of holes occurs within a defect potential well. The inter-well hopping contributes to the DC part of the total conductivity, while intra-well hopping contributes to the pure AC conductivity.

Selected annealed samples were analyzed by X-ray diffraction to determine whether any changes occurred in phase composition,

crystallinity or peak broadening. The obtained diffraction patterns for selected annealed samples (Fig. 10) are characteristic for purely crystalline materials; i.e., the so called amorphous phase is not observed as it was in the case of both non-annealed WSP samples [10].

Our samples exhibited perfect phase stability. Only one phase, orthorhombic perovskite (PDF card no. 22–153), was present in the irradiated volume. Furthermore, diffraction profile analysis carried out within the frame of the Rietveld method in TOPAS 4.2 software revealed no differences either in preferred orientation, grain size or microstrain. Orthorhombic perovskite phase can be matched to composition with about 58 mol.% of TiO_2 in CaO, as indicated in shown diagram (Fig. 11) extracted from literature. The diagrams describing the system under 1300 °C were not found.

Data obtained from reflectance measurements was used for estimation of the band gap of selected samples. Band gap energy of $CaTiO_3$ is 3.65 eV [21]. Three sample types were compared for band gap estimation, WSP 450, GSP 100 and a conventionally sintered

16
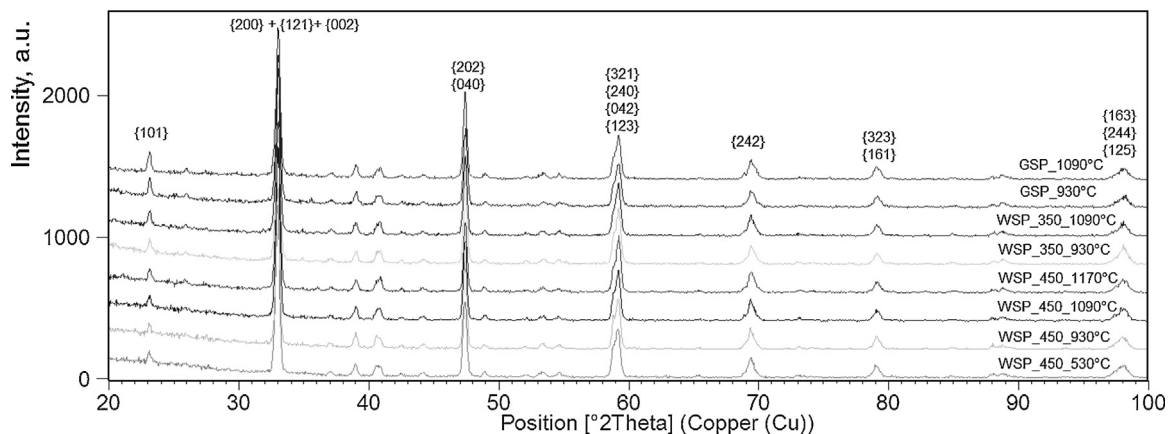
Fig. 10. X-ray diffraction patterns of selected annealed samples.
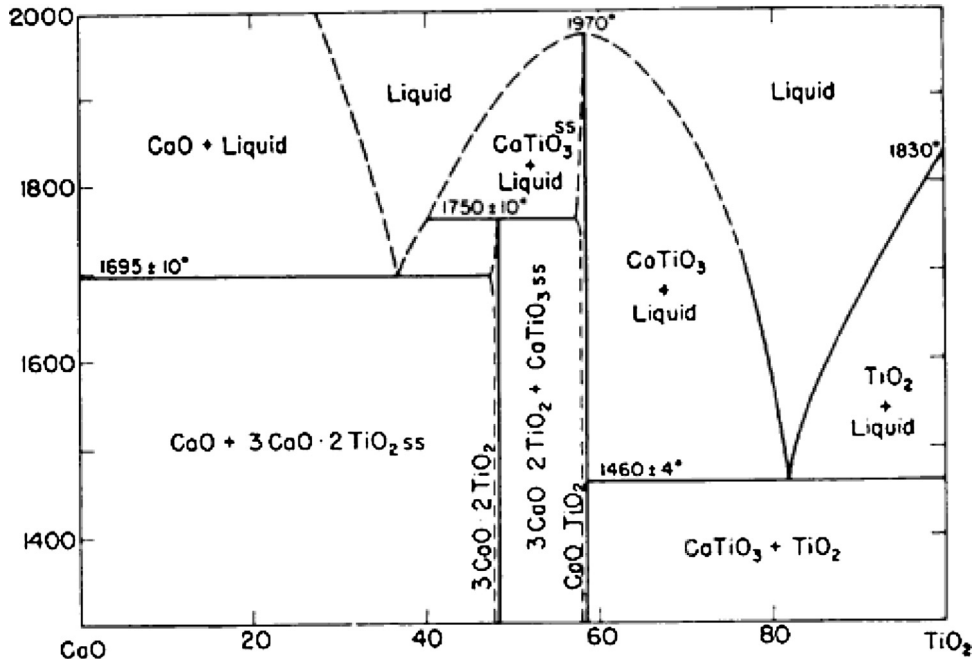
Fig. 11. The phase diagram of the CaTiO₃ [20].
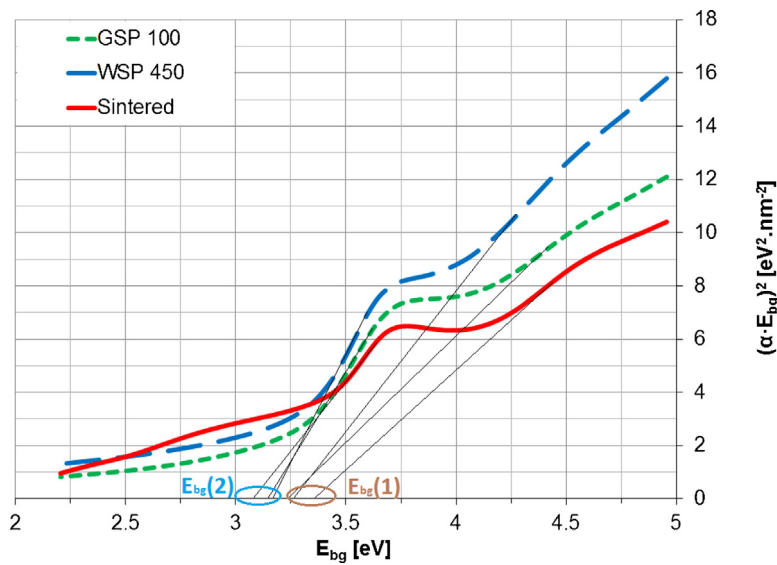
Fig. 12. Estimation of the band gap energy of CaTiO₃.

sample. All three samples have similar E_{bg} versus $(\alpha \times E_{bg})^2$ plots, as shown in Fig. 12.

The band gap energy value (assuming direct transition between valence and conduction band [16,21]) splits into two levels $E_{bg}(1)$ and $E_{bg}(2)$. The main absorption edge at $E_{bg}(1)$ corresponds to non-stoichiometric (oxygen deficient) CaTiO₃ and the secondary absorption edge at $E_{bg}(2)$ corresponds to an absorption tail of delocalized electronic states [22] with low excitation energy. The lower value of $E_{bg}(1)$ for both sprayed CaTiO₃ versus the sintered sample (i.e., red shift) occurs because of the vacancies present in the coatings.

Microstructure of the final CaTiO₃ powder suitable for spraying is given in Fig. 13. Particle size is 63–125 μm.

Porosity was evaluated using image analysis method containing several steps, Fig. 14. Image taken from polished cross-sections by light microscopy was converted to shades of gray in order to define pores. Pores were identified by threshold of the shades of grey.
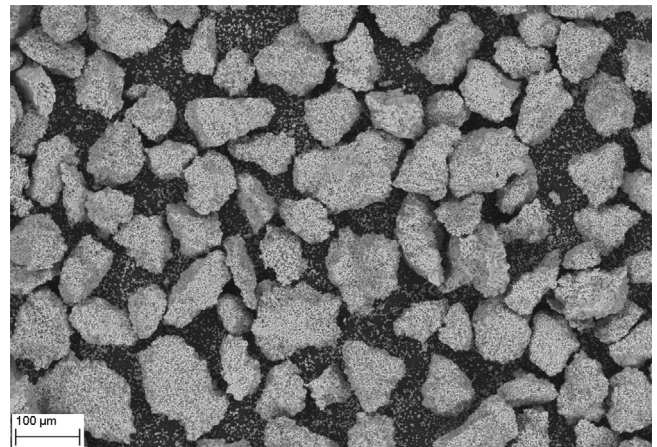
Fig. 13. Feedstock powder.
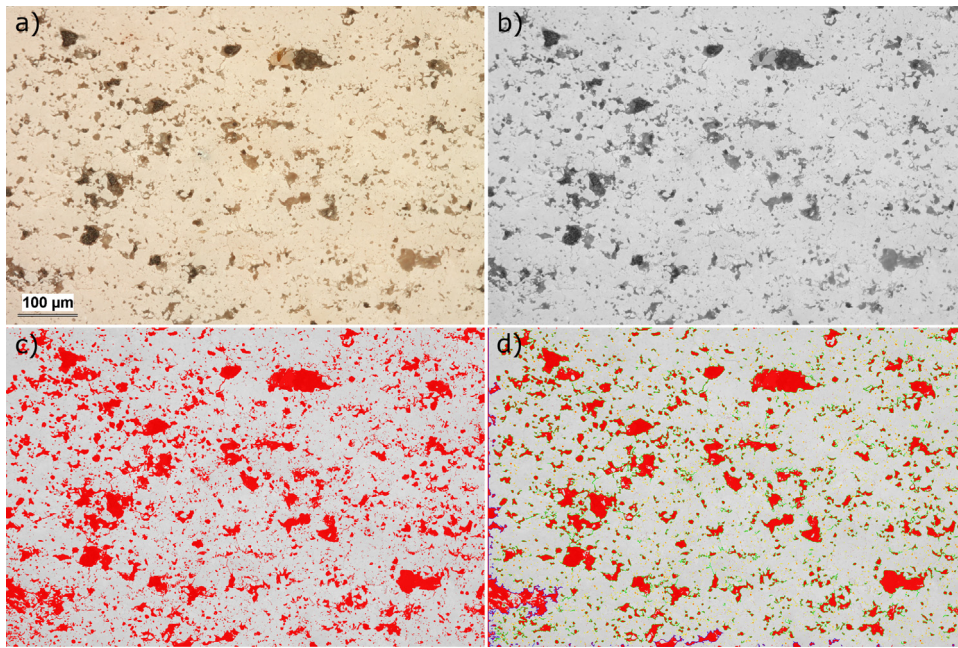
Fig. 14. Porosity evaluation process. (a) Image taken from polished cross-sections by light microscopy at a magnification of 250, (b) conversion to the shades of grey, (c) pores identification, (d) porosity evaluation.

Pores directly connected to the left and bottom side of the image were not counted into the total porosity but pores directly connected to the right and top side of the image were taken into account. This approach minimize uncertainty resulting from unknown total size of these pores.

Results of porosity measurements are shown in Table 2.

Long wide cracks between splats shrank and divided into several smaller ones. Some of the smaller pores closed after annealing. Microstructure became finer with a smaller amount of pores but the number and volume of bigger circular pores, which are present in the as-sprayed state, increased slightly. This results in a higher total circularity of pores of about 6%. Circularity (CIR) of pores (planar 2D projections) is equal to zero for a line and to 1 for a circle. This parameter is slightly higher for GSP 100 samples. These two main effects are the cause of increasing total porosity but the total number of pores was reduced. Increasing of circularity and

Table 2
Results of porosity measurements.

Sample	$T_{anneal.}$ (°C)	Porosity (%)	$N_{Obj.}$ (mm^{-2})	CIR (–)
WSP 350	–	11.7	1990	0.42
	930	14.2	910	0.49
	1090	14.0	1160	0.44
WSP 450	–	13.6	2030	0.38
	530	12.0	1280	0.43
	930	13.9	970	0.47
	1090	18.0	1380	0.40
	1170	16.9	1200	0.42
GSP 100	–	22.8	2560	0.41
	930	19.4	1830	0.50
	1090	25.3	2200	0.53

Porosity character for WSP 450 was changed considerably as can be seen in Fig. 15

Fig. 15. The micrographs of cross-sections of as-sprayed WSP 450 sample a), and WSP 450 sample annealed at 1090 °C b).

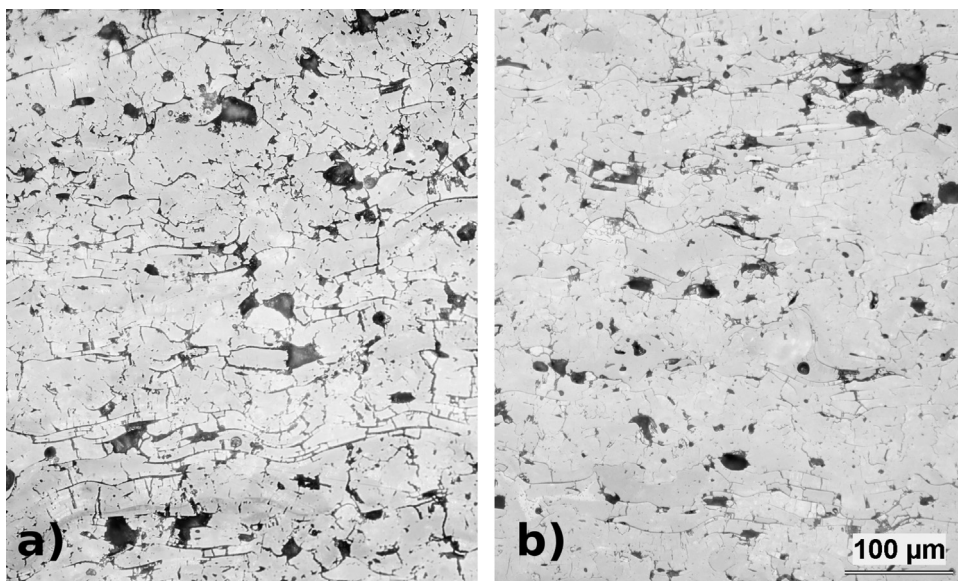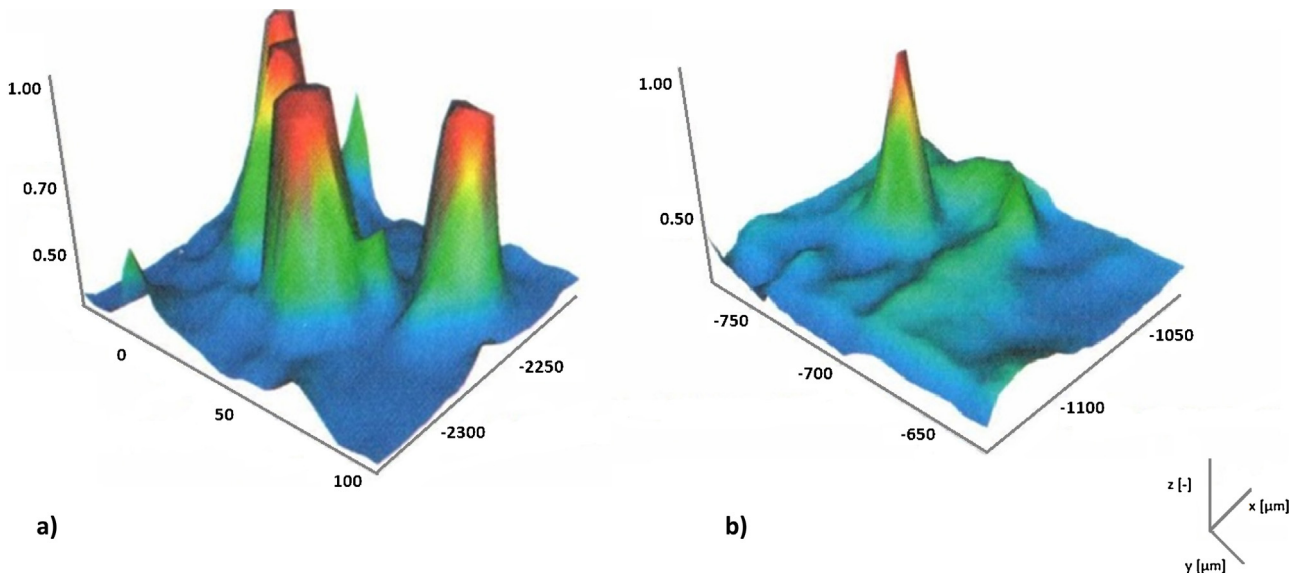**Fig. 16.** Raman map of surface of the sintered CaTiO$_3$ a); Raman map of surface of the as-sprayed WSP 450 b). The value 1 on the z-axis corresponds roughly to 3% TiO$_2$ in CaTiO$_3$.

decreasing of the total number of pores after annealing was observed for all three coatings. In general, porosity increases with increased annealing temperature. The observed trend for total porosity of GSP samples is not too significant taking into account the uncertainty of the porosity measurements. WSP 450 samples exhibit thermal coagulation of pores in the interval between 1090 and 1170 °C. GSP 100 samples have the highest porosity with the highest number of pores. Samples prepared by the WSP system have a similar porosity and number of pores (N. Por.) as well.

Both Figs. 16 and 17 show a Raman map of approx. 120 × 100 μm area on the surface of variously processed CaTiO$_3$.

The height represents the local intensity and presence of chemical bonds corresponding to rutile TiO$_2$. The value 1 on the z-axis corresponds roughly to 3% TiO$_2$ in CaTiO$_3$. Values at the x- and y-axes represent the absolute value of the position in micrometers.

A sintered CaTiO$_3$ sample where isolated islands of rutile are present is given in Fig. 16a). The size of the spots is about 20 μm. Fig. 16b) shows as-sprayed WSP 450. There exist similar spots of "rutile-rich" composition, but they are not as frequent and show a

slightly more "diffused" nature. The character of Raman maps following annealing is completely different. At 690 °C, the maximum local concentration of rutile is just one half of that present in the previous samples as can be seen in Fig. 17a).

The difference between maximum and minimum values decreased. This is similar to what is observed for an annealing temperature of 1010 °C Fig. 17b). This means annealing WSP 450 coatings brought homogenization of the TiO$_2$ composition.

The Raman spectrum itself is displayed in Fig. 18 for the sample annealed at 690 °C.

The spectrum is in good agreement with the literature [23], where the Raman spectrum of CaTiO$_3$ includes eight Raman bands at 183, 227, 247, 288, 339, 470, 494 and 641 cm^{-1}. The band observed at 641 cm^{-1} can be assigned to the Ti–O symmetric stretching vibration. Balachandran and Eror [24] also attributed a band at 639 cm^{-1} to Ti–O stretching. The bands at 470 and 494 cm^{-1} are assigned to Ti–O torsional modes (bending or internal vibration of oxygen cage), in agreement with the literature [24,25]. The bands in the region 225–340 cm^{-1} are tentatively
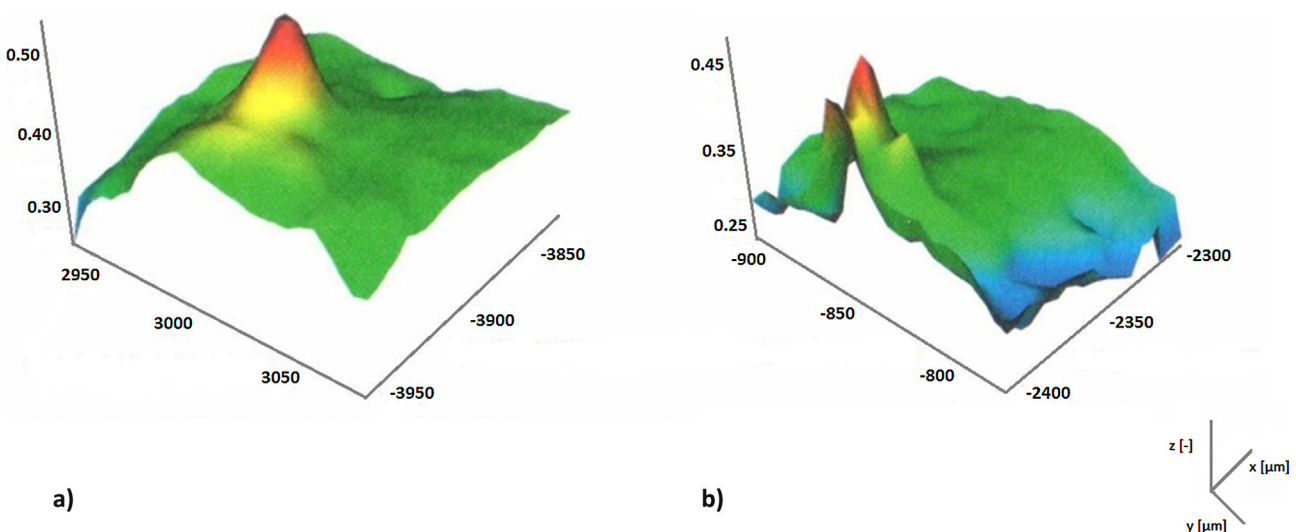

Fig. 17. Raman map of surface of the WSP 450 sample annealed at 690 °C a), Raman map of surface of the WSP 450 sample annealed at 1010 °C b). The value 1 on the z-axis corresponds roughly to 3% TiO$_2$ in CaTiO$_3$.
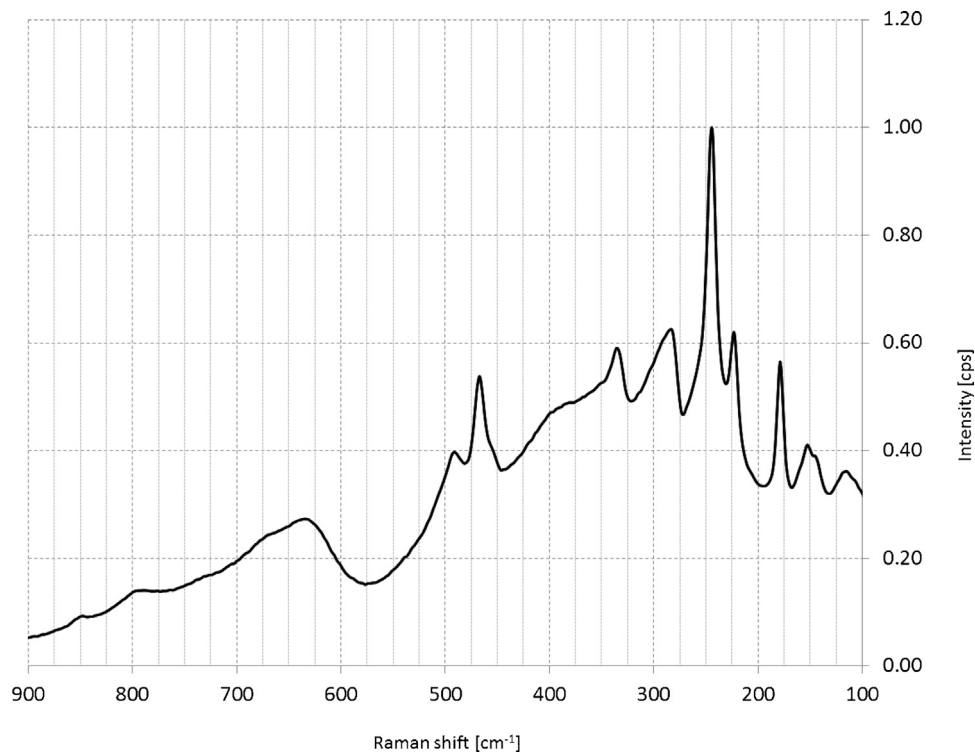
Fig. 18. Raman spectrum of the WSP 450 sample annealed at 690 °C.

assigned to the modes associated with rotations of oxygen cage and the band at 183 cm^{-1} is mainly due to the motion of A-site ions.

According to Raman microanalysis, there exist small islands in the material, where some 3 mol.% of rutile TiO_2 is present. But, according to Fig. 16b), the scanned area was $150 \times 150 \, \mu m$ (i.e., $22,500 \, \mu m^2$) the area of the island with this 3 mol.% of rutile (i.e., red color) is only some $5 \times 5 \, \mu m$ (i.e., $25 \, \mu m^2$). So the area fraction of such an island is only 0.1%. The overall increase of the rutile content in the $CaTiO_3$ is by this way only $3 \times 0.1 = 0.3\%$. We are still below 60 mol.% of TiO_2 in CaO, the melting point decreases very slightly according the binary diagram (Fig. 11) and there exist any intermediary phase formed inside this composition.

High relative permittivity of the WSP as-sprayed samples was highly frequency-dependent. This is associated with slow polarization phenomena which disappeared after annealing. Amorphous content which was observed in the as-sprayed state, affects the mobility of ions in the structure. That is likely the reason for larger similarity between as-sprayed GSP 100 and sintered sample. At very low frequencies this plays an important role. Besides microstructural aspects and partly chemical composition, the electrical character of the grain boundaries was also most probably affected by annealing.

4. Conclusions

This paper describes plasma sprayed calcium titanate. The influence of thermal annealing on dielectric properties was also examined. Samples annealed at a higher temperature exhibit better dielectric properties. By annealing, the loss factor diminished nearly ten times in the frequency range of 10 kHz–3 MHz. Obtained loss factor values after thermal annealing are on the order of 10^{-3}. This is a substantial improvement and properties of all post deposition treated samples correspond to a low loss dielectric materials group. Relative permittivity decreased simultaneously by 20–50 percent compared to the as-sprayed state and becomes almost frequency independent above 10 kHz more or less

for all coatings. All annealed samples only exhibited a pure crystalline orthorhombic perovskite phase. This material will be advantageous for electronics applications on curved surfaces and capacitors. Due to the possibility of coating different shapes and substrates, a combination of plasma spray and thermal annealing presents perspective technology for good dielectric coatings/free-standing parts. Two step process consisting of spraying and annealing could serve preferably as a procedure for fabrication of electronic ceramics that is not a coating but self-supporting parts.

References

[1] S.L. Zhang, C.H.X. Li, Chemical compatibility and properties of suspension plasma-sprayed $SrTiO_3$-based anodes for intermediate-temperature solid oxide fuel cells, J. Power Sources 264 (2014) 195–205.

[2] S.J. Han, Y. Chen, S. Sampath, Role of process conditions on the microstructure, stoichiometry and functional performance of atmospheric plasma sprayed La (Sr)MnO$_3$ coatings, J. Power Sources 259 (2014) 245–254.

[3] M.A. Peña, J.L.G. Fierro, Chemical structures and performance of perovskite oxides, Chem. Rev. 101 (2001) 1981–2018.

[4] W. Janosik, C. Randall, M. Lanagan, Thermodynamic and Electrical Effects of Residual Carbon in Glass Barium Titanate Composites for MLCC Applications, J. Am. Ceram. Soc. 90 (2007) 2415–2419.

[5] E.E.C. Oliveira, A.G. D'Assunção, J.B.L. Oliveira, A.M. Cabral, Small size dual-band rectangular dielectric resonator antenna based on calcium titanate ($CaTiO_3$), Microw. Opt. Technol. Lett. 54 (4) (2012) 976–979.

[6] A. Krause, J. WeberW, A. Jahn, K. Richter, D. Pohl, B. Rellinghaus, U. Schröder, J. Heitmann, T. Mikolajick, Evaluation of the electrical and physical properties of thin calcium titanate high-k insulators for capacitor applications, J. Vac. Sci. Technol. B 29 (1) (2011) 01AC07-5.

[7] C.H.L. Huang, S.H. Lin, Y.B. Chen, New dielectric material system of Nd(Mg$_{1/2}$Ti$_{1/2}$)O$_3$–$CaTiO_3$ with V_2O_5 addition for microwave applications, J. Alloys Compd. 489 (2) (2010) 719–721.

[8] Z. Xing, H. Wang, L. Zhu, X. Zhou, Y. Huang, Properties of the $BaTiO_3$ coating prepared by supersonic plasma spraying, J. Alloys Compd. 582 (2014) 246–252.

[9] P. Ctibor, H. Seiner, J. Sedlacek, Z. Pala, P. Vanek, Phase stabilization in plasma sprayed $BaTiO_3$, Ceram. Int. 39 (2013) 5039–5048.

[10] J. Sedlacek, P. Ctibor, J. Kotlan, Z. Pala, Dielectric properties of $CaTiO_3$ coatings prepared by plasma spraying, Surf. Eng. 29 (5) (2013) 384–389.

[11] K. Neufuss, A. Rudajevova, Thermal properties of the plasma-sprayed $MgTiO_3$–$CaTiO_3$ and $CaTiO_3$, Ceram. Int. 28 (2002) 93–97.

[12] P. Ctibor, J. Sedlacek, Dielectric properties of plasma sprayed titanates, J. Eur. Ceram. Soc. 21 (10–11) (2001) 1685–1688.

[13] R. Ahmadi-Pidani, R. Shoja-Razavi, R. Mozafarinia, H. Jamali, Laser surface modification of plasma sprayed CYSZ thermal barrier coatings, Ceram. Int. 39 (3) (2012) 2473–2480.

[14] J. Ilavsky, J.K. Stalick, Phase composition and its changes during annealing of plasma-sprayed YSZ, Surf. Coat. Technol. 127 (2000) 120–129.

[15] G. Di Girolamo, C. Blasi, L. Pagnotta, M. Schioppa, Phase evolution and thermophysical properties of plasma sprayed thick zirconia coatings after annealing, Ceram. Int. 36 (2010) 2273–2280.

[16] M.K. Reddy, S.V. Manorama, A.R. Reddy, Bandgap studies on anatase titanium dioxide, Mater. Chem. Phys. 78 (2002) 239–245.

[17] T.S. Kumar, R.K. Bhuyan, D. Pamu, Effect of post annealing on structural, optical and dielectric properties of $MgTiO_3$ thin films deposited by RF magnetron sputtering, Appl. Surf. Sci. 264 (2013) 184–190.

[18] M. Ram, S. Chakrabarti, Dielectric and modulus studies on $LiFe_{1/2}Co_{1/2}VO_4$, J. Alloys Compd. 462 (1–2) (2008) 214–219.

[19] U. Akgul, Z. Ergin, M. Sekerci, Y. Atici, AC conductivity and dielectric behavior of $[Cd(phen)_2(SCN)_2]$, Vacuum 82 (3) (2008) 340–345.

[20] R.C. De Vries, R. Roy, E.F.J. Osborn, J. Am. Ceram. Soc. 38 (158) (1955) .

[21] J. Zhuang, Q. Tian, S. Lin, W. Yang, L. Chen, P. Liu, Precursor morphology-controlled formation of perovskites $CaTiO_3$ and their photo-activity for As(III) removal, Appl. Catal. B: Environ. 156–157 (2014) 108–115.

[22] V. Nadtochenko, N. Denisov, A. Gorenberg, Y. Kozlov, P. Chubukov, J.A. Rengifo, C. Pulgarin, J. Kiwi, Correlations for photocatalytic activity and spectral features of the absorption band edge of TiO_2 modified by thiourea, Appl. Catal. B: Environ. 91 (2009) 460–469.

[23] H. Zheng, C. Gyorgyfalva, R. Quimby, H. Bagshaw, R. Ubic, I.M. Reaney, J. Yarwood, Raman spectroscopy of B-site order-disorder in $CaTiO_3$-based microwave ceramics, J. Eur. Ceram. Soc. 23 (2003) 2656–2659.

[24] U. Balachandran, N.G. Eror, Laser-induced Raman scattering in calcium titanate, Solid State Commun. 44 (6) (1982) 815–818.

[25] T. Hirata, K. Ishioka, M. Kitajima, Vibrational spectroscopy and X-ray diffraction of perovskite compounds $Sr_{1-x}M_xTiO_3$ (M = Ca, Mg; $0 < x < 1$), J. Solid State Chem. 124 (1996) 353–359.

4.4 On the dielectric strengths of atmospheric plasma sprayed Al$_2$O$_3$, Y$_2$O$_3$, ZrO$_2$-7% Y$_2$O$_3$ and (Ba,Sr)TiO$_3$ coatings

Presented work was done in cooperation with Center for Thermal Spray Research, State University of New York, Stony Brook, USA. All samples were sprayed using F4 plasma torch and the main interest was in the effect of spray distance on the dielectric breakdown strength of plasma sprayed ceramics. All other spray parameters were kept constant. Not only (Ba,Sr)TiO$_3$ as a titanate related to this thesis but four other widely used material were investigated. Barium-strontium titanate contained both crystalline and amorphous phase. The measured values of dielectric strength increased with increasing of amorphous phase content. It holds true that for other ceramics dielectric breakdown strength decreased with increasing of spray distance. Good homogeneity of studied coatings was confirmed by surprisingly low standard deviations, mostly below 10 % for breakdown strength measurements.

On the dielectric strengths of atmospheric plasma sprayed Al$_2$O$_3$, Y$_2$O$_3$, ZrO$_2$–7% Y$_2$O$_3$ and (Ba,Sr)TiO$_3$ coatings

Jiri Kotlan[a,b,*], Ramachandran Chidambaram Seshadri[c], Sanjay Sampath[c], Pavel Ctibor[a,b], Zdenek Pala[a], Radek Musalek[a]

[a]Materials Engineering Department, Institute of Plasma Physics ASCR, v.v.i., Za Slovankou 3, Prague 8, Czech Republic
[b]Department of Electrotechnology, Faculty of Electrical Engineering, Czech Technical University in Prague, Technicka 2, Prague 6, Czech Republic
[c]Center for Thermal Spray Research, Department of Materials Science & Engineering, Stony Brook University, Stony Brook, NY 11794-2275, USA

Abstract

In article an attempt has been made to investigate the dielectric strengths of selected ceramic coatings namely alumina (Al$_2$O$_3$), yttria (Y$_2$O$_3$), YSZ (ZrO$_2$–7% Y$_2$O$_3$) and ferroelectric BST (Ba$_{0.68}$Sr$_{0.32}$TiO$_3$) deposited using a atmospheric plasma spray process. Samples of each material were deposited under three different spray distances. The hardness, moduli of elasticity, dielectric strengths of the deposits were evaluated. The microstructures and phases were analyzed using optical microscopy and X-ray diffraction analysis respectively. The results show the significant influence of spray distance on dielectric strengths of the coatings. The dielectric strengths as per hierarchy are 17.3 ± 1.0 kV/mm for yttria, 16.6 ± 1.8 kV/mm for alumina, 11.1 ± 1.5 kV/mm for YSZ and 7.8 ± 0.8 kV/mm for BST. The particles temperature and velocity during spraying were analyzed in order to find relation between process parameters and dielectric strengths. Correlation between crystallinity of deposited BST and dielectric strength was found in this study.
© 2015 Elsevier Ltd and Techna Group S.r.l. All rights reserved.

Keywords: B. X-ray methods; B. Grain size; C. Electrical properties; E. Insulators; Dielectric strength

1. Introduction

Conventionally sintered ceramics face limitations because of the high cost and low flexibility in the methods employed for manufacturing the parts. Atmospheric Plasma Spray (APS) technology can be effectively used to deposit ceramic layers on different substrate materials and over large areas without losing both economic and technical virtues. Plasma sprayed ceramics may be used for example in manufacturing of electrical bushings for medium voltage applications such as motors, transformers and capacitors or to cover the large metallic parts of medium voltage devices in order to avoid an electric shock

hazard. APS parameters have significant effect on the resulting microstructure and phases present in the coatings. This structural and phase changes can significantly affect the performance of the deposits when tested for applications in the electrical field [1]. The dielectric strength is an important measure in the field of electrical engineering. Dielectric strength is traditionally defined as breakdown voltage divided by coatings thickness.

The standard dielectric strength measurement technique which requires the immersion of the samples in oil during testing is not recommended for thermal spray deposited materials. Some investigators have observed the doubling of dielectric strength values of oil dipped coatings compared to the values of samples tested in dry condition. This increase in dielectric strength was due to the penetration oil into the pores of the coatings [2]. Nevertheless, the research on the dielectric strength of plasma sprayed ceramics has been limited mostly to

*Corresponding author at: Materials Engineering Department, Institute of Plasma Physics ASCR, v.v.i., Za Slovankou 3, Prague 8, Czech Republic. Tel.: +420 266 053 717.
E-mail address: kotlan@ipp.cas.cz (J. Kotlan).

alumina. Pawlowski [3] reported dielectric strength values ranging between 9 and 18 kV/mm for coatings deposited by spraying different alumina powders. He states that the crucial parameter that can affect the results are the volume percentage of porosity present in the coatings. Toma et al. [4] analyzed the dielectric strengths of plasma alumina coatings having different thicknesses ranging up to 240 μm. The maximum dielectric strength was found to be 24 kV/mm. An ultra-dense alumina coating with a porosity lower than 1 vol% prepared by a low pressure plasma spray technique can exhibit a maximum dielectric strength of 45 kV/mm [5]. Kim et al. [6] showed that there can be slight increase of breakdown voltage for coatings whose surface was ground compared to as-sprayed alumina–titania coatings. Selected dielectric properties of barium strontium titanate (BST) were studied by Dent et al. [7]. The effect of grain size on dielectric strength was investigated for sintered $BaTiO_3$ ceramics. The results showed that dielectric as well as fatigue strengths decrease significantly with increasing amount of coarse grains [8]. It is worth mentioning that the coating materials involved in this study namely the Al_2O_3, Y_2O_3, YSZ and BST have not been compared from the dielectric strength point of view so far. Hence, in the current investigation an attempt was made to systematically analyze and correlate the dielectric strengths of different coating materials with respect to the changes in the temperature and velocity of particles sprayed under different spray distances, vol% of porosity, phase composition, crystallite size and the level of amorphous content present in the coating deposits.

2. Experimental details

2.1. Coating preparation

All the samples were manufactured in the Centre for Thermal Spray Research (CTSR), Stony Brook University, New York using the F4 MB-XL atmospheric plasma spray system (Oerlikon Metco, USA) equipped with Ø 8 mm nozzle and Ø 1.8 mm orthogonal external powder injector. The plasma spray parameters were: Argon flow rate (primary gas) 50 slpm, Hydrogen flow rate (secondary gas) 6 slpm, the input current and voltage supplied to the gun were 550 A and 64 V respectively. The parameters mentioned above were maintained constant to spray all the considered powders. The carrier gas (Ar) flow rates were optimized for each powder since external injection was used. The powders were fed at a constant feed rate of 30 gpm using an Oerlikon Metco twin ten volumetric powder feeder. The carrier gas flow rate was varied between 2–9 slpm in steps of 1 slpm and the Accuraspray-g3 sensor (TECNAR Automation Ltd., St-Bruno, Qc, Canada) was used to measure the temperatures and velocities of particles sprayed under each increment of the carrier gas flow rate at the same spray distance. The center of plasma plume was aligned with the sensor using the spray robot so that the flow center of the spray stream was always within the field of view of the Accuraspray-g3 sensor. The carrier gas flow rate at which the particles achieve the

maximum temperature and velocity was considered as the optimum carrier gas flow setting. This procedure was repeated to optimize the carrier gas flow rate for all the powders. Powders details and feeding conditions are given in Table 1.

The powders were deposited under three different spray distances namely 100 mm, 150 mm and 200 mm. Low carbon steel of thickness 2.3 mm was used as a substrate material. Substrate was grit blasted using 24 mesh corundum grits. The substrates were ultrasonically cleaned with acetone prior to and after grit blasting.

2.2. Characterization of coatings

Dielectric strength measurements were carried out using TuR-WPT 0.8/65 – GPT 3/80 (Veb Transformatorenwerk, Germany) dielectric strength measurement kit. The dielectric strength measurement kit was operated with Ø 6 mm rod which supplied a 50 Hz alternating current (AC) towards the samples. The samples dimension was 50×25 mm^2. The steel substrate served as one of the electrodes. The second rod electrode was placed to the coatings surface. All the edges of the samples were properly covered by vinyl polysiloxane in order to avoid surface discharges that usually occur below the breakdown voltage between electrode and the steel substrate. All the samples were dried in a furnace at 70 °C for 12 h prior to the test in order to get rid of the moisture content in the coating. The applied voltage was increased in steps of 500 V/s until the sample underwent breakdown. The dielectric breakdown was confirmed using the characteristic collapsing/decrease in the voltage with a corresponding increase in value of the current. Since the dielectric strength is defined as the breakdown voltage divided by the coatings thickness, it was computed from the average of 9 breakdown voltage measurements. All the coatings and the feedstock powders were analyzed by X-ray diffraction. The XRD was done using the D8 Discover Bruker diffractometer operated in the Bragg–Brentano mode with filtered CuKα radiation and 1D LynxEye detector. Diffraction patterns were analyzed within the frame of the Rietveld method available in TOPAS 4.2 software.

Metallographic samples were prepared using Tegramin-25 automatic polishing system (Struers, Denmark) to assure identical preparation conditions for all samples. Free-surfaces where electric breakdown took place were observed using a EVO MA 15 scanning electron microscope (Carl Zeiss SMT,

Table 1
Feedstock and spray details.

Material	Producer	Type	Particle size [μm]	Carrier gas flow rate [slpm]
Al_2O_3 (alumina)	Microabrasives Corporation	Microgrit WCA-30	10–35	6.5
Y_2O_3 (yttria)	Norton	Norton 402	10–60	4.5
7 Y_2O_3: ZrO_2 (YSZ)	Saint Gobain	SG-204F	10–45	3.5
(Ba,Sr)TiO$_3$ (BST)	Trans Tech Inc.	$Ba_{0.68}Sr_{0.32}TiO_3$	5–45	7.0

Germany). The porosity was measured on the polished cross-sections of the deposits using light optical microscopy. Ten images of each sample were taken from randomly selected areas at $400\times$ magnification. The volume percentage of porosity was estimated using image analysis software Lucia G (Laboratory Imaging, Prague, Czech Republic). Only the pores which are larger than 3 µm in diameter were taken into account for the porosity measurements. The microhardness measurement was made using SVK-C2 Vickers microhardness tester, (Mitutoyo, Japan). A load of 300 g and a dwell time of 15 s were used to evaluate the hardness. Hardness values were measured at 10 random locations on the polished cross-section of a coating and average values were considered in order to compare the coatings. The modulus of elasticity was measured with an instrumented depth-sensing micro-indentation test [9]. A Fischerscope H100 with a maximum load of 1 N was used to perform these tests. This device simultaneously recorded the applied load and the penetration of the diamond into the material. The mean modulus of elasticity was calculated from the elastic response of the material at the beginning of the unloading. The indentation tests were performed at room temperature on the same polished cross-sections as were used for the SEM and optical microscopy.

3. Results and discussion

3.1. Inflight diagnostics of sprayed particles

The particle velocities and temperatures as obtained from the Accuraspray-g3 sensor are summarized in Table 2 as their averages. The Accuraspray-g3 diagnostic system provides ensemble average data representing the particle characteristics in a measured volume of approximately $\varnothing\ 3\times 25\ mm^2$. The particle velocities and temperatures were obtained from time delay cross-correlation of signals which are recorded at two closely spaced fiber optic sensors and two-color pyrometry respectively. It is not possible to evaluate the distribution and standard deviations of particle velocities and temperatures from the ensemble Accuraspray-g3 data [10].

The melting points of Al_2O_3, Y_2O_3, YSZ and BST are 2072, 2425, 2715, 2080 °C respectively. As expected from the ensemble sensor diagnosis, the particle temperature and velocity decreases with increasing of spray distance irrespective of the materials being sprayed. The YSZ and Y_2O_3 reached temperature above 3000 °C for the shortest spray

distance, 100 mm. Alumina has the highest particles velocity. Even at the spray distance 200 mm the velocity of the alumina particles is above 200 m/s. BST particles have the lowest velocity and mostly the lowest temperature as well. The velocity and temperature gained by the particles in plasma plume depends on the particle diameter, morphology, fusion temperature of the material, mass as well as the injection velocity, which is controlled by the carrier gas flow. Due to smaller inertia, the smaller particles are accelerated and heated up to higher velocities and temperatures by the plasma gas than the larger ones; this phenomenon applies for alumina particles. From Table 2 one could witness that the Y_2O_3 and YSZ particle temperatures measured at 200 mm spray distance are lower than their actual melting points. This suggests that some particles could be in semi-molten state or might have started resolidifying due the longer flight time. Further, the Accuraspray-g3 system averages particle data on the whole measurement volume to one single representing value hence, the results derived from accuraspray diagnostics are typically 10–12% lower than the actual average temperature and velocity values of the particles in the plasma plume [11].

3.2. Dielectric strength of the plasma sprayed deposits

All coatings in this study have approximately the same thickness (h_c) of about 0.5 mm in average which represents a typical thickness of plasma sprayed coatings. The dielectric strength data are summarized in Table 3. The number of spray passes was controlled so as to get approximately the same average coating thickness for the coating sprayed under different spray distances.

The dielectric strength (E_b) decreases with increasing of spray distance except for BST where the observed value is the lowest for a short spray distance. In general, spray conditions with higher velocity and particle temperature result in higher dielectric strength value. Higher velocity and temperature means easier flattening of the impacting droplet on the substrate, to form a lamella, however this simplification is not satisfactory every time (splashing can occur, droplet fragmentation, in-situ annealing) [12]. Standard deviation calculated from nine measured values is below 16% mostly

Table 2
Particles velocities and temperatures during spray process.

Material	Spray distance					
	100 mm		150 mm		200 mm	
	V [m/s]	T [°C]	V [m/s]	T [°C]	V [m/s]	T [°C]
Al_2O_3	264	2660	239	2470	214	2240
Y_2O_3	217	3050	199	2740	171	2440
YSZ	208	3080	181	2810	151	2540
BST	177	2530	167	2440	128	2330

Table 3
Dielectric strength results.

Sample	h_c [mm]	E_b [kV/mm]	st. dev [kV/mm]	st. dev [%]
$Al_2O_3 - 100$	0.502	16.6	1.8	10.8
$Al_2O_3 - 150$	0.687	13.9	0.9	6.5
$Al_2O_3 - 200$	0.549	13.5	1.2	8.9
$Y_2O_3 - 100$	0.521	17.3	1.0	5.8
$Y_2O_3 - 150$	0.554	14.4	1.3	9.0
$Y_2O_3 - 200$	0.531	11.6	1.0	8.6
YSZ – 100	0.473	11.1	1.5	13.5
YSZ – 150	0.564	10.0	0.6	6.0
YSZ – 200	0.432	7.8	0.9	11.5
BST – 100	0.421	5.1	0.8	15.7
BST – 150	0.561	7.8	0.8	10.3
BST – 200	0.450	6.4	0.4	6.3

even lower than 10%. This variability in the measured values is due to the anisotropic nature of the plasma sprayed deposits.

3.3. Phase analysis of the thermal spray deposits

The XRD patterns of the surfaces of coatings deposited under different spray distances are compared with their corresponding feedstocks as shown in Figs. 1–4. In all the figures, vertical shift was introduced in order to make the comparison more illustrative. The identified phases are denoted by special symbols above the corresponding reflections.

For all the XRD patterns, Rietveld refinement was performed with the aim to (i) verify the presence of the identified phases, (ii) refine lattice parameters of the identified crystalline phases, (iii) estimate degree of crystallinity in BST coatings and (iv) calculate average sizes of crystallites or, more precisely, coherently scattering domains (CDD). Selected results are presented in Table 4.

The feedstock used for alumina coatings contains not only corundum, or α-Al$_2$O$_3$, but also around 7 wt% of sodium rich β-alumina as seen in Fig. 1 [13], which is a standard minor phase in alumina powders (i.e. fused and crushed) fabricated by the Bayer process (digestion of bauxite). However, the plasma sprayed coatings consists dominantly of the so called metastable aluminas, in particular cubic γ and tetragonal δ (Fig. 1), which are commonly observed after plasma spraying [14]. There are traces of corundum in the coatings amounting to several wt%, but these are probably unmelted particles embedded in the coating [15]. There are no major differences
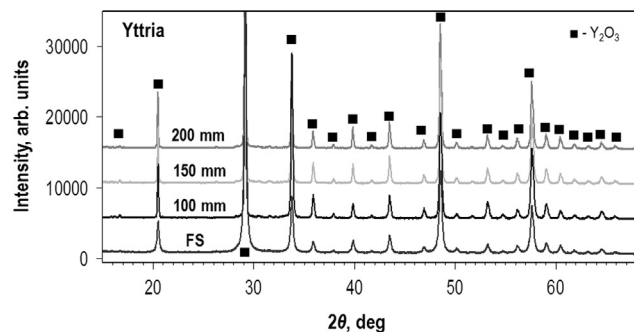
in the phase composition of coating surfaces sprayed under different spray distances.

In case of Y$_2$O$_3$, both the feedstock and coatings show presence of only cubic Y$_2$O$_3$ as displayed in Fig. 2. The diffraction profiles of the feedstock are broadened and, hence, the established CDD is an order of magnitude lower than for the coatings. Moreover, there is a clear tendency of increase in CDD with increasing spray distance. Taking into account dielectric strength values from Table 3, we observe decreasing E_b with increasing CDD of Y$_2$O$_3$. The increase in dielectric strength with corresponding decrease of grain size for sintered materials was reported in the past [16,17] for barium titanates. Ferroelectric ceramics, such as BaTiO$_3$, consist of ferroelectric grains and insulating grain boundaries representing an obstacle for charge carriers' movement. Thus, the volume of the grains and grain boundaries changes with grain size variation. In the case of yttrium oxide, we observe that the variation in grain size and grain boundary area seems to play an important role in the dielectric breakdown strength even for ceramics which is not ferroelectric.

From Fig. 3 it is visible that the YSZ deposits contains both monoclinic (m-ZrO$_2$) and tetragonal (t-ZrO$_2$) zirconia. The powder feed stock contains a large amount (around 10 wt%.) of m-ZrO$_2$. A lowest level of 1.6 wt% m-ZrO$_2$ was ascertained for coatings sprayed with a spray distance of 150 mm. The other two SD have approximately the same amount of m-ZrO$_2$ reaching around 2.8 wt%. The YSZ is the only exception where the CDD does not increase with SD which is probably because of the fact that it was closer to its melting point at the longest spray distance and CDD decreased due to recrystallization.

The BST feed stock has both BST and BaTiO$_3$ as major phases, whereas the coatings show the presence of BST and an
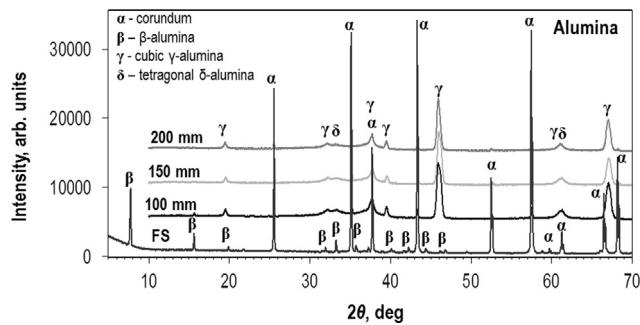

Fig. 1. XRD patterns of alumina feedstock (FS) and as-sprayed surfaces of three coatings.

Fig. 2. XRD patterns of yttria FS and as-sprayed surfaces of three coatings.
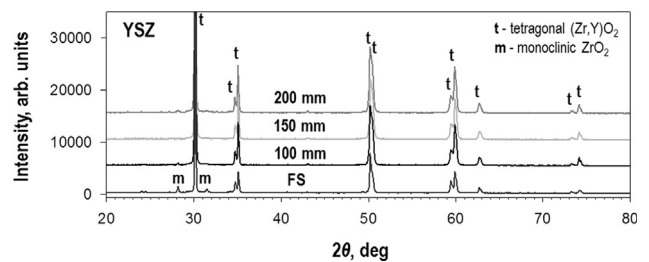

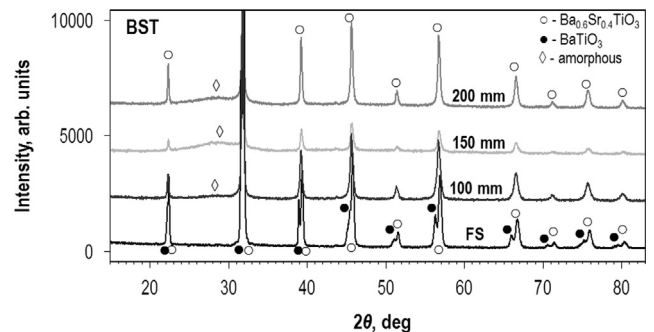Fig. 3. XRD patterns of YSZ FS and as-sprayed surfaces of three coatings.

Fig. 4. XRD patterns of BST FS and as-sprayed surfaces of three coatings.

Table 4
Selected results from Rietveld refinement.

Phase	Feedstock		Spray distance					
			100 mm		150 mm		200 mm	
	Lattice parameters [Å]	CDD [nm]	Lattice parameters [Å]	CDD [nm]	Lattice parameters [Å]	CDD [nm]	lattice parameters [Å]	CDD [nm]
Al_2O_3	n.a.	n.a.	n.a.	n.a.	n.a.	n.a.	n.a.	n.a.
Y_2O_3	10.6065 ± 0.0003	37 ± 1	10.6028 ± 0.0002	281 ± 13	10.6034 ± 0.0002	325 ± 12	10.6046 ± 0.0002	364 ± 15
t-ZrO_2 in	$a=3.6154 \pm 0.0001$	> 500	$a=3.6142 \pm 0.0001$	194 ± 4	$a=3.6146 \pm 0.0001$	224 ± 5	$a=3.6145 \pm 0.0001$	197 ± 4
YSZ	$c=5.1633 \pm 0.0001$		$c=5.1618 \pm 0.0001$		$c=5.1621 \pm 0.0001$		$c=5.1624 \pm 0.0002$	
BST	3.9632 ± 0.0001	55 ± 1	3.9719 ± 0.0002	47 ± 1	3.9721 ± 0.0003	55 ± 2	3.9716 ± 0.0001	70 ± 1

amorphous content, which could be inferred from Fig. 4. The stoichiometry of barium and strontium atoms occupying the (0, 0, 0) site in primitive cubic lattice, as refined by the Rietveld method, was similar in the deposits sprayed under 100 and 150 mm spray distances, i.e. $Ba_{0.35}Sr_{0.65}$, which is less balanced compared to $Ba_{0.45}Sr_{0.55}$ for 200 mm. In case of the BST feedstock the refined occupancies show $Ba_{0.60}Sr_{0.40}$ stoichiometry which is slightly different from the information provided by feedstock supplier, i.e. $Ba_{0.68}Sr_{0.32}TiO_3$. Fig. 5 clearly indicates that there is a clear correlation between the amorphous content in BST coatings and the obtained E_b values. Tanaka et al. [18] showed the influence of crystallinity on dielectric strength on low-density polyethylene. The authors elucidated that the increase in crystallinity makes the mean free-path of the charge carriers longer, resulting in lower dielectric strength values. The only parallel found in the literature is an observation concerning the crystallinity in PEEK polymer [19]. All samples in our study have fully crystalline structure except BST. By comparing the crystallinity and dielectric strength values for BST it was observed that BST seems to follow the behavioral trend of a PEEK polymer. In our case, the BST samples exhibit increased dielectric strength with increasing levels of amorphous content. Two phenomena i.e., the crystallinity and dielectric strength are acting against each other in the case of BST samples. The increase of CDD and amorphous phase supports the aforementioned claims.

3.4. Microstructural observations of the coatings

Microstructures of coatings deposited at a spray distance 100 mm are displayed in Fig. 6. Y_2O_3 samples have the lowest porosity among all other samples (Table 5). The porosity value is close to 5 vol% for all spray distances. The most porous material in this study is YSZ. Evaluated porosity of YSZ samples range up to 9.2% and the standard deviation is relatively high compared to other samples. The melting point of YSZ is the highest among the considered materials, hence there is a possibility that some of the YSZ particles might have started to re-solidify inflight when sprayed at the spray distance of 200 mm. The porosity naturally decreases the dielectric strength of materials but the differences in total porosity at different spray distances with respect to standard
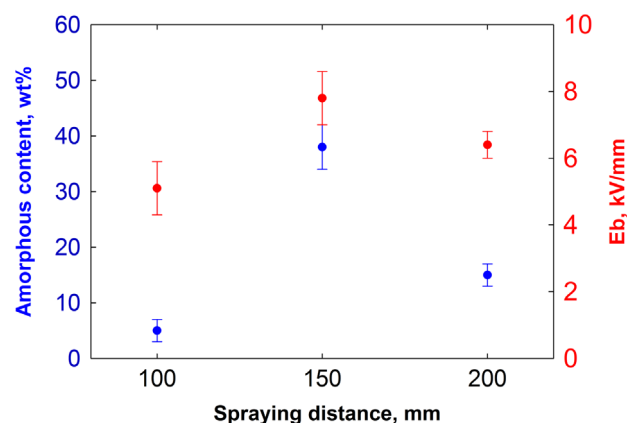

Fig. 5. Amorphous content in BST coatings and measured E_b values versus spray distance.

deviation are not significant in our case. Typical lamellar microstructure of the plasma spray deposits greatly affects the behavior of the samples in the electric field [20].

Vickers hardness data are given in Fig. 7. As expected significant differences for studied materials were observed. The highest value over 1750 HV has alumina sprayed at spray distance 100 mm. Even the lowest value for the longest spray distance, 200 mm, is more than three times higher compared to values observed for BST and Y_2O_3. In general hardness decreases with increasing of spray distance for all samples. Modulus of elasticity dependence on spray distance is given in Fig. 8. The modulus of elasticity and hardness of a thermal spray deposited material are governed not only by the intrinsic elastic properties of constituents forming the structure, but also by the interlamellar bonding between the splats and pore density. In plasma sprayed ceramics, the coating elastic properties are significantly lower compared to bulk counterparts. The Yttria and BST were found to have the lowest modulus and alumina possess the highest modulus followed by the YSZ. The same kind of trend is observed also in case of microhardness. There is a clear correlation between particle diagnostic results on one side and modulus of elasticity and hardness of the coatings on the other. Considering porosity, its low values are obtained for the shortest spray distance. However there is no clear correlation between the evaluated mechanical properties and dielectric strengths of the coatings under consideration.
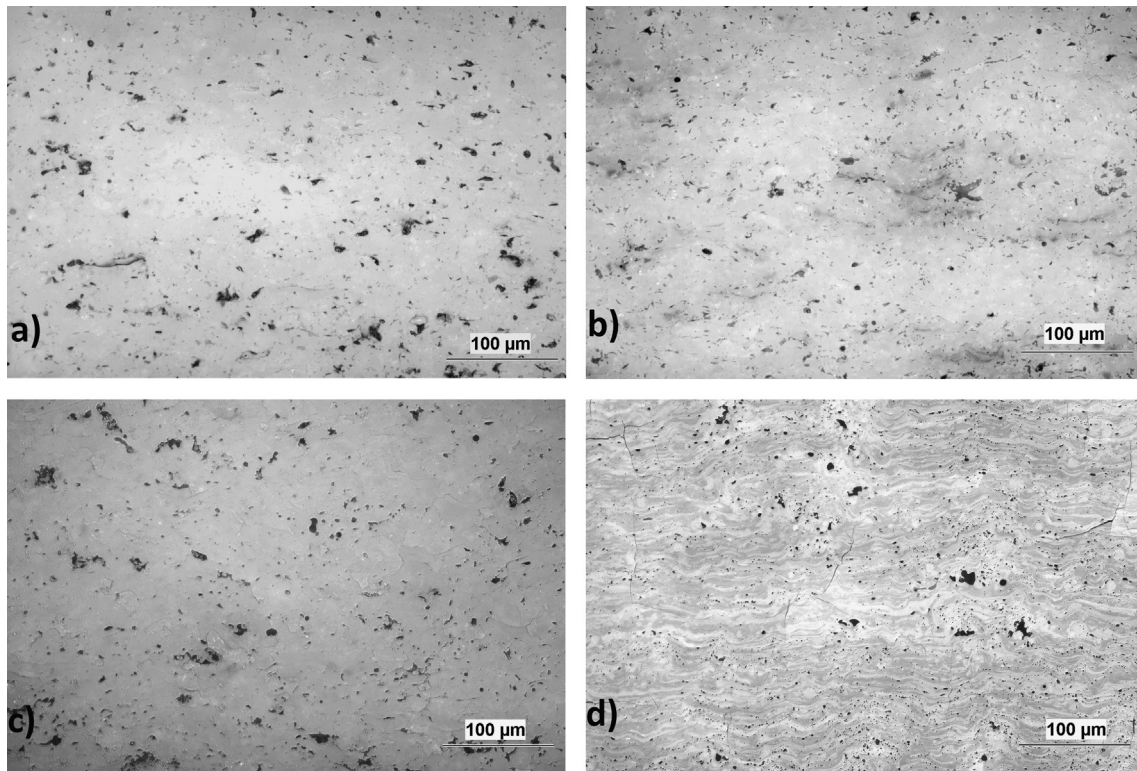
Fig. 6. Cross sections at 400 magnification of (a) alumina 100, (b) Y_2O_3 100, (c) YSZ 100 and (d) BST 100.

Table 5
Porosity measurements data.

Sample	Porosity [%]
$Al_2O_3 - 100$	5.4 ± 1.2
$Al_2O_3 - 150$	4.4 ± 0.4
$Al_2O_3 - 200$	6.2 ± 0.6
$Y_2O_3 - 100$	5.2 ± 1.2
$Y_2O_3 - 150$	5.0 ± 0.9
$Y_2O_3 - 200$	4.9 ± 0.8
YSZ $-$ 100	7.0 ± 1.3
YSZ $-$ 150	9.2 ± 1.9
YSZ $-$ 200	8.6 ± 1.7
BST $-$ 100	5.4 ± 0.6
BST $-$ 150	4.9 ± 0.9
BST $-$ 200	8.6 ± 1.8
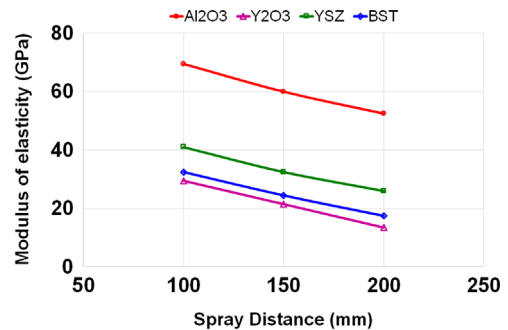
Fig. 8. Comparison of effective modulus of elasticity of the deposits.

3.5. Analysis of surface morphologies of samples after dielectric strength test

As-sprayed surface of the Y_2O_3 coatings sprayed with 100 mm spray distance seems to possess a lot of black spots. These black spots are caused by the inflight oxygen reduction which takes place in the naturally reducing plasma gas atmosphere. Longer spray distances are helpful for the fabrication of pure white coatings. Under longer spray distances the re-oxidation of the particles can occur due to the relatively low ambient temperature and presence of abundant oxygen [21]. The surfaces of coatings after break-down were analyzed using SEM and the pictures are shown in Fig. 9.
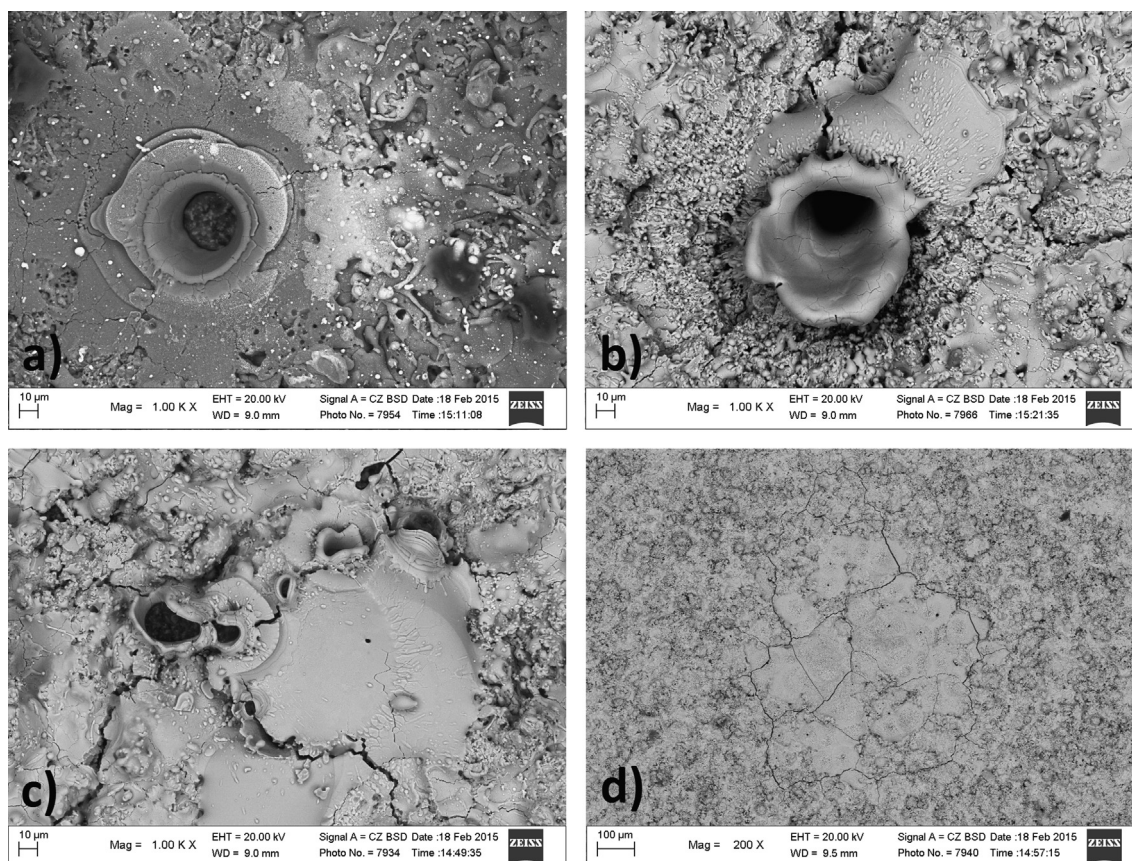

Fig. 7. Comparison of Vicker's microhardness of the deposits.

Fig. 9. Free surfaces of coatings sprayed under 100 mm spray distance after dielectric breakdown (a) Al_2O_3, (b) Y_2O_3, (c) YSZ and (d) BST.

The electrical discharge has provoked channel formation through the coatings. Typical diameters of the channels range between 15 and 25 μm. The BST coating displayed larger areas of remelted material after breakdown, whereas other materials display clear channel formations. The breakdown affected surface area is much larger in case of BST compare to other materials. Typical diameter of this area is about 500 μm. This effect might have taken place due to low energy demand of the BST to transit from solidus to liquidus phase. Self-healing effect after solidification is not observed in BST, probably due to the extensive crack formation on the surface.

4. Conclusions

In this article an attempt was made to investigate and compare the dielectric strengths of plasma sprayed ceramic deposits prepared from commercially available feedstock powders. Dense coatings with higher microhardness and modulus were obtained under a shortest spray distance of 100 mm. The largest scatter of dielectric strength values is seen for yttria coatings where also strong correlation with crystallite size is observed. In case of Y_2O_3 coatings, the dielectric strength is around 17 kV/mm for coating with smallest crystallite size about 280 nm, but dielectric strength decreases to around 11.5 kV/mm in coating which has a crystallite size of 365 nm. Moreover, the crystallite size was found to increase with increasing spray distances. Among the considered materials, BST exhibits the lowest dielectric strength in the 5–8 kV/mm range. BST coatings contain both crystalline and amorphous phases and the measured values of dielectric strength increase with increasing levels of amorphous content. The surface area of the BST coating which gets affected the dielectric strength test was about one order magnitude larger compared to other materials considered in this investigation. Except for BST, which is the only coating with amorphous content, it holds true that the hotter particles with higher velocities form a harder coating with high modulus values which can in turn result in higher dielectric strength values. Taking into account dielectric strength values and mechanical properties of the considered materials, the plasma sprayed alumina seems to be the most perspective material for industrial applications; especially samples prepared at spray distance 100 mm exhibit good dielectric strength and high hardness and modulus of elasticity as well.

References

[1] N. Branland, E. Meillot, P. Fauchais, A. Vardelle, F. Gitzhofer, M. Boulos, Relationships between microstructure and electrical properties of RF and DC plasma-sprayed titania coatings, J. Therm. Spray Technol. 15 (2006) 53–62.

[2] M. Niittymaki, K. Lahti, T. Suhonen, J. Metsajoki, Dielectric breakdown strength of thermally sprayed ceramic coatings: effects of different test arrangements, J. Therm. Spray Technol. 24 (2015) 542–551.

[3] L. Pawlowski, The relationship between structure and dielectric properties in plasma-sprayed alumina coatings, Surf. Coat. Technol. 35 (1988) 285–298.

[4] F. Toma, Comparative study of the electrical properties and characteristics of thermally sprayed alumina and spinel coatings, J. Therm. Spray Technol. 20 (2011) 195–204.

[5] E.J. Young, E. Mateeva, J.J. Moore, B. Mishra, M. Loch, Low pressure plasma spray coatings, Thin Solid Films 377–378 (2000) 788–792.

[6] H.J. Kim, S. Odoul, C.H. Lee, Y.G. Kweon, The electrical insulation behavior and sealing effects of plasma-sprayed alumina–titania coatings, Surf. Coat. Technol. 140 (2001) 293–301.

[7] A.H. Dent, A. Patel, J. Gutleber, E. Tormey, S. Sampath, H. Herman, High velocity oxy-fuel and plasma deposition of $BaTiO_3$ and (Ba,Sr) TiO_3, Mater. Sci. Eng. B 87 (2001) 23–30.

[8] S.C. Lu, Y.H. Chen, W.H. Tuan, J. Shieh, C.Y. Chen, Effect of microstructure on dielectric and fatigue strengths of $BaTiO_3$, J. Eur. Ceram. Soc. 30 (2010) 2569–2576.

[9] L.J. Loubet, G. Meille, in: P.J. Blau, B.R. Lawn (Eds.), Microindentation Techniques in Materials Science Engineering, ASTM STP 889, Philadelphia, 1986, pp. 72–89.

[10] G. Mauer, R. Vaßen, D. Stöver, Comparison and applications of DPV-2000 and Accuraspray-g3 diagnostic systems, J. Therm. Spray Technol. 16 (2007) 414–424.

[11] J. Colmenares-Angulo, K. Shinoda, T. Wentz, W. Zhang, Y. Tan, S. Sampath, On the response of different particle state sensors to deliberate process variations, J. Therm. Spray Technol. 20 (2011) 1035–1048.

[12] P. Fauchais, M. Fukumoto, A. Vardelle, M. Vardelle, Knowledge concerning splat formation: an invited review, J. Therm. Spray Technol. 13 (2004) 337–360.

[13] R.R. Ridgway, A.A. Klein, W.J. O'Leary, The Preparation and properties of so-called Beta Alumina, Trans. Electrochem. Soc 70 (1936) 71–88.

[14] P. Chraska, J. Dubsky, K. Neufuss, J. Pisacka, Alumina-base plasma-sprayed materials part I: phase stability of alumina and alumina-chromia, J. Therm. Spray Technol. 6 (1997) 320–326.

[15] P. Ctibor, O. Roussel, A. Tricoire, Unmelted particles in plasma sprayed coatings, J. Eur. Ceram. Soc. 23 (2003) 2993–2999.

[16] T. Tunkasiri, G. Rujijanagul, Dielectric strength of fine grained barium titanate ceramics, J. Mater. Sci. Lett. 15 (1996) 1767–1769.

[17] Z. Song, H. Liu, S. Zhang, Z. Wang, Y. Shi, H. Hao, et al., Effect of grain size on the energy storage properties of $(Ba_{0.4}Sr_{0.6})TiO_3$ paraelectric ceramics, J. Eur. Ceram. Soc. 34 (2014) 1209–1217.

[18] Y. Tanaka, N. Ohnuma, K. Katsunami, Y. Ohki, Effects of crystallinity and electron mean-free-path on dielectric strength of low-density polyethylene, Electr. Insul. IEEE. Trans. 26 (1991) 258–265.

[19] T.W. Giants, Crystallinity and dielectric properties of PEEK. poly(ether ether ketone), Dielectr. and Electr. Insul. IEEE Trans. 1 (1994) 991–999.

[20] P. Ctibor, J. Sedlacek, Dielectric properties of plasma sprayed titanates, J. Eur. Ceram. Soc. 21 (2001) 1685–1688.

[21] H.K. Seok, E.Y. Choi, P.R. Cha, M.C. Son, B.L. Choi, et al., Characterization of plasma-sprayed Y_2O_3 coating and investigation of its visual aspect change, Surf. Coat. Technol 205 (2011) 3341–3346.
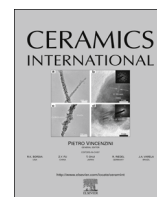
4.5 The role of amorphous phase content on the electrical properties of atmospheric plasma sprayed (Ba,Sr)TiO$_3$ coatings

Motivation for this paper came from interesting results obtained in previous paper where correlation between amorphous phase content and electrical breakdown strength was observed. This study studied electrical properties of barium-strontium titanate prepared by APS. Different spray distances resulted in presence of different amount of amorphous material content in the coating. Change in relative permittivity value or loss factor due to the high content of amorphous contents is approximately four times. Sample containing 38 wt.% of amorphous phase content (the highest of all samples) exhibited four orders of magnitude higher electrical resistivity when compare to the sample with only 5 wt.% of amorphous phase content. Not only amorphous phase content affects the electrical properties but there is also contribution of oxygen vacancies, preferably generated at short spray distances due to the oxygen reduction in plasma atmosphere.

The role of amorphous phase content on the electrical properties of atmospheric plasma sprayed (Ba,Sr)TiO₃ coatings

Jiri Kotlan [a,b,*], Ramachandran Chidambaram Seshadri [c], Sanjay Sampath [c], Pavel Ctibor [a]

[a] Materials Engineering Department, Institute of Plasma Physics CAS, v.v.i., Za Slovankou 3, Prague 8, Czech Republic
[b] Department of Electrotechnology, Faculty of Electrical Engineering, Czech Technical University in Prague, Technicka 2, Prague 6, Czech Republic
[c] Center for Thermal Spray Research, Department of Materials Science & Engineering, Stony Brook University, Stony Brook, NY 11794-2275, USA

ABSTRACT

(Ba,Sr)TiO₃ coatings deposited on carbon steel substrates were successfully prepared by an atmospheric plasma spray system. Three sets of samples containing different amount of both crystalline and amorphous phases were deposited and consequently studied in order to determine their electrical properties. The results show a clear correlation existing between the amorphous phase content and coating´s electrical properties. The resistivity increases with increase of amorphous phase content. Relative permittivity for low frequencies decreases and become more stable with frequency tuning when amorphous phase content increased. The maximum relative permittivity value is in the range 75–200 for frequency 1 kHz. The loss factor varies between 0.23 and 0.03 for all studied samples. The loss factor is at the lower limit of these values and frequency much less dependent when the coating contains 15 wt% of amorphous phase and more. The band gap of all samples is between 2.75 eV and 2.90 eV. Microstructure and hardness were evaluated in order to determine basic mechanical properties of deposits.

© 2016 Elsevier Ltd and Techna Group S.r.l. All rights reserved.

1. Introduction

Ferroelectric and paraelectric ceramics play an important role in electronic applications, since these materials have high relative permittivity values. High permittivity value allows the material to act as gates in dielectric devices. The BaTiO₃ which belong the aforementioned category of materials is extensively studied and applied in a wide variety of applications such as multilayer ceramic thermistors, piezoelectric transducers, capacitors and actuators [1]. This group of materials is principally produced by powder sintering or high temperature co-firing (HTCC) methods. Disadvantage of conventional powder sintering technologies lies in the fact that they cannot be easily used in coatings or direct writing technology. Atmospheric Plasma Spray (APS) technology can be effectively used to deposit ceramic layers on different substrate materials and over large areas at moderate to low deposition temperatures [2]. Barium titanate and its doped variants were and still are extensively used for its excellent ferroelectric, piezoelectric and thermoelectric properties in electronic industry [3,4]. Sintered (Ba₀.₄Sr₀.₆)TiO₃ ceramics was studied in order to determine the effect of grain boundary on the energy storage

properties and dielectric breakdown strength [5]. There are a few articles available in the open literature, which deals with the study on the dielectric properties of plasma and HVOF deposited barium strontium titanate (BST) coatings [6–8]. A significant influence of the amorphous phase content on the dielectric constant values was observed on BaTiO₃ coatings that were prepared by various spray deposition techniques. BaTiO₃ coatings sprayed by the supersonic plasma spray system (HEPJet) showed that that defects like porosity and voids can reduce the piezoelectric effect in the resultant coatings [9]. Among the spray parameters, the spray distance was found to significantly affect the photocatalytic activity of plasma sprayed BaTiO₃ coatings [10]. The importance of substrate temperature during plasma spray deposition of coatings was demonstrated in a study, which showed that with the increase in substrate temperature the inter-splat bonding increases and this consequently results in the increase in the relative permittivity values [11]. Solidification of molten particles during plasma spraying is accompanied by extremely high cooling rates [12]. Rapid cooling promotes the formation of amorphous phases in the coating and thus various material properties are affected by the degree of crystallinity. Thermal annealing is important post-deposition process which can be effectively used to tailor the dielectric properties of atmospheric plasma sprayed dielectric ceramic deposits [13]. In our previous publication which focused on electrical breakdown strengths of selected atmospheric plasma sprayed ceramics, it was found that the electrical breakdown

strength increased with increasing levels of amorphous content in $(Ba,Sr)TiO_3$ coatings [14]. The current investigation is focused on studying the role of amorphous phase content on mechanical and some electrical properties of about 0.5 mm thick coatings. We report namely the DC resistivity, relative permittivity and loss factor of plasma deposited $(Ba,Sr)TiO_3$ coatings prepared under different spray conditions. The influence of spray distance is a key parameter in this study. The relative permittivity and loss factor were studied in the frequency range from 50 Hz to 1 MHz.

2. Experimental details

2.1. Coating preparation

Three sets of samples sprayed at different spray distances namely 100 mm, 150 mm and 200 mm were prepared and the corresponding coatings were labeled as BST 100, BST 150 and BST 200. The Accuraspray-g3 sensor (TECNAR Automation Ltd., St-Bruno, Qc, Canada) was used to measure the surface temperatures and velocities of the sprayed particles. Coatings were deposited on grit blasted substrates having dimensions $25 \times 230 \times 2.3$ mm^3 made out of low carbon steel. Coatings thicknesses were 0.36 mm, 0.48 mm and 0.41 mm for BST 100, BST 150 and BST 200 respectively. The spray parameters and powder details are listed out in Table 1.

2.2. Characterization of coatings

All the coatings and the feedstock powder were analyzed by X-ray diffraction. The XRD was done using the D8 Discover Bruker diffractometer operated in the Bragg-Brentano mode with filtered Cu$K\alpha$ radiation and 1D LynxEye detector. Diffraction patterns were analyzed within the frame of the Rietveld method available in TOPAS 4.2 software. Samples were cut and ground to the dimensions of approximately $25 \times 20 \times 2.8$ mm^3. A three electrode measuring system was employed for all electrical properties measurements. Carbon steel substrate of thickness 2.3 mm was used as one of the electrodes. Two other aluminum electrodes were sputtered on the coating surface under reduced pressure. Capacity measurements were carried-out in a frequency range from 50 Hz to 1 MHz. For low frequency measurements (50 Hz–100 kHz) a Hioki 3522–50 LCR HiTester was used. The device was set to four times the average of all values. The Agilent 4285 instrument equipped with Agilent 16451B sample fixture module was employed to measure frequency range measurements between 75 kHz to 1 MHz. The frequency step was progressively increased and applied AC voltage of 1 V kept constant in both devices. The electric field was applied along the spray direction (i.e., perpendicular to the substrate surface). The relative permittivity ε_r was calculated from measured capacities and specimen dimensions using equation $\varepsilon_r = (C \cdot d)/(A \cdot \varepsilon_0)$ where C (F) is

electrical capacity of the sample, d (m) is samples thickness, A (m^2) is area of measuring electrode and ε_0 is permittivity of vacuum (8.854e − 12 F/m). The same LCR-meters were, at the same moment, used for the loss factor measurement. Loss factor ($tg\,\delta$) was measured for the same frequencies as capacity. The volume resistivity was measured on the same samples for capacity measurements using Keithley 6517B high resistance meter. Applied voltage for all resistance measurements was set to 100 ± 0.16 V. Customized Keithely 6104 shielded test enclosure was used in order to avoid error from ambient noise. Resistivity was calculated from measured resistance and specimen dimensions using equation $\rho = (R \cdot A)/d$ where R (Ω) is electrical resistance of the sample, A (m^2) is area of measuring electrode and d (m) is samples thickness. All electrical properties measurements shows electrical response of the whole coating-substrate system because the substrate served as one of the electrodes (earlier described in [14]). Diffuse reflectance was measured by UV–vis-NIR scanning spectrophotometer (Shimadzu, Japan) with a multi-purpose large sample compartment and corresponding band-gap energy was estimated. The reflectance curves obtained between 200 and 2000 nm were converted to absorbance and recalculated [15] to band-gap energy, E_{bg}. Metallographic samples were prepared using Tegramin-25 automatic polishing system (Struers, Denmark) to ensure identical preparation conditions for all samples. Cross sections were observed using EVO MA 15 scanning electron microscope (Carl Zeiss SMT, Germany) equipped with EDX detector. The porosity was measured on the polished cross-sections of the deposits using light optical microscopy. Ten images of each sample were taken from randomly selected areas at $400 \times$ magnification. The volume percentage of porosity was estimated using image analysis software Lucia G (Laboratory Imaging, Prague, Czech Republic). Only the pores which are larger than 3 μm in diameter were taken into account for the porosity measurements. The microhardness measurement was made using SVK-C2 Vickers microhardness tester, (Mitutoyo, Japan). A load of 300 g and a dwell time of 15 s were used to evaluate the hardness. Hardness values were measured at 10 random locations on the polished cross-section of a coating and average values were considered in order to compare the coatings. The indentation tests were performed at room temperature on the same polished cross-sections as were used for the SEM and optical microscopy.

3. Results and discussion

3.1. Inflight diagnostics of sprayed particles

The average velocities and surface temperatures of the particles obtained from the Accuraspray-g3 sensor are summarized in Table 2. The working of Accuraspray-g3 ensemble particle stream sensor data can be referred elsewhere [16]. The melting point BST is 2080 °C. It could be inferred from the ensemble sensor diagnosis data that, the particle temperature and velocity decreases with increasing of spray distance. The velocities of particles measured at 200 mm spray distances is significantly lower than the velocities measured at 100 mm and 150 mm spray distances. Particles

Table 1
APS spray parameters employed for this study.

Parameter	Value/Unit
Torch/nozzle diameter	60 kW F4-MB-XL/ 8 mm
Injector type/diameter and angle	Single external/ 1.8 mm/ 90°
Argon/Hydrogen/carrier gas flow rates	50/6/7 lpm
Powder make/size/Feed rate	$(Ba,Sr)TiO_3$ powder (Trans Tech Inc., USA)/ 5–45 μm/ 30 gpm
Spray distance	100, 150 and 200 mm
Current/voltage	550 A/ 64 V
Raster speed/step (over-lap) size	1000 mmps/ 3 mm

Table 2
In-flight surface temperature and velocities of the BST particles at different distances.

Spray distance (mm)	Surface Temperature (°C)	Velocity (m/s)
100	2530	177
150	2440	167
200	2330	128

Fig. 1. XRD patterns of BST FS and as-sprayed surfaces of three coatings.

Fig. 2. The time evolution of DC resistance measurement for the BST 150 sample.
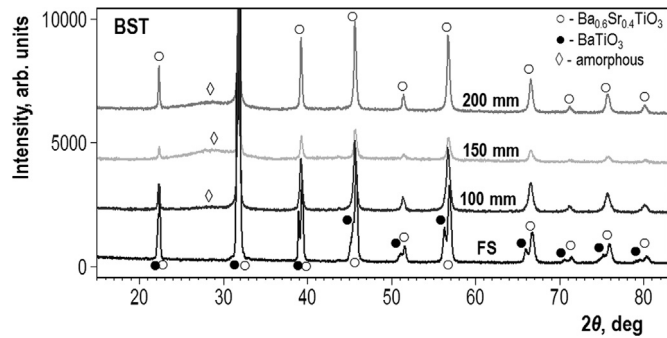
Fig. 3. Volume resistivity results.

temperature seems to decrease to at least 100 °C with every 50 mm increment in the spray distance.

3.2. Phase analysis of the thermal spray deposits

The XRD patterns of the surfaces of the coatings deposited under different spray distances are compared with the feedstock powder, Fig. 1. In the figure, vertical shift was introduced in order to make the comparison more illustrative. The identified phases are denoted by special symbols above the corresponding reflections.

Rietveld refinement was performed with the aim to (a) verify the presence of the identified phases, (b) refine lattice parameters of the identified crystalline phases, (c) calculate average sizes of crystallites or, more precisely, coherently scattering domains (CDD) and (d) estimate amorphous content in coatings. Results are presented in Table 3.

The BST feed stock has both BST and $BaTiO_3$ as major phases, whereas the coatings show the presence of BST and an amorphous content, which could be inferred from Fig. 1. The stoichiometry of barium and strontium atoms occupying the (0, 0, 0) site in primitive cubic lattice, as refined by Rietveld method, was similar in the deposits sprayed under 100 and 150 mm spray distances, i.e. $Ba_{0.35}Sr_{0.65}$, which is less balanced compared to $Ba_{0.45}Sr_{0.55}$ for 200 mm. In case of the BST feedstock the refined occupancies show $Ba_{0.60}Sr_{0.40}$ stoichiometry which is slightly different from the information provided by feedstock supplier, i.e. $Ba_{0.68}Sr_{0.32}TiO_3$.

3.3. Electrical properties of the deposits

The DC resistance was measured until the resistance value was fully stabilized. Measuring time step size was set to one data point per second (dps) and the data were continuously recorded and processed until stabilization was established. It took between 60 and 90 minutes for the DC resistance to stabilize. This behavior is associated with the dielectric polarization, i.e. capacitance charging. When all transient processes are done, the resistance value represents the real DC resistance. For illustration, the time evolution of DC resistance for one of the BST 150 samples is given, Fig. 2.

Obtained results show that samples sprayed at 150 mm have the highest DC resistivity and samples sprayed at 100 mm have in
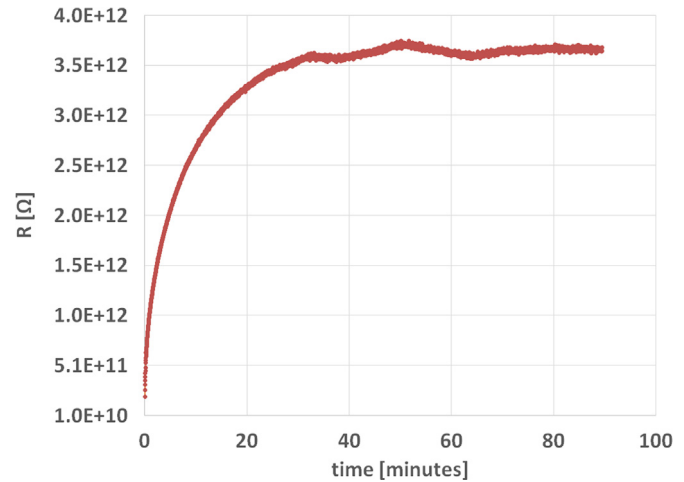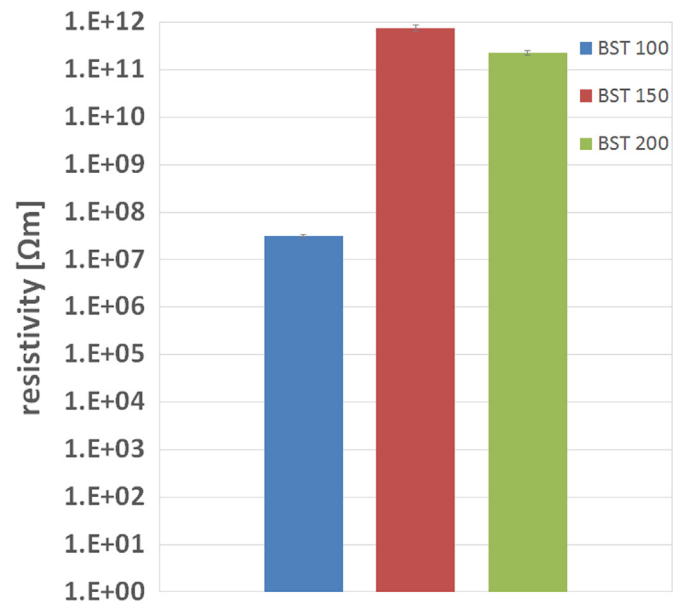
four orders of magnitude lower value, Fig. 3. Standard deviation for all samples sprayed at different spray distances is lower than 10%. A clear correlation between amorphous phase content in coatings and DC resistivity was observed. Samples with high amorphous phase content exhibit high resistivity.

Frequency dependence of relative permittivity decreases with increasing of amorphous content in the coating, Fig. 4. Sample BST 150 with estimated amorphous content of about 38 wt% has weak frequency dependence and significantly lower permittivity value especially in low frequency range when compared to other samples. Standard deviation is lower than 3 for all measured frequencies. Two other samples exhibit higher permittivity value as well as bigger standard deviation. BST 100 has similar frequency dependence as BST 200. That holds true for low frequencies. For high frequency range is the behavior rather like for BST 150.

Frequency dependence of loss factor, that represents power losses in dielectrics, is given, Fig. 5. BST 100 sample exhibits significantly higher loss factor when compared with two other samples. High loss factor as well as low DC resistivity is commonly associated with presence of oxygen vacancies in the coatings [17]. Stoichiometry is affected in a reducing plasma atmosphere of APS process. The re-oxidation of particles can take place with increase

Table 3
Rietveld analysis results of feedstock and coating deposits.

Sample ID	Lattice parameters (Å)	CDD (nm)	Amorphous content (wt%)
Feed Stock	3.9632 ± 0.0001	55 ± 1	–
BST 100	3.9719 ± 0.0002	47 ± 1	5
BST 150	3.9721 ± 0.0003	55 ± 2	38
BST 200	3.9716 ± 0.0001	70 ± 1	15

Fig. 4. Frequency dependence of relative permittivity.

Fig. 5. Frequency dependence of loss factor.

Fig. 6. The band gap estimation.

conduction band [20]. Band gap values for plasma sprayed $BaTiO_3$ were reported between 2.64 eV and 3.25 eV [10]. Similar value 3.2 eV was determined for $SrTiO_3$ single crystal [21]. Different run of the curve corresponding to BST 100 spectra represents lower absorbance for radiation energies below 3 eV.

3.5. Microstructural observations of the coatings

Microstructures of coatings are displayed in Fig. 7. All coatings contain typical lamellar microstructure. BST 100 and BST 150 samples have similar porosity, $5.4 \pm 0.6\%$ and $4.9 \pm 0.6\%$ respectively.

Sample sprayed at longest spray distance exhibits slightly higher porosity with higher standard deviation as well. Value of $8.6 \pm 1.8\%$ shows that spray distance is most likely too long and resulting in less compacted coating. Please note, that typical spray distance for plasma spraying using F4 plasma torch is rarely longer than 150 mm. When the coating´s electrical properties and porosity values were compared, it is realizable that porosity is not the main factor affecting coatings behavior in the electrical field.

Vickers hardness data show decrease in hardness with increasing of spray distance. Observed values are 555, 477 and 325 $HV_{0.3}$ for BST 100, BST 150 and BST 200 respectively. Standard deviation for all measurements was below ± 15 $HV_{0.3}$. Hardness of a thermal spray deposited material is governed not only by the intrinsic elastic properties of constituents forming the structure, but also by the interlamellar bonding between the splats and pore density. In plasma sprayed ceramics, the coating elastic properties are significantly lower compared to bulk counterparts. There is a clear correlation between particle diagnostic results on one side and hardness of the coatings on the other. Considering porosity, its low values are obtained for the shortest spray distance.

4. Conclusions

In this article, an attempt was made to investigate the effect of
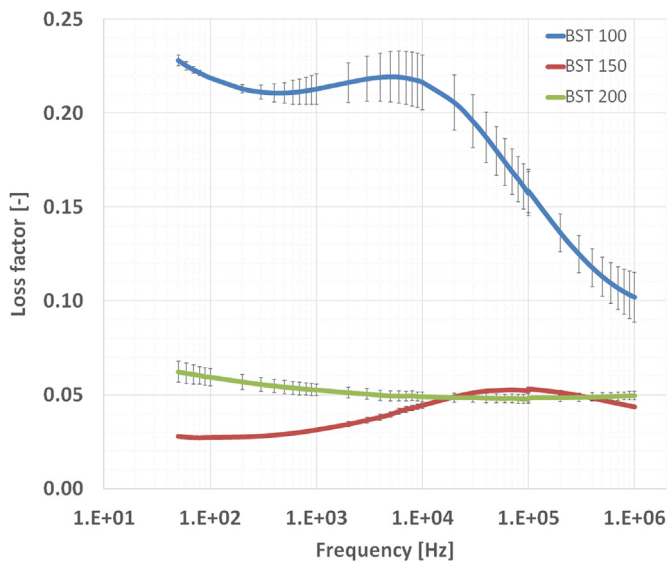
of spray distance [18,19]. This is also illustrated by DC resistivity measurements Fig. 3. BST 100 has significantly lower resistivity as well as the highest loss factor among all the samples. Nevertheless, dielectric properties are most likely affected by degree of crystallinity in the coating. This two effects takes place in the case of BST coating. Frequency stable permittivity as well as loss factor values are advantageous for applications where the signal frequency is tuned.

3.4. Optical properties of the coatings

To assess the shape and the position of the absorption edge of the material we measured the total reflectance R_{total} by integration sphere. Following assumption that the transmittance is zero, the absorptance is then calculated as $1–R_{total}$. The relation between absorption coefficient α and $1–R_{total}$ is however not as straightforward. Data obtained from reflectance measurements was used for estimation of the band gap. The band-gap estimation is given, Fig. 6.

The band gap lies between 2.75 eV and 2.9 eV for all spray distances when assuming direct transition between valence and
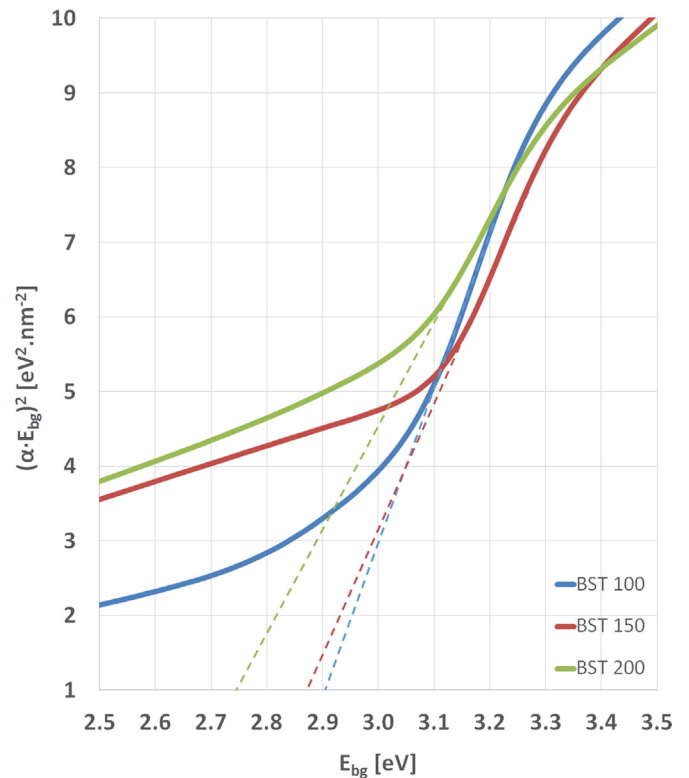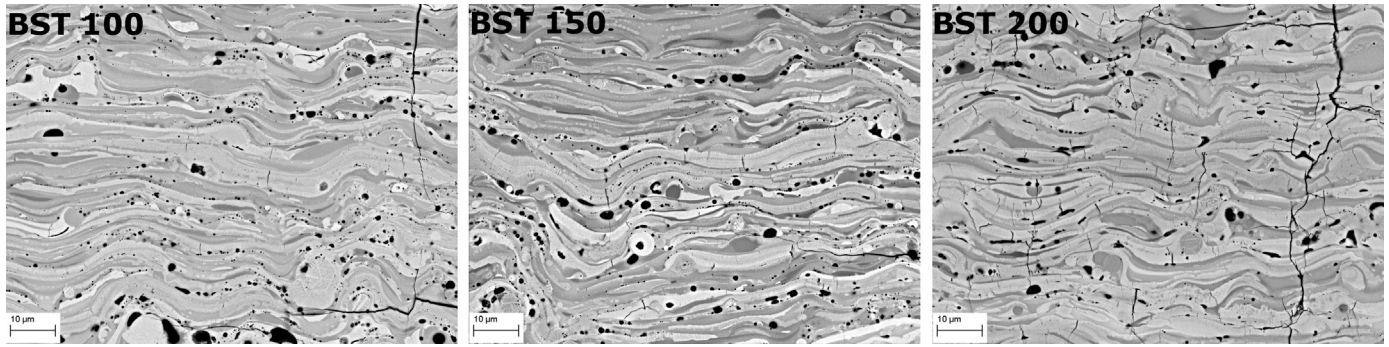
Fig. 7. SEM observations on polished cross sections of deposits.

amorphous phase content on electrical properties of atmospheric plasma sprayed $(Ba,Sr)TiO_3$ coatings. Three set of samples were plasma spray deposited using different spray distances. Final coatings contained 5, 15 and 38 wt% of amorphous phase. Results of DC resistivity measurements show clear correlation between amorphous phase content and electrical resistivity. Sample BST 150 containing 38 wt% of amorphous phase exhibits four orders of magnitude higher resistivity when compared to the BST 100 with 5 wt% of amorphous phase. Not only degree of crystallinity but also oxygen vacancies, preferably generated at short spray distances due to reduction in plasma atmosphere, affected the conductivity of the deposits. Loss factor value is linked to the resistivity of the material because a conduction mechanism of electrical losses is associated with electrical resistivity. BST 100 exhibits the highest relative permittivity for low frequencies as well as the highest loss factor for the whole frequency range. Other two samples containing significantly higher amorphous phase content have loss factor nearly ten times lower and much less dependent on frequency. Frequency dependence of relative permittivity for BST 150 and BST 200 is linear and the absolute value decreases with increase of amorphous phase content.

In general, increase in amorphous phase content results in an increase in DC resistivity and reduction in relative permittivity value for low frequencies. Frequency dependence of relative permittivity is weak for samples containing 15 wt% of amorphous phase content and more. Sample BST 200, with 15 wt% of amorphous phase content, exhibits the best electrical properties of all studied samples due to relatively high permittivity value and low frequency dependence on relative permittivity (200 for 1 kHz) and relatively low loss factor (0.05) in the whole frequency range. In contrary, its porosity is the highest and microhardness is the lowest. The porosity is therefore not the main parameter affecting coatings electrical properties. Based on literature research this level of mechanical properties is satisfactory.

Acknowledgments

References

[1] N. Setter, R. Waser, Electroceramic materials, Acta Mater. 48 (2000) 151–178.
[2] S. Sampath, Thermal spray applications in electronics and sensors: past, present, and future, J. Therm. Spray Technol. 19 (5) (2010) 921–949.
[3] Ce-Wen Nan, M.I. Bichurin, Shuxiang Dong, D. Viehland, G. Srinivasan, Multiferroic magnetoelectric composites: historical perspective, status, and future directions, J. Appl. Phys. 103 (2008) 031101.
[4] M.M. Vijatović, J.D. Bobić, B.D. Stojanović, History and challenges of barium titanate: Part II, Sci. Sinter. 40 (2008) 235–244.
[5] Z. Song, H. Liu, H. Hao, S. Zhang, M. Cao, Z. Yao, Z. Wang, W. Hu, Y. Shi, B. Hu, The effect of grain boundary on the energy storage properties of $(Ba_{0.4}Sr_{0.6})$ TiO_3 paraelectric ceramics by varying grain sizes, IEEE Trans. Ultrason. Ferroelectr. Freq. Control 62 (4) (2015) 609–616.
[6] A.H. Dent, A. Patel, J. Gutleber, E. Tormey, S. Sampath, H. Herman, High velocity oxy-fuel and plasma deposition of $BaTiO_3$ and $(Ba, Sr)TiO_3$, Mater. Sci. Eng. B87 (2001) 23–30.
[7] K. Ahn, B.W. Wessels, S. Sampath, Dielectric properties of plasma-spray-deposited $BaTiO_3$ and $Ba_{0.68}Sr_{0.32}TiO_3$ thick films, J. Mater. Res. 18 (5) (2003) 1227–1231.
[8] K. Ahn, B.W. Wessels, R. Greenlaw, S. Sampath, Dielectric Properties of Spray Deposited $BaTiO_3$ and $Ba_{0.68}Sr_{0.32}TiO_3$, Materials Research Society Proceedings: Electroactive Polymers and Rapid Prototyping, Direct Write Electronics, 2001.
[9] Z. Xing, H. Wang, L. Zhu, X. Zhou, Y. Huang, Properties of the $BaTiO_3$ coating prepared by supersonic plasma spraying, J. Alloy. Compd. 582 (2014) 246–252.
[10] P. Ctibor, H. Ageorges, V. Štengl, N. Murafa, I. Píš, T. Zahoranová, V. Nehasil, Z. Pala, Structure and properties of plasma sprayed $BaTiO3$ coatings: spray parameters versus structure and photocatalytic activity, Ceram. Int. 37 (2011) 2561–2567.
[11] A.H. Pakseresht, M.R. Rahimipour, M.R. Vaezi, M. Salehi, Effect of splat morphology on the microstructure and dielectricproperties of plasma sprayed barium titanate films, Appl. Surf. Sci. 324 (2015) 797–806.
[12] S. Sampath, H. Herman, Rapid solidification and microstructure development during plasma spray deposition, J. Therm. Spray Technol. 5 (4) (1996) 445–456.
[13] P. Ctibor, J. Sedlacek, Z. Pala, Structure and properties of plasma sprayed $BaTiO_3$ coatings after thermal posttreatment, Ceram. Int. 41 (6) (2015) 7453–7460.
[14] J. Kotlan, R.C. Seshadri, S. Sampath, P. Ctibor, Z. Pala, R. Musalek, On the dielectric strengths of atmospheric plasma sprayed Al_2O_3, Y_2O_3, ZrO_2–7% Y_2O_3 and $(Ba,Sr)TiO_3$ coatings, Ceram. Int. 41 (9) (2015) 11169–11176.
[15] M.K. Reddy, S.V. Manorama, A.R. Reddy, Bandgap studies on anatase titanium dioxide, Mater. Chem. Phys. 78 (2002) 239–245.
[16] G. Mauer, R. Vaßen, D. Stöver, Comparison and applications of DPV-2000 and accuraspray-g3 diagnostic systems, J. Therm. Spray Technol. 16 (2007) 414–424.
[17] A. Kalabukhov, R. Gunnarsson, J. Börjesson, E. Olsson, T. Claeson, D. Winkler, Effect of oxygen vacancies in the $SrTiO_3$ substrate on the electrical properties of the $LaAlO_3/SrTiO_3$ interface, Phys. Rev. B 75 (2007) 121404(R).
[18] H.B. Xiong, L.L. Zheng, L. Li, A. Vaidya, Melting and oxidation behavior of in-flight particles in plasma spray process, Int. J. Heat Mass Transf. 48 (2005) 5121–5133.
[19] H.K. Seok, E.Y. Choi, P.R. Cha, M.C. Son, B.L. Choi, et al., Characterization of plasma-sprayed Y_2O_3 coating and investigation of its visual aspect change, Surf. Coat. Technol. 205 (2011) 3341–3346.
[20] M.K. Reddy, S.V. Manorama, A.R. Reddy, Bandgap studies on anatase titanium dioxide, Mater. Chem. Phys. 78 (2002) 239–245.
[21] A. Kalabukhov, R. Gunnarsson, J. Börjesson, E. Olsson, T. Claeson, D. Winkler, Effect of oxygen vacancies in the $SrTiO_3$ substrate on the electrical properties of the $LaAlO_3$ $SrTiO_3$ interface, Phys. Rev. B 75 (12) (2007) 121404.

4.6 On reactive suspension plasma spraying of calcium titanate

All previous papers in this thesis studied plasma deposited titanates with focus on the role of spray parameters on their physical properties. This paper presented a new technique for deposition of calcium titanate. This promising material was studied in the first three papers of the collection. Standard manufacturing process of calcium titanate lies in reactive sintering of calcium titanate precursors which are calcium carbonate and titania. The paper shows possibility to deposit calcium titanate not only from calcium titanate powder as shown in previous papers but due to the high entalpy of WSP-H plasma torch chemical reaction of precursors took place during interaction with plasma yet and consequent additional reaction on the substrate was observed as well. Coating's deposition process need to be improved for any application as dielectric material but tailoring of coatings microstructure was not the aim ot this study. Important is that a novel reactive plasma spraying technique was successfully introduced.

On reactive suspension plasma spraying of calcium titanate

Jiri Kotlan[a,b,*], Zdenek Pala[a], Radek Musalek[a], Pavel Ctibor[a]

[a]Materials Engineering Department, Institute of Plasma Physics CAS, v. v. i., Za Slovankou 3, 182 00 Prague 8, Czech Republic
[b]Department of Electrotechnology, Faculty of Electrical Engineering, Czech Technical University in Prague, Technicka 2, 166 27 Prague 6, Czech Republic

Abstract

This study shows possibility of preparation of calcium titanate powder and coatings by reactive suspension plasma spraying. Suspension of mixture of calcium carbonate ($CaCO_3$) and titanium dioxide (TiO_2) powders in ethanol was fed into hybrid plasma torch with a DC-arc stabilized by a water–argon mixture (WSP®-H 500). Various feeding distances and angles were used in order to optimize suspension feeding conditions. In the next step, the coatings were deposited on stainless steel substrates and the effect of substrate temperature on microstructure and chemical and phase composition of the coatings was studied. Captured in-flight particles and deposits were analysed by X-ray diffraction (XRD) and scanning electron microscopy SEM equipped with EDX detector. Obtained results confirm that chemical reaction of $CaCO_3$ and TiO_2 forming $CaTiO_3$ perovskite takes place during the interaction of suspension with plasma jet. The conditions of rapid cooling during spraying process result in the presence of metastable $CaTiO_3$ high-temperature tetragonal and cubic phases. Increase in the substrate temperature increases the content of the calcium titanate in the deposit and the coatings microstructure becomes more compact. Obtained results show that WSP®-H technology may be used for deposition of the $CaTiO_3$ powders and coatings by reactive plasma spraying.
© 2015 Elsevier Ltd and Techna Group S.r.l. All rights reserved.

1. Introduction

Employing suspensions in thermal spray technology brings a new opportunity for deposition of functional coatings. Fine particles dispersed in the liquid allow to build coatings microstructure from submicron or even nano-sized particles. Much finer splats (up to two orders of magnitude smaller) when compared to the spraying from conventional powder feedstock can be achieved [1,2]. That may result in interesting materials properties such as low thermal conductivity, improved hardness or fracture toughness [3,4].

Reactive plasma spraying has recently become widely studied around the world. In general, this term may denote two different spraying approaches. First, reactions between the sprayed material and surrounding reactive atmosphere. This approach is used e.g. for formation of hard titanium nitride composites in nitrogen-rich atmosphere [5–8]. In the second approach, reactions between feedstock constituents take place [9–11].

Calcium titanate which was deposited from conventional powder feedstock in our previous studies [12,13] seems to be a promising candidate for reactive plasma spraying. This material shows interesting dielectric properties perspective for electronics industry [14–17]. The goal of this study was to achieve formation of calcium titanate ($CaTiO_3$) during plasma spraying by reaction between titanium dioxide (TiO_2) and calcium carbonate ($CaCO_3$). This approach would eliminate the need of several feedstock preparation steps, including calcination, crushing and sieving, thus significantly reducing manufacturing costs with benefits of fine microstructure.

The hybrid water-stabilized plasma torch was employed in this study. The high enthalpy of this torch is promising for suspension processing due to a high achievable feed rate up to tens of kilograms of powder per hour for conventional powders.

Possibility of suspension processing by water stabilized plasma technology has been already demonstrated on suspension spraying of YSZ [18].

The focus of the paper is in introduction of potentially interesting novel method of production of $CaTiO_3$ powders and layers by reactive suspension plasma spraying. In this study, plasma treated particles were analysed in order to evaluate in-flight chemical and phase composition changes to get information about feedstocks reaction during in-flight stage. The optimized spraying conditions providing high amount of desirable perovskite phase in the product were used in coating deposition experiments with a deliberately controlled substrate temperature.

2. Experimental procedure

The mixture of commercial purity calcium carbonate ($CaCO_3$ – calcite) and finer titanium dioxide (TiO_2 – anatase) powders was prepared with mass ratio (56 wt% $CaCO_3$, 44 wt% TiO_2) required for the formation of stoichiometric calcium titanate ($CaTiO_3$) and used as an initial material for this study. The same approach is commonly used also for commercial sintering of bulk calcium titanate dielectrics. The laser diffraction particle size analysis of the mixed feedstock performed with Mastersizer 3000 (Malvern Instruments, UK) shows bi-modal distribution of the particle distribution with two distinguishable peaks at 3 µm and 0.5 µm for $CaCO_3$ and TiO_2, respectively (Fig. 1). Tendency of formation of agglomerates in liquid with particle size in the range of tens of microns to about 200 µm is also observable from Fig. 1. Sprayable suspension of this mixture in ethanol (20 wt% solids) was prepared by mechanical mixing followed by ultrasonic agitation.

Hybrid Argon-Water stabilized plasma torch WSP®-H 500 (Institute of Plasma Physics CAS, v.v.i., CZ) operated at Argon flowrate 15 slpm and power of 150 kW (500 A, 300 V) and with external radial injection was used for plasma spraying. First, in-flight particles of sprayed suspension were capture into water bath. Particles were analysed in order to determine the optimal feeding conditions which were in the next step used for deposition of suspension on AISI 304 steel substrates. Grit-blasted substrates ($120 \times 25 \times 4$ mm^3) were mounted to a static sample holder and prior to the deposition degreased by acetone. Substrate temperature was evaluated during deposition by K-type thermocouple attached to the rear side of the substrate.
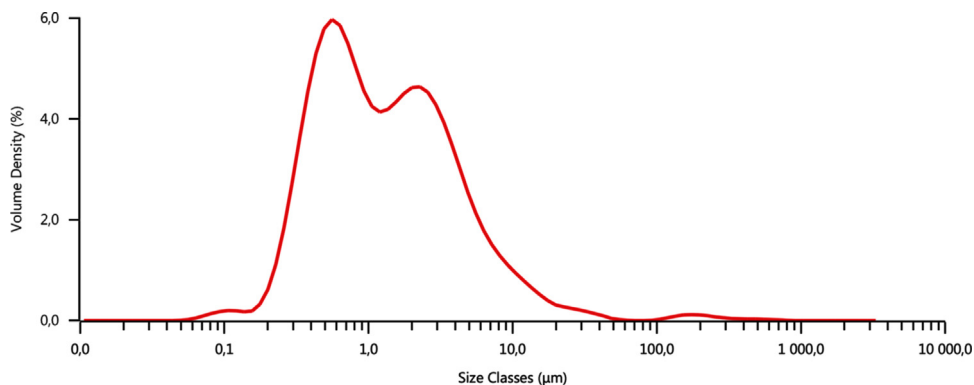
Pneumatic feeding system (Institute of Plasma Physics CAS, v.v.i., CZ) with separate purging liquid (ethanol) and suspension tanks with ultrasonic agitation was used for liquid injection through the sapphire nozzle with circular orifice (diameter 0.5 mm) providing a laminar liquid stream. Spray-Cam system (Control Vision Inc., USA) using 905 nm laser was used for optimization of the droplets trajectory by variation of suspension injection pressure and visualization of the liquid stream break-up in the plasma jet.

First, nine in-flight experiments with different feeding conditions were carried out in order to find optimum feeding conditions to maximize efficiency of the calcium titanate formation. Feeding distance (i.e. distance between the plasma nozzle and the feeding point) and the feeding angle were varied (see Fig. 2). Based on the obtained results, four deposition experiments with different substrate temperature were performed with optimized feeding conditions in order to observe expected effect of deposition temperature on the coating microstructure.

All samples, as well as in-flight captured particles, were analysed by X-ray diffraction. Measurements were performed on D8 Discover Bruker diffractometer in Bragg–Brentano setup using filtered CuKα radiation and 1D LynxEye detector. Diffraction patterns were analyzed by Rietveld method in TOPAS 4.2 software employing principles from [19,20]. The quantitative Rietveld refinement was performed with structural files from ICSD (Inorganic Crystal Structure Database). Materialographic samples were prepared on automatic polishing system Tegramin-25 (Struers, Denmark) to assure identical preparation conditions for all samples. Polished cross-sections and free-surfaces were observed using EVO MA 15 scanning electron microscope (Carl Zeiss SMT, Germany) equipped with EDX detector. Microhardness measurements were carried out using microhardness tester Nexus 4504 (Innovatest, the Netherlands) equipped with a Vickers indenter. The load 100 g was used. Obtained value is an average value from 20 indentations.

3. Results and discussion

3.1. Injection optimization

External feeding allowed to set different injection angles and feeding distance. A total of nine conditions (see further) were performed as is illustrated in Fig. 2.

Fig. 1. Particle distribution in feedstock powder (mixture of $CaCO_3$ and TiO_2).
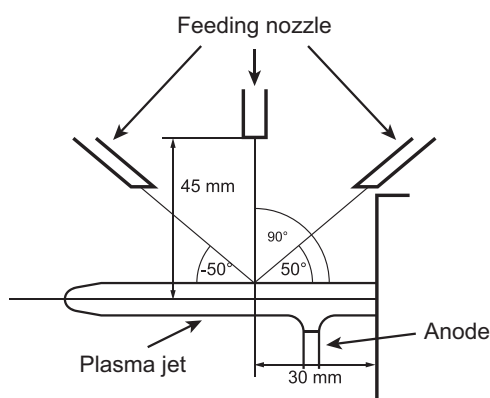
Fig. 2. Three different feeding angles for 30 mm feeding distance. The same angles for feeding nozzle were used for feeding distances 50 mm and 70 mm.

Table 1
Optimal pressure in the suspension vessel and appropriate feed rate at different feeding arrangements.

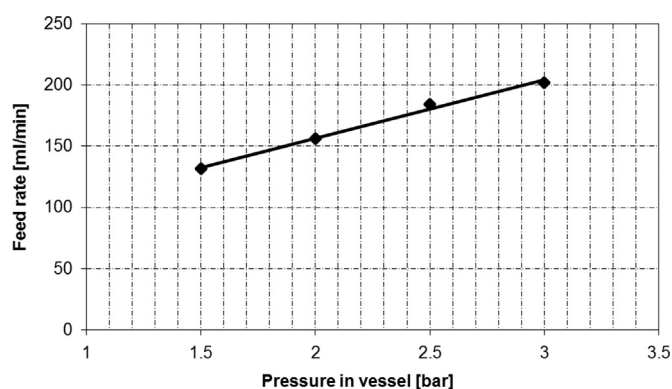|		Feeding angle [°]		
		−50	50	90
		Pressure in vessel [bar] (Feed rate [ml/min])		
Feeding distance [mm]	30	2.20 (165)	2.50 (185)	2.00 (155)
	50	1.00 (110)	1.50 (131)	1.30 (125)
	70	0.75 (95)	0.90 (105)	0.85 (100)

Fig. 3. Feed rate dependence on the vessel pressure for 0.5 mm output nozzle.

The suspension flow rate depends on the adjustable tank pressure which controls a feeding pressure at the injector. This pressure has to be adjusted for each feeding setup due to different plasma flow characteristic at the injection point position. Plasma density and velocity naturally decreases with the increasing distance from the plasma torch nozzle. That results in fact that the pressure in the feeding system needs to be lower for longer feeding distance in order to properly penetrate the suspension into the plasma jet and not to overshoot the plasma core. Feed rate dependence on pressure in the suspension vessel is shown in Fig. 3.

It is obvious, that lower feeding pressure leads to lower feedrate which influences also the momentum of the liquid stream. Moreover, liquid stream break-up is substantially influenced by the choice of injection point and relative velocity of the stream with respect to the plasma axis (feeding angle). Due to the complexity of the injection process feeding pressure was optimized with the SprayCam system in order to achieve optimum suspension trajectory. Optimal pressure values in suspension vessel for used setup are given Table 1. The liquid stream penetration into the core of the plasma jet and fragmentation of the stream may be illustrated in Fig. 4. In general, injection angle substantially affects liquid stream

breakdown and particles trajectory in the plasma jet. Particles trajectory is narrow and droplet dwell time in the plasma jet is longer when positive injection angle is used, because the most of the particles penetrate directly into core of the plasma jet. Using negative angle and injection perpendicular to the plasma jet results in less homogenous penetration into the jet and wide angle of particle projection causing insufficient thermal treatment of the feedstock (see Fig. 4).

3.2. In-flight stage

Deposition conditions were optimized in nine spraying experiments. Feeding distance and feeding angles were varied from 30 mm to 70 mm and −50° to 90°, respectively (see Table 1). Successful transformation of $CaCO_3$ and TiO_2 powders into $CaTiO_3$ during plasma processing may be illustrated on the comparison of dried suspension and in-flight captured particles in Fig. 5.

The Fig. 5. – left shows good homogenization of the feedstock and that finer TiO_2 formed around $CaCO_3$ particles agglomerates with typical size about 100 nm. Suspension fragmented in plasma jet formed droplets containing numerous particles of both feedstock powders dispersed in the ethanol solvent. After evaporation of ethanol, feedstock powders were fused forming spherical particles of up to 10 μm in diameter.

Successful formation of calcium titanate is evident from the comparison of XRD patterns of the feedstock and plasma-treated powders, Fig. 6. According to the Rietveld refinement, the feedstock powder contained anatase and two crystalline forms of $CaCO_3$, orthorhombic aragonite and trigonal calcite, with weight fractions of 50:6:44 wt% for calcite, aragonite and anatase, respectively. The phase composition of plasma-treated powders is markedly different with desired $CaTiO_3$ perovskite phases with overall content up to 80 wt% according to the Rietveld refinement, Table 2.

Perovskite diffraction profiles exhibited visible asymmetry (e.g. diffraction profile at 33° 2θ of pattern II in Fig. 6) which can be attributed to the presence of orthorhombic, tetragonal and cubic perovskite phases. Indeed, the Rwp factors characterizing quality of the fits of Rietveld refinement [21] improve significantly when the high temperature phases are taken into account, i.e. $Rwp=12.6$ only for orthorhombic perovskite, $Rwp=8.3$ with inclusion of tetragonal phase and $Rwp=7.7$ with orthorhombic, tetragonal and cubic crystalline forms (see Fig. 7). Please note that there is a significant overlap of tetragonal and cubic phases'
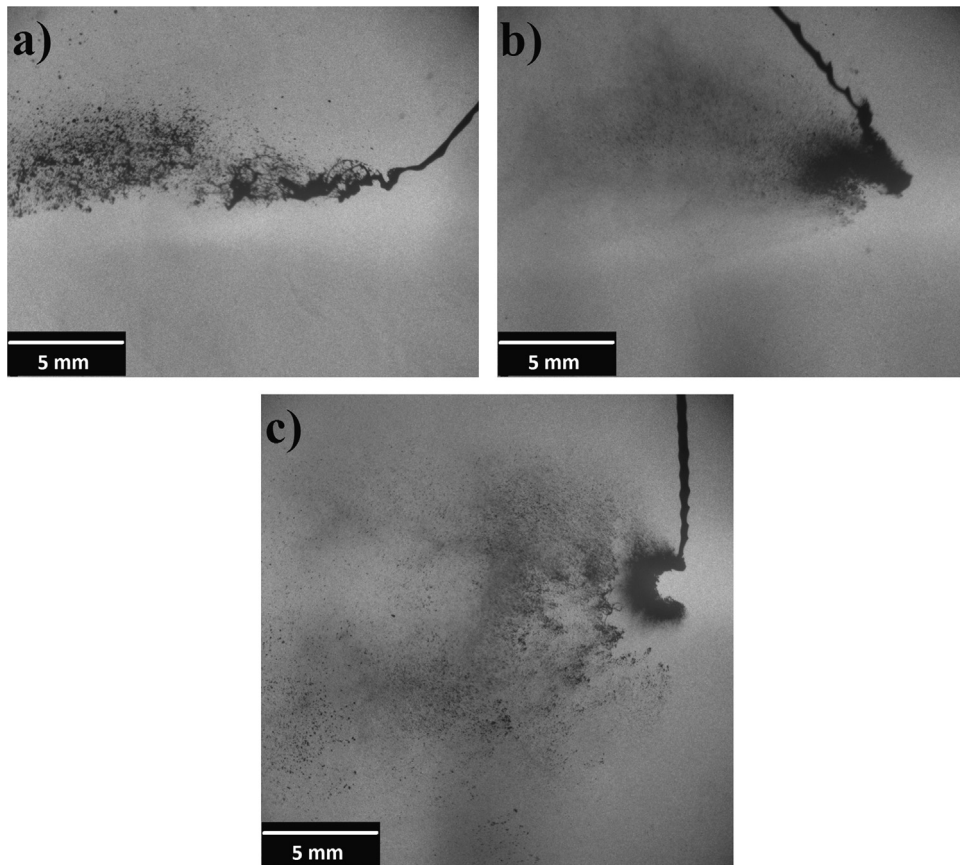
Fig. 4. Suspension penetration into plasma jet for 30 mm feeding distance and (a) 50° feeding angle, (b) −50° feeding angle and (c) 90° feeding angle.

diffraction profiles which leads to a reduced accuracy of the mutual weight ratio of these phases. The occurrence of high-temperature or metastable phases in either plasma as-sprayed deposits or plasma processed powders is not anomalous as shown by e.g. [22–24] with the most notable case being the stabilized tetragonal zirconia with monoclinic to tetragonal phase transition range 990–1220 °C [25]. Moreover, tetragonal and high-temperature cubic BaTiO$_3$ perovskites were detected by XRD in nanostructures prepared by hydrothermal method [26].

The highest overall content of calcium titanate phases was observed for the setup with 50 mm feeding distance, 50° feeding angle and 1.5 bar feeding pressure. However, setup with 30 mm feeding distance, 50° feeding angle and 2.5 feeding pressure (further noted as "optimum") was chosen for the following deposition experiments due to significantly higher feed rate (11.1 vs 7.9 l per hour) which is desirable for efficiency of the spraying process. Please note that the used feed rate is rather high when compared to the standard atmospheric plasma spraying of suspensions [27,28]. Results of phase analysis of the captured in-flight particles are in a good agreement with optimization of suspension injection as visualized with SprayCam. The fact, that the content of calcium titanate is the highest for the positive angle +50° for all feeding distances confirms the expectation from the shadowgraphy observation that positive angle provides the most appropriate thermal treatment and particles trajectory along the plasma jet axis.

3.3. Coating deposition

Four experiments were carried out with spraying on static stainless steel substrate. Feeding conditions (feeding distance 30 mm, feeding angle 50°, feed rate 11.1 l/h) were chosen according to the previous optimization, see Section 3.2. The spraying distance was set to 100 mm as a compromise between demanded deposition velocity and heat transfer to the substrate. Traversal speed of the robot handling the plasma spray torch 400 mm/s was used.

During the experiment, substrate temperature was controlled by number of preheating and spraying passes in order to study its expected influence on the coating microstructure and phase composition, in particular presence of metastable high-temperature phases, Table 3. Each spray cycle began when the substrate temperature reached the targeted value of the preheating temperature, see Fig. 8.

Spraying at higher substrate temperatures enabled deposition with more cycles due to lower demands on cooling, resulting in relatively more stable temperature during the whole process. However, the coatings with "cauliflower-like" microstructure (Fig. 9) were successfully deposited for all deposition conditions on the whole coated surface with a similar deposition efficiency (2–4 μm per spraying pass, Table 3).

Cross-sections of selected samples are illustrated in Fig. 10. All coatings exhibited a rather porous lamellar microstructure typical
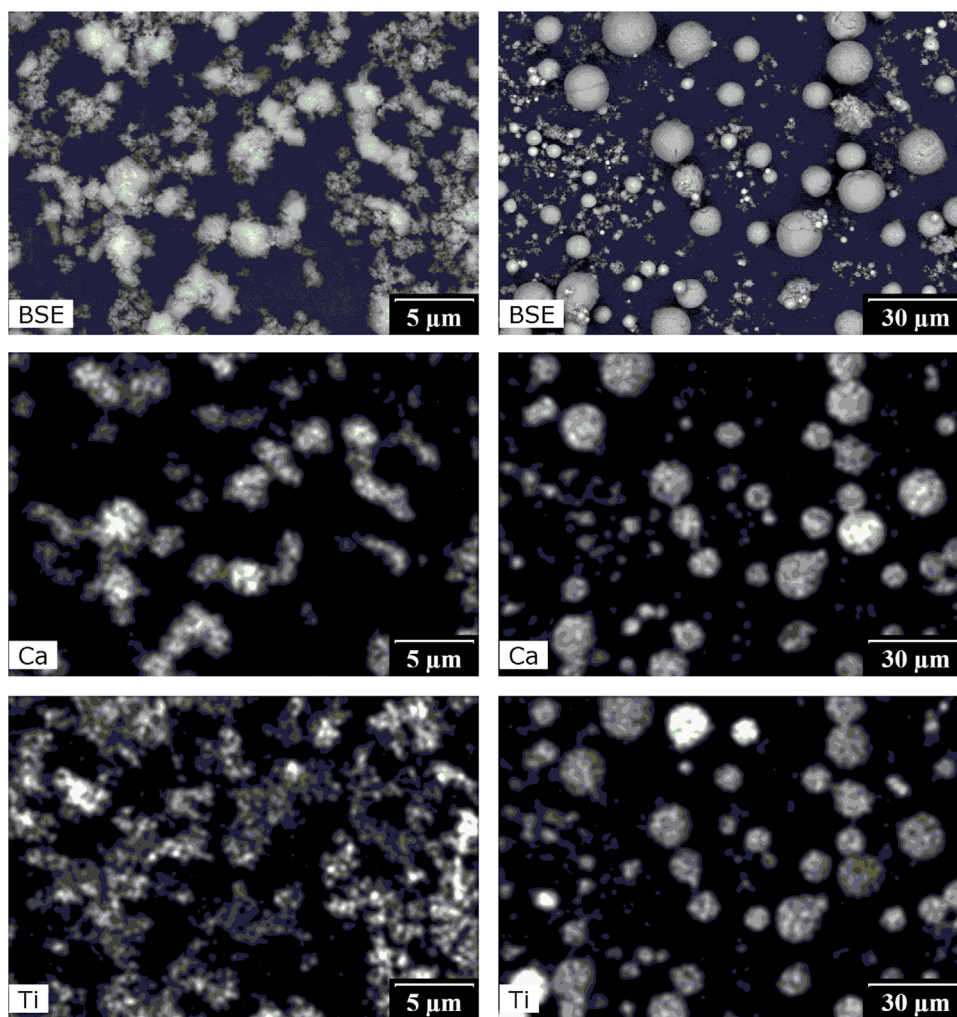
Fig. 5. EDX maps of mixture of $CaCO_3$ and TiO_2 feedstock powder (left) and plasma-treated particles collected after plasma processing (right). Feeding distance 30 mm, feeding angle 50°. Please note different magnifications.
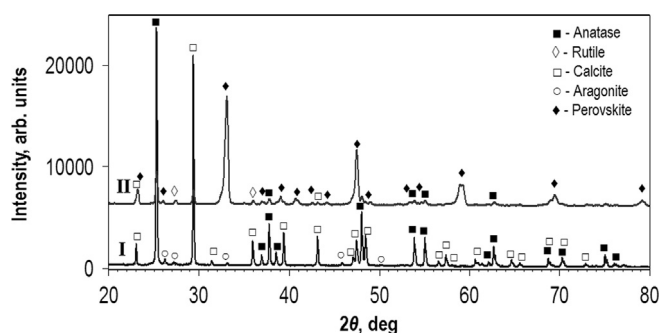

Fig. 6. Powder diffraction patterns and phase identification of feedstock powder (I) and powder processed with feeding distance 30 mm and feeding angle 50° (II).

for suspension plasma sprayed coatings consisting of flattened and spherical splats and containing both open and submicron-sized closed spherical pores. Lack of contrast in the images obtained with BSE detector in SEM indicates a satisfactory homogeneity of the deposit. Increase in the substrate temperature

Table 2

Phase composition of in-flight captured particles for different feeding conditions.

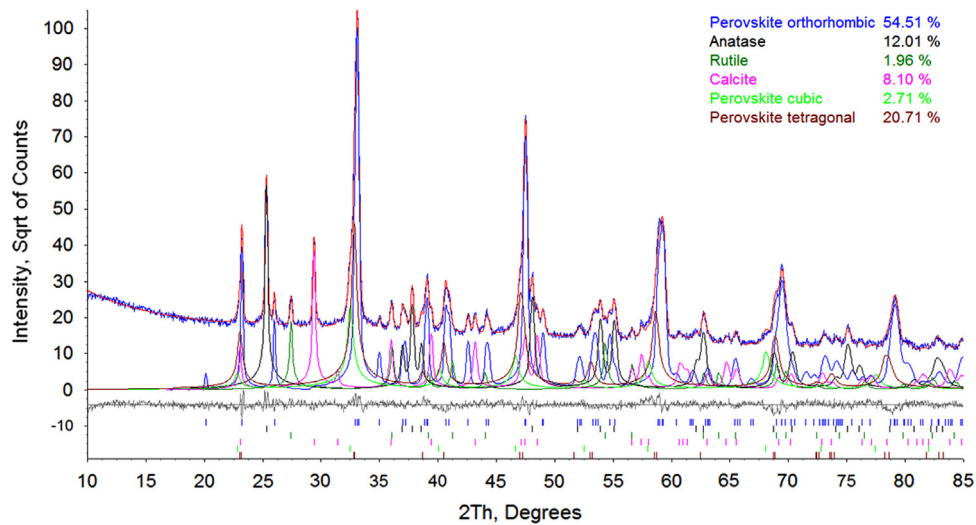|			Feeding angle [°]		
		Material	−50	50	90
			Phase content [%]		
Feeding distance [mm]	30	$CaTiO_3$ phases	41.6	77.9	68.7
		TiO_2 (Anatase)	27.1	12.0	17.9
		TiO_2 (Rutile)	19.3	2.0	4.5
		$CaCO_3$ (Aragonite)	–	–	–
		$CaCO_3$ (Calcite)	12.0	8.1	8.9
	50	$CaTiO_3$ phases	36.8	81.4	21.0
		TiO_2 (Anatase)	29.3	10.2	37.6
		TiO_2 (Rutile)	22.3	1.9	4.9
		$CaCO_3$ (Aragonite)	–	–	2.9
		$CaCO_3$ (Calcite)	11.6	6.5	33.6
	70	$CaTiO_3$ phases	67.3	72.6	56.4
		TiO_2 (Anatase)	17.5	17.0	23.1
		TiO_2 (Rutile)	9.7	1.1	3.0
		$CaCO_3$ (Aragonite)	0.2	–	1.3
		$CaCO_3$ (Calcite)	5.3	9.3	16.2

Fig. 7. Rietveld refinement of powder processed with feeding distance 30 mm and feeding angle 50°.

Table 3
Spraying setup and coating's characteristics.

Sample notation	A	B	C	D
Number of preheating passes	1	3	4	5
Preheating temperature [°C]	170	370	450	530
Number of spray passes (cycles × passes)	8 × 2	12 × 2	17 × 2	23 × 2
Coating thickness [µm]	45 ± 11	90 ± 12	60 ± 21	130 ± 24
Thickness per pass [µm]	2.8	3.8	1.8	2.8
Microhardness [HVM0.1]	–*	138 ± 53	111 ± 29	155 ± 57

Note: * – Hardness measurement not available due to insufficient coating thickness.

Fig. 8. Substrate temperature history for all samples.

had a positive effect on flattening ratio of deposited splats resulting in more compact coating (Fig. 10-right).

XRD diffraction patterns for all the coatings are shown in Fig. 11 and results of Rietveld refinement are in Table 4. From the comparison of Tables 2 and 4, it is obvious, that all coatings contained significantly higher amount of perovskite phases when compared to the captured in-flight particles (up to 96.4 wt% for the condition D), which indicates that some additional perovskite formation from residual $CaCO_3$ and TiO_2 takes place even after the deposition on the substrate. Moreover, higher substrate temperature favors desirable orthorhombic phase formation. Furthermore, content of tetragonal and cubic perovskite phases in the deposits decreased with an increase of the substrate temperature which was observable also on decrease of asymmetry of perovskite profiles. This may be explained by the fact that the lower substrate temperatures result in higher cooling rates which promotes preservation of metastable tetragonal and cubic high-temperature phases.

Microhardness values are listed in Table 3. Relatively low hardness values of the presented coatings are not surprising as the coatings microstructure contains numerous voids, i.e. pores and cracks both on micrometric and sub-micrometric scale. However,

the bonding of the splats in the areas of low porosity is high enough to cause not only crushing of the splats under the sharp Vickers indenter and debonding of the splats but also formation of cracks network in the vicinity of the indents (Fig. 12).

4. Conclusions

Calcium titanate powders and coatings were successfully prepared by reactive plasma spraying of ethanol-based suspension containing $CaCO_3$ and TiO_2 powders using WSP®-H 500 spray system. Feeding conditions were optimized in order to maximize efficiency of $CaTiO_3$ formation during in-flight stage. XRD analysis of in-flight captured particles showed a high content of perovskite in the form of orthorhombic $CaTiO_3$ as well as high temperature metastable tetragonal and cubic phases.

Four deposition experiments with controlled substrate temperature and feeding rate of 11.1 l of suspension per hour were carried out. Substrates preheated to more than 450 °C
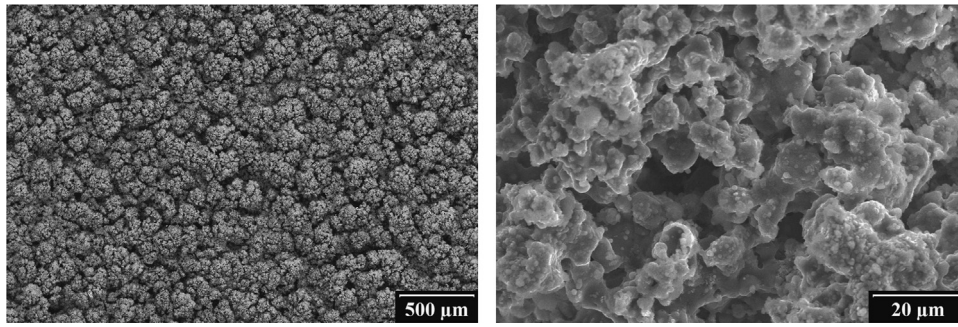
Fig. 9. Free surface of sample D. Variable pressure SE detector. SEM-VPSE.
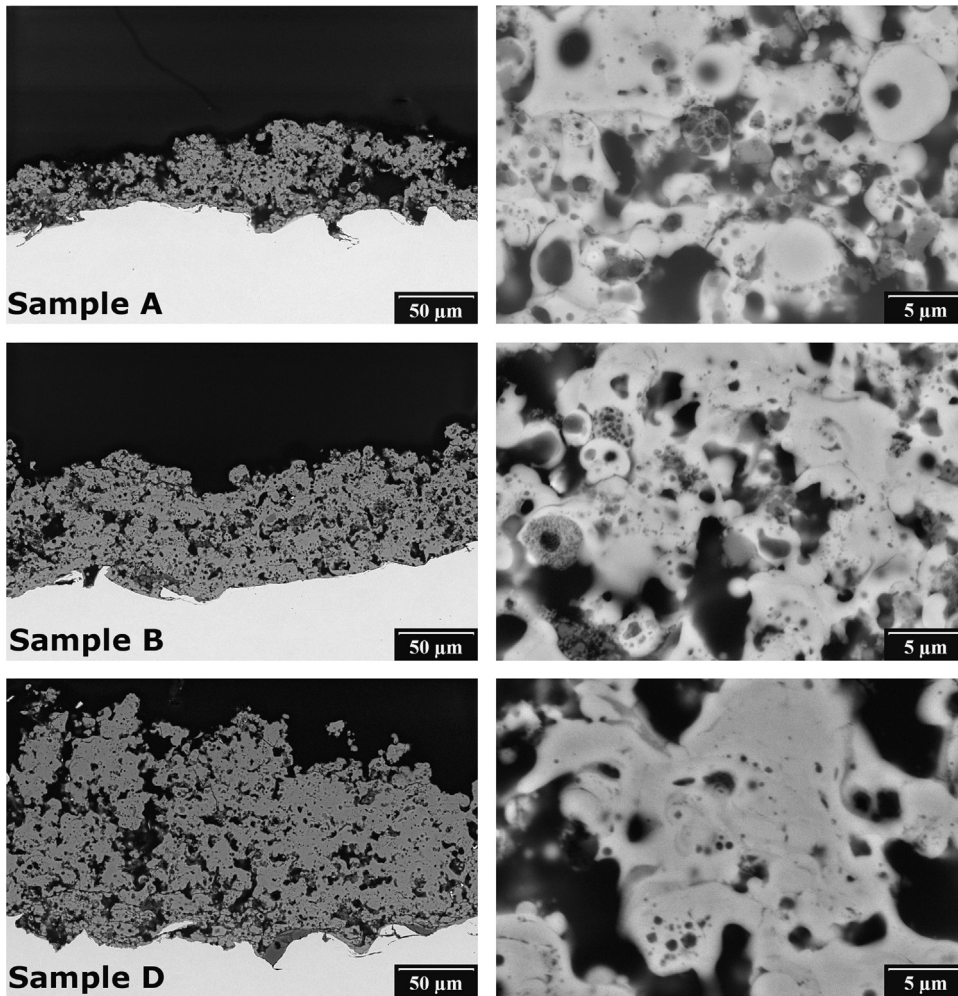
Fig. 10. Coatings cross-sections. Back-scattered electron SEM image.

contained more than 95 wt% of desired calcium titanate phases. From the results, it is obvious that all coatings contained significantly higher amount of perovskite phases when compared to the captured in-flight particles, which implies that some additional perovskite formation from the residual $CaCO_3$ and TiO_2 takes place even after the deposition on the substrate.

Content of tetragonal and cubic perovskite phases in the deposits decreased with an increase of the substrate temperature. Contrary, lower substrate temperatures resulted in higher cooling rates which promoted preservation of metastable high temperature phases. Presented techniques based on reactive suspension plasma spraying may be potentially used for the

Fig. 11. Juxtaposition of XRD patterns of the deposited coatings.

Table 4
Rietveld refinement results for deposited coatings in wt%.

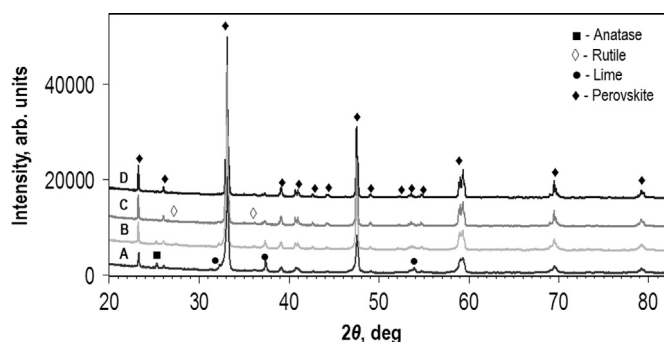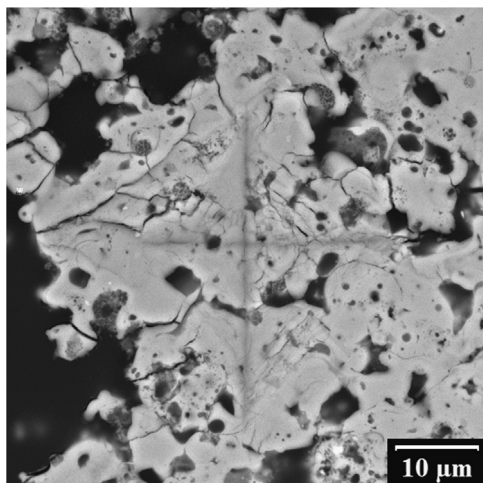| Coating	Perovskites			Anatase	Rutile	Lime	Calcite
	Orthorhombic	Tetragonal	Cubic				
A	90.1			1.4	2	6	< 1
	59.2	23.9	7				
B	92.4			< 1	3.4	3.8	–
	65.4	19	8				
C	95.4			–	2.8	1.8	–
	93.5	1.9	–				
D	96.4			–	2.9	< 1	–
	96.4	–	–				

Fig. 12. Vickers indent on cross-section of sample D.

CaTiO$_3$ coating deposition or preparation of spheroidized CaTiO$_3$ powders.

Acknowledgment

References

[1] C.C. Koch, Nanostructured Material-processing, Properties and Applications, Noyes Publications/William Andrew Publisher, Norwich, NY, USA, 2002.

[2] P. Fauchais, V. Rat, J. Coudert, R. Etchart-Salas, G. Montavon, Operating parameters for suspension and solution plasma-spray coatings, Surf. Coat. Technol. 202 (18) (2008) 4309–4317.

[3] P. Carpio, Q. Blochet, B. Pateyron, L. Pawlowski, M.D. Salvador, A. Borrell, E. Sanchez, Correlation of thermal conductivity of suspension plasma sprayed yttria stabilized zirconia coatings with some microstructural effects, Mater. Lett. 107 (2013) 370–373.

[4] E. Bannier, M. Vicent, E. Rayón, R. Benavente, M.D. Salvador, E. Sánchez, Effect of TiO$_2$ addition on the microstructure and nanomechanical properties of Al$_2$O$_3$ Suspension Plasma Sprayed coatings, Appl. Surf. Sci. 316 (2014) 141–146.

[5] L. Xiao, D. Yan, J. He, L. Zhu, Y. Dong, J. Zhang, X. Li, Nanostructured TiN coating prepared by reactive plasma spraying in atmosphere, Appl. Surf. Sci. 253 (18) (2007) 7535–7539.

[6] A. Kobayashi, Formation of TiN coatings by gas tunnel type plasma reactive spraying, Surf. Coat. Technol. 132 (2–3) (2000) 152–157.

[7] T. Bacci, L. Bertamini, F. Ferrari, F.P. Galliano, E. Galvanetto, Reactive plasma spraying of titanium in nitrogen containing plasma gas, Mater. Sci. Eng. A 283 (1–2) (2000) 189–195.

[8] E. Galvanetto, F.P. Galliano, F. Borgioli, U. Bardi, A. Lavacchi, XRD and XPS study on reactive plasma sprayed titanium–titanium nitride coatings, Thin Solid Films 384 (2) (2001) 223–229.

[9] J. Xu, B. Zou, X. Fan, S. Zhao, Y. Hui, Y. Wang, X. Zhou, X. Cai, S. Tao, H. Maa, X. Cao, Reactive plasma spraying synthesis and characterization of TiB2–TiC–Al$_2$O$_3$/Al composite coatings on a magnesium alloy, J. Alloy. Compd. 596 (2014) 10–18.

[10] L. Wang, D. Yan, Y. Yang, Y. Dong, X. Chen, J. Zhang, Structure and properties of nanostructured ceramic matrix composite coatings prepared in-situ by reactive plasma spraying micro-sized Al–Fe$_2$O$_3$–Cr$_2$O$_3$ powders, Ceram. Int. 40 (2014) 6481–6486.

[11] B. Zou, S. Tao, W. Huang, Z.S. Khan, X. Fan, L. Gu, Y. Wang, J. Xu, X. Cai, H. Ma, X. Cao, Synthesis and characterization of in situ TiC–TiB$_2$ composite coatings by reactive plasma spraying on a magnesium alloy, Appl. Surf. Sci. 264 (2013) 879–885.

[12] J. Sedlacek, P. Ctibor, J. Kotlan, Z. Pala, Dielectric properties of CaTiO$_3$ coatings prepared by plasma spraying, Surf. Eng. 29 (5) (2013) 384–389.

[13] J. Kotlan, P. Ctibor, Z. Pala, P. Homola, V. Nehasil, Improving dielectric properties of plasma sprayed calcium titanate (CaTiO$_3$) coatings by thermal annealing, Ceram. Int. 40 (2014) 13049–13055.

[14] R.C. Kell, A.C. Greenham, G.C.E. Olds, High-permittivity temperature-stable ceramic dielectrics with low microwave loss, J. Am. Ceram. Soc. 56 (7) (1973) 352–354.

[15] B. Jancar, D. Suvorov, M. Valant, Microwave dielectric properties and microstructural characteristics of aliovalently doped perovskite ceramics based on CaTiO$_3$, Key Eng. Mater. 206–213 (2002) 1289–1292.

[16] E.E.C. Oliveira, A.G. D'Assunção, J.B.L. Oliveira, A.M. Cabral, Small size dual-band rectangular dielectric resonator antenna based on calcium titanate (CaTiO$_3$), Microw. Opt. Technol. Lett. 54 (4) (2012) 976–979.

[17] A. Krause, W. Weber, A. Jahn, K. Richter, D. Pohl, B. Rellinghaus, U. Schröder, J. Heitmann, T. Mikolajick, Evaluation of the electrical and physical properties of thin calcium titanate high-k insulators for capacitor applications, J. Vac. Sci. Technol. B29 (1) (2011) 01AC07–05A.

[18] R. Mušálek, G. Bertolissi, J. Medřický, J. Kotlan, Z. Pala, N. Curry, Feasibility of suspension spraying of yttria-stabilized zirconia with water-stabilized plasma torch, Surf. Coat. Technol. 268 (2015) 58–[162.

[19] R.W. Cheary, A. Coelho, A fundamental parameters approach to X-ray line-profile fitting, J. Appl. Crystallogr. 25 (2) (1992) 109–121.

[20] L.B. McCusker, R.B. Von Dreele, D.E. Cox, D. Louer, P. Scardi, Rietveld refinement guidelines, J. Appl. Crystallogr. 32 (1) (1999) 36–50.

[21] B.H. Toby, R factors in Rietveld analysis: how good is good enough?, Powder Diffr. 21 (2006) 67–70.

[22] R. McPherson, Formation of metastable phases in flame- and plasma-prepared alumina, J. Mater. Sci. 8 (6) (1973) 851–858.

[23] S. Sampath, H. Herman, Rapid solidification and microstructure development during plasma spray deposition, J. Therm. Spray Technol. 5 (1996) 445–456.

[24] P. Chraska, J. Dubsky, K. Neufuss, J. Pisacka, Alumina-base plasma-sprayed materials Part I: Phase stability of alumina and alumina-chromia, J. Therm. Spray Technol. 6 (3) (1997) 320–326.

[25] R.N. Patil, E.C. Subbarao, Monoclinic-tetragonal phase transition in zirconia: mechanism, pretransformation and coexistence, Acta Crystallogr. Sect. A: Cryst. Phys. Diffr. Theor. Gen. Crystallogr. 26 (1970) 535–542.

[26] W. Dong, B. Li, Y. Li, X. Wang, L. An, C. Li, B. Chen, G. Wang, Z. Shi, General approach to well-defined perovskite $MTiO_3$ (M = Ba, Sr, Ca, and Mg) nanostructures, J. Phys. Chem. C 115 (10) (2011) 3918–3925.

[27] P. Fauchais, G. Montavon, Latest developments in suspension and liquid precursor thermal spraying, J. Therm. Spray. Technol. 19 (1–2) (2010) 226–239.

[28] A. Joulia, G. Bolelli, E. Gualtieri, L. Lusvarghi, S. Valerif, M. Vardelle, S. Rossignol, A. Vardelle, Comparing the deposition mechanisms in suspension plasma spray (SPS) and solution precursor plasma spray (SPPS) deposition of yttria-stabilised zirconia (YSZ), J. Eur. Ceram. Soc. 34 (15) (2014) 3925–3940.

Chapter 5

Conclusions

This thesis presents work done within the frame of the topic "Property studies of plasma sprayed titanates". Barium titanate is the most known material from group of titanates. It received a lot of attention world-widely. Chemical and microstructural changes may take place during plasma spraying. Final electrical properties of deposited barium titanate are behind expectations due to this unwanted processes. It could be general conclusion based on the literature research. With respect to these findings, calcium titanate was chosen as an alternative material from group of titanates for the main part of this thesis. Calcium titanate was deposited by APS as well as WSP technique. Presented results showed possibility of employing plasma spraying and consequent thermal annealing as a technique for deposition good dielectric layer. Less reductive plasma atmosphere seems to be way to obtain as-sprayed coating with sufficient dielectric properties.

Plasma deposited coatings could serve as electrical breakdown barrier especially for application where a good resistance against mechanical load is required. Alumina and yttria had electrical breakdown value over 16 kV/mm. This is satisfactory for many applications. However, behavior of the coatings was investigated in normal atmosphere only. For broader employing in specific applications is necessary to study how air humidity or thermal cycling affects coatings breakdown strength.

Rapid cooling of deposited particles may result in formation of amorphous phases in the coating. One example of this effects is presented in paper focused on the role of amorphous phase content on the electrical properties of plasma deposited barium-strontium titanate. Response to an electric field applied to the coating was significantly different for all coatings, containing different amorphous phase content, studied in this paper. Samples containing high amount of amorphous phase content exhibited lower relative permittivity as well as lower loss factor whereas DC resistivity was higher. Not only amorphous phase content but the oxygen deficiency played role in the coatings properties. The same material deposited at same spray conditions where only spray distance varied may exhibit surprisingly different electrical properties. Controlling of amorphous phase content to tailor coatings electric properties could be interesting topic for further work.

Reactive thermal spraying has a great potential for deposition functional coatings. This technique is based on chemical reaction of sprayed materials during or even after deposition onto the substrate. In general, this process may denote two different spraying approaches. First, reaction between the sprayed material and surrounding atmosphere. In the second approach, which was used in the last paper of this collection, reaction between feedstock constituents took place. The work introduced a novel method for preparation of calcium titanate powder or coatings. Fine powders of calcium carbonate and titania mixed in stoichiometric ratio necessary for formation of calcium titanate were dispersed in ethanol in order to avoid clogging problem during feeding of such fine powders. Feeding optimization played important role in this study with result that feeding angle is very important parameter. The best results were obtained when suspension was injected downstream to plasma jet. Penetration and consequently thermal treatment of injected particles were significantly better when compared to the perpendicular or upstream plasma jet injection. The unique side result of this study was in stabilization of metastable high temperature tetragonal a cubic crystalline phases. Increase in substrate temperature resulted in an increase of amount of calcium titanate in the coating up to more than 96 wt.%.

Finally, calcium titanate as well as other titanates may be useful as dielectrics in application where plasma spraying has added value for manufacturing process. Not only large area coatings or free standing tubes but advance in covering various substrates at low or middle substrate temperature give advantage for application of plasma deposited layers.

Bibliography

[1] H. Herman. Plasma-sprayed coatings. *Scientific American*, 259(3):112–117, sep 1988.

[2] Science learning. `http://sciencelearn.org.nz/Contexts/Gases-and-Plasmas/Looking-Closer/Plasma-spray-coating`. Accessed: 2016-06-20.

[3] J. Jenista, H. Takana, N. Nishiyama, M. Bartlova, V. Aubrecht, P. Krenek, M. Hrabovsky, T. Kavka, V. Sember, and A. Maslani. Integrated parametric study of a hybrid-stabilized argon–water arc under subsonic, transonic and supersonic plasma flow regimes. *Journal of Physics D: Applied Physics*, 44(43):435204, oct 2011.

[4] P. Ctibor, H. Ageorges, V. Stengl, N. Murafa, I. Pis, T. Zahoranova, V. Nehasil, and Z. Pala. Structure and properties of plasma sprayed BaTiO3 coatings: Spray parameters versus structure and photocatalytic activity. *Ceramics International*, 37(7):2561–2567, sep 2011.

[5] A.H. Pakseresht, M.R. Rahimipour, M.R. Vaezi, and M. Salehi. Effect of splat morphology on the microstructure and dielectric properties of plasma sprayed barium titanate films. *Applied Surface Science*, 324:797–806, jan 2015.

[6] F.L. Toma, S. Scheitz, L.M. Berger, V. Sauchuk, M. Kusnezoff, and S. Thiele. Comparative study of the electrical properties and characteristics of thermally sprayed alumina and spinel coatings. *Journal of Thermal Spray Technology*, 20(1-2):195–204, nov 2010.

[7] H.J. Kim, S. Odoul, C.H. Lee, and Y.G. Kweon. The electrical insulation behavior and sealing effects of plasma-sprayed alumina–titania coatings. *Surface and Coatings Technology*, 140(3):293–301, jun 2001.

[8] S.K. Asl and M.H. Sohi. Effect of grit-blasting parameters on the surface roughness and adhesion strength of sprayed coating. *Surface and Interface Analysis*, 42(6-7):551–554, feb 2010.

[9] P. Ctibor, O. Roussel, and A. Tricoire. Unmelted particles in plasma sprayed coatings. *Journal of the European Ceramic Society*, 23(16):2993–2999, dec 2003.

[10] T. Kavka, J. Matejicek, P. Ctibor, and M. Hrabovsky. Spraying of metallic powders by hybrid gas/water torch and the effects of inert gas shrouding. *Journal of Thermal Spray Technology*, 21(3-4):695–705, dec 2011.

[11] G. Mauer, M.O. Jarligo, D.E. Mack, and R. Vaßen. Plasma-sprayed thermal barrier coatings: New materials, processing issues, and solutions. *Journal of Thermal Spray Technology*, 22(5):646–658, feb 2013.

[12] J. Marthe, E. Meillot, G. Jeandel, F. Enguehard, and J. Ilavsky. Enhancement of scattering and reflectance properties of plasma-sprayed alumina coatings by controlling the porosity. *Surface and Coatings Technology*, 220:80–84, apr 2013.

[13] C.C. Stahr, S. Saaro, L.M. Berger, J. Dubsky, K. Neufuss, and M. Herrmann. Dependence of the stabilization of α-alumina on the spray process. *Journal of Thermal Spray Technology*, 16(5-6):822–830, oct 2007.

[14] H. Gerdien and A. Lotz. Wasserstabilisierter lichtbogen. *Wiss Veroff Siemenswerk*, 2(489):489–492, 1922.

[15] M. Hrabovsky, V. Kopecky, V. Sember, T. Kavka, O. Chumak, and M. Konrad. Properties of hybrid water/gas DC arc plasma torch. *IEEE Trans. Plasma Sci.*, 34(4):1566–1575, aug 2006.

[16] L. Pawlowski. The relationship between structure and dielectric properties in plasma-sprayed alumina coatings. *Surface and Coatings Technology*, 35(3-4):285–298, nov 1988.

[17] P. Chraska, J. Dubsky, K. Neufuss, and J. Pisacka. Alumina-base plasma-sprayed materials part i: Phase stability of alumina and alumina-chromia. *Journal of Thermal Spray Technology*, 6(3):320–326, sep 1997.

[18] L. Pawlowski. *The Science and Engineering of Thermal Spray Coatings, 2nd Edition.* John Wiley & Sons, Ltd., 2008.

[19] P. Ctibor, J. Sedlacek, and K. Neufuss. Influence of chemical composition on dielectric properties of al2o3 and ZrO2 plasma deposits. *Ceramics International*, 29(5):527–532, jan 2003.

[20] A.H. Dent, A. Patel, J. Gutleber, E. Tormey, S. Sampath, and H. Herman. High velocity oxy-fuel and plasma deposition of BaTiO3 and (ba,sr)TiO3. *Materials Science and Engineering: B*, 87(1):23–30, oct 2001.

[21] K. Ahn, B.W. Wessels, and S. Sampath. Dielectric properties of plasma-spray-deposited BaTiO3 and ba0.68Sr0.32Tio3 thick films. *Journal of Materials Research*, 18(05):1227–1231, may 2003.

[22] P. Ctibor, H. Ageorges, J. Sedlacek, and R. Ctvrtlik. Structure and properties of plasma sprayed BaTiO3 coatings. *Ceramics International*, 36(7):2155–2162, sep 2010.

[23] Z. Xing, H. Wang, L. Zhu, X. Zhou, and Y. Huang. Properties of the BaTiO3 coating prepared by supersonic plasma spraying. *Journal of Alloys and Compounds*, 582:246–252, jan 2014.

[24] P. Ctibor, J. Sedlacek, and Z. Pala. Structure and properties of plasma sprayed BaTiO3 coatings after thermal posttreatment. *Ceramics International*, 41(6):7453–7460, jul 2015.

[25] A.H. Pakseresht, M.R. Rahimipour, M.R. Vaezi, and M. Salehi. Effect of heat treatment on the microstructure and dielectric properties of plasma-sprayed barium titanate films. *International Journal of Materials Research*, 107(1):28–34, jan 2016.

[26] P. Ctibor, J. Sedlacek, K. Neufuss, J. Dubsky, and P. Chraska. Dielectric properties of plasma-sprayed silicates. *Ceramics International*, 31(2):315–321, jan 2005.

[27] P. Ctibor, B. Nevrla, Z. Pala, J. Sedlacek, J. Soumar, T. Kubatik, K. Neufuss, M. Vilemova, and J. Medricky. Study on the plasma sprayed amorphous diopside and annealed fine-grained crystalline diopside. *Ceramics International*, 41(9):10578–10586, nov 2015.

[28] E.J. Young, E. Mateeva, J.J. Moore, B. Mishra, and M. Loch. Low pressure plasma spray coatings. *Thin Solid Films*, 377-378:788–792, dec 2000.

[29] G. Berard, P. Brun, J. Lacombe, G. Montavon, A. Denoirjean, and G. Antou. Influence of a sealing treatment on the behavior of plasma-sprayed alumina coatings operating in extreme environments. *Journal of Thermal Spray Technology*, 17(3):410–419, jul 2008.

Appendix A

List of Publications Related to the Thesis

All authors have the same contribution for all papers in appendices to this thesis.

A.1 Papers in Impacted Journals

[1*] J. Sedlacek, P. Ctibor, J. Kotlan, and Z. Pala. Dielectric properties of $CaTiO_3$ coatings prepared by plasma spraying. *Surface Engineering*, 29(5):384-389, jun 2013.

[2*] J. Kotlan, P. Ctibor, Z. Pala, P. Homola, and V. Nehasil. Improving dielectric properties of plasma sprayed calcium titanate ($CaTiO_3$) coatings by thermal annealing. *Ceramics International*, 40(8):13049-13055, sep 2014.

Cited in:

[2*.1] J.E. Arce, A.E. Arce, Y. Aguilar, L. Yate, S. Moya, C. Rincon, and O. Gutierrez. Calcium phosphate – calcium titanate composite coatings for orthopedic applications. *Ceramics International*, 42(8):10322-10331, jun 2016.

[2*.2] J. Zhu, Z. Ma, L. Gao, Y. Liu, F. Wang, T. Li, and Z. Yan. Plasma spraying of $La_{1-x}Sr_xTiO_{3+\delta}$ coating. *Science of Advanced Materials*, 7(12):2611-2616, dec 2015.

[3*] P. Ctibor, J. Kotlan, Z. Pala, J. Sedlacek, Z. Hajkova, and T.M. Grygar. Calcium titanate ($CaTiO_3$) dielectrics prepared by plasma spray and post-deposition thermal treatment. *Materials Research Bulletin*, 72:123-132, dec 2015.

Cited in:

[3*.1] V.S. Puli, R. Picchini, C. Orozco, and C.V. Ramana. Controlled and enhanced dielectric properties of high-titanium containing $Li_xTi_{0.1}Ni_{1-x}O$ via chemical composition-tailoring. *Chemical Physics Letters*, 649:115118, apr 2016.

[4*] J. Kotlan, R.C. Seshadri, S. Sampath, P. Ctibor, Z. Pala, and R. Musalek. On the dielectric strengths of atmospheric plasma sprayed Al_2O_3, Y_2O_3, ZrO_2-7% Y_2O_3 and $(Ba,Sr)TiO_3$ coatings. *Ceramics International*, 41(9):11169-11176, nov 2015.

[5*] J. Kotlan, R.C. Seshadri, S. Sampath, and P. Ctibor. The role of amorphous phase content on the electrical properties of atmospheric plasma sprayed $(Ba,Sr)TiO_3$ coatings. *Ceramics International*, 42(9):11010-11014, jul 2016.

[6*] J. Kotlan, Z. Pala, R. Musalek, and P. Ctibor. On reactive suspension plasma spraying of calcium titanate. *Ceramics International*, 42(3):4607-4615, feb 2016.

Cited in:

[6*.1] V. Brozek, P. Pokorny, P. Bouska, J. Stoulil, and L. Mastny. Corrosion properties of chromia based eco - friendly coatings on mild steel. *Metalurgija*, 55(4):675-678, nov 2016.

A.2   Other Publications

[7*] J. Kotlan, P. Ctibor, Z. Pala. Plasma Sprayed and Annealed Calcium Titanate Dielectrics. *In The Proceedings of the 1st International Porous and Powder Materials Symposium and Exhibition*, PPM 2013. Izmir: University of Izmir, 2013, p. 207-211. ISBN 978-975-6590-05-8.

[8*] J. Kotlan, R. Musalek, J. Medricky, P. Ctibor, Z. Pala. Suspension Precursor Plasma Spraying as a Technique For Preparing Calcium Titanate Coatings. *In 9th International Materials Technology Conference and Exhibition.* Selangor: Institute of Materials Malaysia, 2014, art. no. ISCT-OS-01.

[9*] J. Kotlan, S.J. Han, P. Ctibor, Z. Pala, H. Seiner. High temperature characterisation of thick ceramic dielectric coatings prepared by high feed-rate plasma spray system. *In Book of abstracts of The 11th International Conference of Pacific Rim Ceramic Societies.* Seoul: The Korean Ceramic Society, 2015, art. no. ThN2-4, p. 615.

Appendix B

List of Publications without Relation to the Thesis

B.1 Papers in Impacted Journals

[1**] P. Ctibor, I. Pis, J. Kotlan, Z. Pala, I. Khalakhan, V. Stengl, and P. Homola. Microstructure and properties of plasma-sprayed mixture of Cr_2O_3 and TiO_2. *Journal of Thermal Spray Technology*, 22(7):1163-1169, jul 2013.

Cited in:

[1**.1] N.N. Li, G.L. Li, H.D. Wang, J.J. Kang, S.H. Dong, and H.J. Wang. Influence of TiO_2 content on the mechanical and tribological properties of Cr_2O_3-based coating. *Materials & Design*, 88:906-914, dec 2015.

[1**.2] A.H. Navidpour, M. Salehi, M. Amirnasr, H.R. Salimijazi, M.A. Azarpour, Siahkali, Y. Kalantari, and M. Mohammadnezhad. Photocatalytic iron oxide coatings produced by thermal spraying process. *Journal of Thermal Spray Technology*, 2 (8):1487-1497, oct 2015.

[2**] P. Ctibor, K. Neufuss, Z. Pala, J. Kotlan, and J. Soumar. Dielectric and mechanical properties of plasma-sprayed olivine. *Romanian Reports in Physics*, 67(2):600-616, 2015.

[3**] R. Musalek, G. Bertolissi, J. Medricky, J. Kotlan, Z. Pala, and N. Curry. Feasibility of suspension spraying of yttria-stabilized zirconia with water-stabilized plasma torch. *Surface and Coatings Technology*, 268:58-62, apr 2015.

Cited in:

[3**.1] V. Brozek, P. Pokorny, P. Bouska, J. Stoulil, and L. Mastny. Corrosion properties of chromia based eco - friendly coatings on mild steel. *Metalurgija*, 55(4):675-678, nov 2016.

[4**] P. Ctibor, R.C. Seshadri, J. Henych, V. Nehasil, Z. Pala, J. Kotlan. Photocatalytic and electrochemical properties of single and multilayer substoichiometric titanium oxide coatings prepared by atmospheric plasma spraying. *Journal of Advances Ceramics*, 5(2):126-136, jul 2016.

B.2 Other Publications

[5**] P. Ctibor, J. Kotlan, Z. Pala, K. Neufuss, J. Soumar. Plasma spraying of natural olivine and its dielectric, mechanical and optical characterization. *In 16th International Conference on Plasma Physics and Applications*. Bucharest: National institute for lasers, plasma and radiation physics, 2013, art. no. O-04, p. 36. ISSN 2344-0481.